Device modeling of dye-sensitized solar cells

Juan Bisquert[1] and Rudolph A. Marcus[2]

[1]Photovoltaics and Optoelectronic Devices Group, Departament de Física, Universitat Jaume I, 12071 Castelló, Spain

[2]Noyes Laboratory of Chemical Physics, California Institute of Technology, Pasadena CA 91125 USA.

Contents

Juan Bisquert and Rudolph A. Marcus
"Device modeling of dye-sensitized solar cells"
Computational Photovoltaics, *Topics in Current Chemistry* (2013), David Beljonne and Jérôme Cornil Eds.

The original publication is available at www.springerlink.com

Introduction

Standard dye-sensitized solar cells (DSC)[1] are composed of three main elements, as indicated in Fig. 1(a): the electron transport material (ETM), the hole transport material (HTM) and the light absorber. The ETM is a mesoporous structured wide band gap metal oxide semiconductor that provides a high internal area framework to maintain the light absorber rigidly anchored or sticked to the surface. We will refer to mesoporous anatase TiO_2 as the archetypal ETM. Conventionally the light absorber is a monolayer of metal-organic dye such as the well known N719 ruthenium bypyridil dye. In recent years an enormous variety of dyes have been investigated, and particularly porphyrin dyes have shown very powerful results, elevating power conversion efficiency to 12%.[2] In addition, solid light absorbers of different classes, either colloidal quantum dots, or uniform nanometer-thick light absorbing layer, have become increasingly investigated.[3-5] Finally, the preferred HTM was a liquid electrolyte containing redox couple I_3^- / I^- and a number of coadsorbents to control the surface conditioning of the TiO_2 metal oxide. Recently, rather effective redox shuttles based on transition metal complexes were applied to high performance devices.[6] Fully solid hole conductors have been widely used as well. In general the selection of the HTM depends critically on the type of absorber, and these choices also determine the counterelectrode.[7]

Device modeling can serve different finalities. It may be used to gain detailed scientific insight into a range of phenomena occurring in the DSC. Or it may be aimed at technical characterization to support the quality of fabrication of devices. Among the two extremes, a widely used type of application of the methods is to compare a set of DSC prepared with some variation of materials or procedures, in order to extract information about the internal mechanisms. Therefore modeling DSC and solar cells in general may have a wide variety of purposes.

The following overview aims to present a reasonably short summary of the state of the art and recent exciting developments with a view to broad possible applications of these methods. We aim to cover a series of fundamental factors that have appeared crucial to the operation of the DSC over many years of research: causes of fundamental electron transfer rate that govern recombination; energy disorder affecting electronic states in electron conductor; and the general modeling approach incorporating such fundamental properties to small perturbation techniques, that have provided outstanding control over the internal state of the device and the mechanisms lying behind the photovoltaic performance. We will be concerned by description of the basis of impedance spectroscopy results, the causes and measurements of the electron

lifetime, and how these understandings establish properties of current-voltage curves.

1. The electron subsystem

In cells, in which the absorber is a molecular dye, and the HTM is a liquid conductor with low viscosity, the injection of photogenerated electrons into TiO_2 is very fast, in the ps domain, and main modelling issues are referred to the electron subsystem. Provided that dye regeneration is sufficiently fast, the HTM can be viewed simply as an homogeneous medium that regenerates the oxidized dye and therefore provides (the oxidized) species that may accept electrons from TiO_2. It is therefore assumed in a starting approach that the Fermi level of the hole species is flat and stable and any kind of kinetics in the absorber or HTM can be safely neglected. In contrast, for thin inorganic absorber of quantum dot absorber, a number of additional issues occur, because the carrier dynamics in the absorber cannot be neglected.[7-9] Furthermore, for viscous electrolytes, or solid HTM, it is necessary to describe the transport of the ionic or electronic species.[10]

Let us for the moment set aside the problems of dynamics in the absorber and HTM and we consider the description of electrons in ETM, which is a central problem to the modelling of dye solar cells.

From the point of view of energetics the basic modelling uses two main levels, indicated in Fig. 1(b): a transport level usually identified with a conduction band level, E_c, and the electrochemical potential of electrons that is usually called the Fermi level, E_{Fn}. The energy level E_c is significant for issues of charge transfer as in injection from the dye and recombination,[11] while the Fermi level determines the photovoltage in the DSC and establishes how electron transport is driven by diffusion.[12] Normally the TiO_2 nanoparticles (or wires, tubes, etc.) provide a well connected structure and the energy level is defined globally in the nanostructured film as shown in Fig. 1(b). Electron density in the transport level n_c is defined as

$$n_c = N_c e^{(E_{Fn}-E_c)/k_BT} \tag{1}$$

where k_BT is thermal energy and N_c is an effective total density of states. The Fermi level in the absence of bias voltage E_{F0} is called the "equilibrium Fermi level". The electron density at equilibrium is

$$n_{c0} = N_c e^{(E_{F0}-E_c)/k_BT} \tag{2}$$

and we may write

$$n_c = n_{c0} e^{(E_{Fn} - E_{F0})/k_B T} \tag{3}$$

Consider for the sake of clarity a pulse of electrons injected from the substrate into the metal oxide nanostructure. The electrons diffuse into the ETM, and the electron motion can be viewed as a random walk process,[13] in which a carrier at each step has a chance to either continue random walk or recombine with the acceptor ionic species, or holes in the HTM. The probability to move away from the injection point is governed by the diffusion length L_n, as suggested in Fig. 1(b). This parameter plays a key role in the modelling of DSC[14] since the size of L_n compared to film thickness L critically determines the collection efficiency[15] of the solar cell. In addition a large $L_n >> L$ implies that carrier gradients are small in most conditions. This feature greatly simplifies modelling, as said above, because one considers homogeneous distribution of carriers and may focus exclusively on the time dependence of the processes. This case will be developed in the next section to formulate an important description of the performance of a DSC.

2. The fundamental diode model

According to a fundamental conservation argument, in a film where electrons can be generated, diffuse, and recombine, as in Fig. 1(b), electron density at position x is controlled by the equation,

$$\frac{\partial n_c}{\partial t} = -\frac{\partial J_n}{\partial x} + G(x) - U_n(x) \tag{4}$$

where J_n is the electron flux, related to the free electron diffusion coefficient, D_0, by Fick's law

$$J_n = -D_0 \frac{\partial n_c}{\partial x} \tag{5}$$

G is a local generation rate, and U_n is a recombination rate. At the extraction contact the carrier density is controlled by the voltage. The voltage is given by the rise of the electrons Fermi level, with respect to the redox level, as indicated in Fig. 1(b)

$$qV = E_{Fn}(x = 0) - E_{redox} \tag{6}$$

Note that we use a positive voltage for raising the Fermi level of electrons. This convention has an opposite sign with respect to the voltage in electrochemistry, but it is convenient for the description of the DSC, where the active contact is that of electrons and provides a negative voltage. The convention of Eq. (6) makes the normal photovoltage positive.

At initial equilibrium we have $E_{F0} = E_{redox}$, and we assume here that the redox level remains stationary even though the electron density may increase. Therefore we have the following expression for the voltage in the device

$$qV = E_{Fn} - E_{F0} \tag{7}$$

where q is the elementary charge, and therefore

$$n_c(x=0) = n_{c0} e^{qV/k_B T} \tag{8}$$

The selective boundary at $x = L$ imposes the condition

$$J_n(L) = 0 \tag{9}$$

Let us assume reasonably homogeneous carrier distribution in the mesoporous TiO_2 film. This model with fast transport and Fermi levels is shown in Fig. 2. By spatial integration of Eq. (4) along the thickness of the device, we obtain

$$\frac{\partial(n_c L)}{\partial t} = J_n(0) + \int_0^L G(x)dx - LU_n \tag{10}$$

Variations of the total carrier number $n_c L$ correspond to the sum of three effects: electrons going out and into the device through the contact, in the flux $J_n(0)$; generation, and finally, recombination. We start by considering steady state condition, in which $\partial n_c / \partial t = 0$. From Eq. (10)

$$-J_n(0) = \int_0^L G(x)dx - LU_n \tag{11}$$

There is a full balance of the three terms of Eq. (10) as suggested in Fig. 2(a). The steady state regime is the true domain of operation of a solar cell for electrical power production under sunlight. On the other hand, most characterization techniques involve time dependence in order to provide detailed kinetic information about the system, and these conditions will be described later on.

Working at steady state we have to describe simply two variables: the electrical current density in the outer circuit

$$j = qJ_n(0) \tag{12}$$

as a function of the voltage. V is related to concentration by Eq. (8). The concentration enters the balance equation (11) via the recombination term. A phenomenological model that gives good results in many cases is the following [14,16]

$$U_n = k_{rec}\left(n_c{}^{\beta} - n_{c0}{}^{\beta}\right) \tag{13}$$

Eq. (13) consists on a power β of the free carrier density and is called the β-recombination model. This parameter usually has experimental values 0.6-0.75. The recombination rate in Eq. (13) is composed of two terms: a dark generation rate, that we express as a current density

$$j_0 = qLk_{rec}n_{c0}{}^{\beta} \tag{14}$$

and the recombination current

$$j_{rec} = qLk_{rec}n_c{}^{\beta} \tag{15}$$

The latter term can also be expressed

$$j_{rec} = j_0 e^{q\beta V/k_B T} \tag{16}$$

Finally photogeneration in Eq. (11) gives the photocurrent as follows

$$j_{ph} = q\int_0^d G_\Phi dx \tag{17}$$

In summary we have that

$$j = j_{ph} - j_{rec} + j_0 \tag{18}$$

j_{rec}, as discussed before, is the recombination current that we have described in Eq. (16) as j_0 (the recombination current at thermal equilibrium) enhanced by the applied voltage. Therefore we may write Eq. (18) as

$$j = j_{ph} - j_0\left(e^{qV/mk_B T} - 1\right) \tag{19}$$

We observe that the diode quality factor relates to the recombination exponent as $m = 1/\beta$.[17]

3. Features of current-voltage curves: photocurrent and photovoltage

The simple model of Fig. 2 and Eq. (19) appears deceptively primitive at first sight but in fact it has important applications as it contains the main features for the description of the current voltage (jV) curve of the DSC. There are two main assumptions to this model, (a) the first is a total decoupling of photocurrent and recombination; these two features are viewed as independent phenomena. The second feature is (b) carrier density is independent of position. Both assumptions are a good approximation so far as the diffusion length is very large. But how well are they realized?

If the carrier collection efficiency is very good, then photocurrent, j_{ph}, is determined by the light absorption and charge injection features that are measured by Incident Photon to Current conversion efficiency (IPCE), also known as the External Quantum Efficiency (EQE).[18] Examples of the absorption spectra of efficient dyes are shown in Fig. 3,[19] and the corresponding IPCE is shown below in the Figure together with the final photovoltaic performance. In this type of highly efficient DSC, the measured current can indeed be viewed as completely decoupled from recombination, as in the model of Eq. (19). The convolution of IPCE with the solar spectrum describes very well the actual value of j_{ph}. However in cells with low collection efficiency one should be careful to calculate correctly the collection efficiency starting from diffusion lengths.[20] Another important consideration to describe photocurrent is optical modeling, including features as glass reflection, scatter layers, and photonic crystal light absorption.[21-26]

Next main feature is recombination of electrons, which is described in this simple model by j_{rec} in Eq. (16). Now recombination describes the shape of the jV curve apart from the additive j_{ph} term. Therefore recombination determines the fill factor and open-circuit voltage V_{oc} of the solar cell. A vast number of papers and studies have been devoted to obtaining comparative information of DSCs with varying characteristics and we will review here a number of features. As example we consider the data in Fig. 4(a) that correspond to a series of DSC with different electrolytes but otherwise identical conditions of film thickness, dye (N719) and so on.[27]

We should first of all remark that experimentally it is usually not possible to obtain j_{rec} from the jV due to complications such as the series resistance that is always present and affects the voltage. The voltage associated to separation of Fermi levels is called V_F, and it is obtained from the measured voltage V_{app} by correction of the voltage drop at series resistance. In Fig. 4(b) the jV curve is shown with respect to V_F. In this case the downward bending of the curve towards high voltages must be due to recombination and the curves correspond to Eq. (19).

To avoid the sempiternal problem of uncertainty of jV curve modeling, it has become widely accepted in the DSC area to use the technique of impedance spectroscopy (IS), that separates different resistive components[28,29] by means of an equivalent circuit analysis that takes into account the spectral shapes. One key point about IS applied to DSC is that it provides a direct probe of recombination via the recombination resistance, R_{rec},

$$R_{rec} = \left(\frac{\partial\, j_{rec}}{\partial V_F} \right)^{-1} \tag{20}$$

Obviously R_{rec} consists on a derivative of the recombination flux.

Assuming that R_{rec} is measured, as in Fig. 4, we wish to obtain the parameters for recombination in the DSC. For example from the model of Eq. (16) we obtain the explicit dependence

$$R_{rec} = R_0 \exp\left[-\frac{\beta q V_F}{k_B T} \right] \tag{21}$$

where

$$R_0 = \frac{k_B T}{\beta q j_0} \tag{22}$$

Therefore from the measurement of impedance spectroscopy the recombination parameters j_0 and β can be derived. In general, as it may be observed in Fig. 4(b), R_{rec} approaches quite well the single exponential behaviour given in Eq. (21). Another example of the recombination resistance in a family of similar DSCs is shown in Fig. 5(b). These results provide strong support to the recombination model of Eq. (13). Therefore we may aim at a more fundamental discussion of the parameters j_0 and β in terms of electron transfer, depending on surface conditions, TiO_2 properties, etc.[30-34]

Fig. 4(c) shows that the variation of electrolyte conditions produces a very large impact on recombination parameters. This is due to two different factors: the shift of the conduction band, and the change of interfacial kinetics, induced by the specific properties of the electrolyte. These questions will be treated in more detail in a later section, after we have introduced the disordered DOS in TiO_2. In all the cells of Fig. 4 the redox couple is the same, but other redox couples based on cobalt or copper can be used and the variations are investigated using similar methods.[35-39]

It has been therefore established that we are able to measure recombination with great accuracy, and it is a challenge of great significance both from fundamental and applied stances, to be able to describe by a comprehensive theory these observations. We will carry out this discussion below, but first we need to develop a number of points concerning the disorder in the electron subsystem. It should be pointed out, however, that the exponential dependence of the recombination resistance on voltage, which is characteristic in high performance liquid electrolyte DSC, is not universal, and different types of behaviour have

been occasionally reported.[40,41]

Another important method of application of the recombination resistance is that by integration of (20) we can recover j_{rec}. In addition, for the simple model of Eq. (16) integration is not even needed as the following expression[27] can be used

$$j = j_{ph} + j_0 - \frac{k_B T}{\beta q} \frac{1}{R_{rec}(V_F)} \tag{23}$$

Therefore from the impedance data it is possible to reconstruct the jV curve, as shown in Fig. 4(a), with a great control over the elements that intervene in the curve. A similar method has been derived for organic solar cells.[42]

We must also discuss the second assumption of the fundamental diode model of Fig. 2, which is a homogeneous carrier density. Clearly this assumption is better realized close to open circuit than in short circuit conditions, as in latter case the electron Fermi level must come to the equilibrium value, at the contact, while the carrier density is still high in the rest of the device, see Fig. 6.[43] However, the region of jV curve close to open circuit is the most significant one, in cells in which the collection efficiency is high, as it is in this voltage region where we wish to measure recombination, in order to obtain an understanding of the factors controlling fill factor and V_{oc}. It is therefore important to check that homogeneous distribution is a good hypothesis, and this has been done in the data shown in Fig. 5, that indicate that the distributed transmission line elements[44] (measured at open circuit conditions), that will be discussed in Section 12, are independent of the TiO_2 film thickness in the DSC, for a significant variation of film sizes.[45] This result shows that local impedances in the film are independent of thickness, indicating nearly homogeneous carrier distribution.

4. Interfaces and mass transport

Let us consider a more detailed modelling of the device operation beyond the homogeneous model discussed in the previous section. Modelling the DSC and in general any complex nanostructured device requires to consider four main aspects.

(1) The number of types of transport species: charged and neutral, ionic and electronic.

(2) The spatial distribution of the charge carriers, that relates to important properties such as shielding, macroscopic electrical fields and the main transport mechanisms.

(3) The structure of interfaces, particularly at the contacts, including a description of interfacial capacitances.

(4) The energy axis, governed by disorder at each material,[17] and by energy level

alignment at interfaces.[46]

The device is therefore formed by some geometry and morphology that sets the first constraint in establishing regions where the carriers can be distributed, either in motion or stationary. Such regions have boundaries that are described by suitable boundary conditions, and in particular the contacts, in which electronic carriers communicate with the external circuit, are critically important for the operation of solar cells.[47]

Having set morphologies and boundaries, there are two different dimensionalities, namely the *spatial space* which can be described with one or more dimensions, and the *energy space*. At each point an energy diagram gives the allowed energy levels for a type of carriers, or their combination, as indicated in Fig. 1(a) and in quantitative detail in Fig. 7. Energy levels for electronic carriers may be stationary states, also called localized states or traps, or extended states that allow fast transport. Transport may also proceed by hopping between localized states,[48] but this formalism is not usually adopted in DSC, in which the transport of electrons is well described by the multiple trapping model.[49] The relative energy alignment at interfaces provides essential constraints for the kinetics of charge or energy transfer.

Based on these general properties that allow to describe the model, one formulates a series of macroscopic equations and boundary conditions that provide, as a result, carrier densities and carrier dynamics, expressed as output current densities, either for steady state or any desired transient condition. In this paper we focus our attention on phenomenological modeling using macroscopic equations. A first model, presented in the previous section, contains only one kind of carriers (electrons in TiO_2) and no spatial dimension at all (once the photocurrent is calculated by an integration of generation term), since all the points are considered at the same density. This model is fairly useful, as discussed above, however, for a deeper understanding of the microscopic electronic phenomena it is necessary to include the energy axis, distinguishing free and trapped electrons, which makes a very large effect for all measured kinetic parameters of the DSC. This description is discussed below.[49-52]

Instead of the phenomenological transport and conservation equations one may adopt a more fundamental point of viewin which electronic states are modelled individually and the transfer rates between states allow us to analyze the global dynamics by Monte Carlo simulation.[13] These methods have been also applied widely, they permit to establish arbitrary morphologies and to investigate complex effects such as percolation and nonthermalized electron transport.[53-57] Still a more fundamental approach consists in a simulation of the molecular details of the components of the system. This approach can produce very valuable

knowledge about the structure of interfaces and the origin of the observed energy distribution features, and the nature of excited or intermediate states for charge transfer phenomena.[58-60] Microscopic simulation methods have been widely explored in the field of organic materials, and they have important applications for the investigation of carrier and energy transport in organic solids.[61-63]

A very important aspect of the modeling of a DSC, beyond the zero-dimensional homogeneous model, is to consider a 1 dimensional model, adapted to the standard sandwich –type cell, where equation (4) allows the consideration of gradients like those shown in Fig. 6 to calculate photocurrents and other quantities. In the steady state we have

$$-\frac{\partial J_n}{\partial x} + G(x) - U_n(x) = 0 \qquad (24)$$

This type of model, generally denoted diffusion-recombination model, has been very widely used, with many extensions and variants.[43,64-72] It is interesting to recall that Eq. (24), and its many extensions, are based on a macrohomogeneous approach[73-75] in which the mixture of nanoporous ETM and the HTM inside the pores is viewed as a unique medium that hosts both species, with certain probabilities of carrier exchanges between ETM and HTM, corresponding to electron injection, regeneration, electron-hole recombination, etc. In a highly concentrated electrolyte, the Debye length is very short, and shielding by electroneutrality prevents the formation of long range electrical fields in the semiconductor nanostructure. When the electrons are injected into a nanostructured metal oxide, positive ions move to the surface of the charged nanoparticles and neutralize long range electrical fields. Therefore electron transport is driven by concentration gradient, i.e. by diffusion.[15] This property is quite general for a number of photovoltaic and electrochemical cells, such as inorganic composite solar cells formed by nanoscale elements,[76] classical electrochemical systems when a supporting electrolyte is used,[77] and also crystalline p-silicon solar cells, in which injected electrons are much less than the majority carrier holes.[78,79]

The crucial mechanism of shielding of electrical fields simplifies considerably the modeling tasks, is illustrated in Fig. 8. There the increase of electron Fermi level in the nanostructure is easily allowed by the large quantity of compensating charges in the HTM, so that the holes in the latter medium (or ions) effectively play the role of a majority carrier. If the shielding is effective, then the cell voltage is readily explained by the change of the Fermi level at the left contact, see Fig. 8. It should be emphasized that the *voltage* is the amount of work necessary to carry an electron from one plate of the device to the other. This work

involves the measurement of an electrical current with an electrometer and is given by the *difference of electron Fermi levels* between the two plates,[80,81] which is the rationale for Eq. (6). It is also true that a change of voltage between the contacts, requires that somewhere, in the device, occurs as well a modification of *electrostatic potentials* (reflected by a change of the vacuum level diagram). There is a widespread tendency to look for a change of *band bending* as a source of photovoltage in a solar cell. In the area of DSC the question of potential barriers was a matter of concern that promoted many discussions.[82-84] It is now well established that the origin of photovoltage is a kinetic balance of excess carriers as expressed by Eq. (4), a result that was conclusively demonstrated by Gregg et al.[83] Monitoring the Fermi level variation is a definitive explanation of photovoltage but still begs the question about the location of the electrical field, and this can be reasoned as shown in Fig. 9. The figure suggests that the change of electrostatic potential, reflected in a change of the vacuum level associated with the photovoltage, i.e. the difference of electrostatic potentials between dark and light, is absorbed at the interface between the SnO_2 transparent conducting oxide (TCO) and the TiO_2. This interface has been repeatedly discussed in the literature.[85-91] Due to effective shielding as mentioned above, the electrical field at the surface of the substrate does not penetrate deeply into the mesostructure.

In principle the diagrams of Figs. 8 and 9 do not seem consistent with the fact that the conduction band of TiO_2 and SnO_2, is normally reported at -4.3 and -4.8 eV, respectively, with respect to the vacuum level. At acidic pH, corresponding to the DSC electrolytes, the TCO conduction band should be higher, but it achieves equilibrium with the redox level, which is about -4.8 eV vs. vacuum for I_3^-/I^-, see Fig. 7, and deeper for other redox couples, that consequently are able to produce a higher photovoltage.[92] The remarkable point is the high position of the TiO_2 conduction band,[84] that is facilitated by specific coadsorbents, which allow a large photovoltage to be achieved.[93] It must be remarked, therefore, that the overall picture in Fig. 9 considers the equilibration by interfacial charging at several interfaces: the TCO/electrolyte, and TiO_2/electrolyte. As a result of these properties the Fermi level in the TCO finally raises under illumination, pulled up by the electrons in TiO_2 so that the TCO/TiO_2 junction forms an excellent selective contact to electrons that is responsible to a large extent for the good operational properties of the DSC. For comparison, the operation of the cathode in bulk heterojunction solar cell seems more problematic, as the initial offset of work functions is shared by both a surface dipole and band bending entering the bulk of the blend.[94]

The previous model erases all electrical fields and interfacial barriers in the mesostructure, which is viewed in effect as a homogeneous medium. However, in semiconductor mesostructures, filled with a HTM, one can also allow for the presence of electrical field and semiconductor barrier at the internal interface ETM/HTM. The prevalence of one approach or the other one, i.e., a macrohomogeneous model that only contemplates the Fermi level, or the explicit presence of internal interface barriers, depends on doping densities, size of semiconductor particles or wires, and Debye length both in the semiconductor nanostructure and in the HTM. [95-97]

The diffusion-recombination model has been developed largely for the liquid electrolyte containing iodide/triodide, that has a very high conductivity, and generally introduces no problem for transport. It was shown that improving the conditions of shielding in liquid electrolyte enhances the observed electron diffusion coefficient.[98] A high concentration electrolyte provides excellent shielding and a flat reference E_{redox}. However, energetically the I_3^-/I^- redox level is too high, see Fig. 7, for example measurement of tris(1,10-phenanthroline)cobalt(II/III) redox couple is 230 mV deeper (more positive redox potential) than iodide electrolyte.[37] In consequence cobalt electrolytes, and also solid organic hole conductors, have been widely explored. It should be noticed in Fig. 7 that Co(II/III) redox couple stands too deep to regenerate oxidized standard ruthenium bypyridill dye. Therefore both the dye and the redox couple have been simultaneously optimized for high performance[99,100] and this approach has provided large rewards in terms of power conversion efficiency.[2]

A number of solid electrolytes have been amply investigated, OMETAD being the most well known[101-103] but also other materials such as CuSCN[104] and P3HT[3,105] showed promising results. In such solid conductors the free carrier density is not so high as in the liquid one, and easy shielding and electroneutrality is not warranted but need to be carefully investigated. IS studies of these DSC with solid hole conductor using either organic or inorganic absorber have shown that the transport of holes in these HTM is usually an issue that introduces a large additional resistance affecting the fill factor of the solar cell.[104-106] Using high extinction solid absorbers such as Sb_2S_3 sensitizer, it was reported that in planar, thin layer configurations, the solid cells provide a sizable photocurrent, but a poor fill factor.[105] It is concluded that the role of mesostructure is not only to provide a large internal area for carrier generation. Charge compensation to satisfy electroneutrality is also a central property of mesoporous DSC. The questions will very likely be more intensively investigated with perovskite absorbers, which

very likely are genuine ambipolar transport materials that do not strictly need fast separation of carriers into different phases.[4,5,107]

The one dimensional diffusion-recombination model neglects the transport in the electrolyte and shielding conditions. A standard, more general approach to multiple carrier transport problems[77] is solved using a set of equations that comprises:

-Diffusion-drift equation for each carrier

-Poisson equation that determines the macroscopic electrical fields

-The boundary conditions

These equations must be combined with statements on energy distributions and charge transfer rates. Early models applied the idea of ambipolar diffusion,[108] which is based on the coupling of just two types of carriers by electroneutrality.[109,110] There have been many attempts to develop a general set of equations able to model the DSC behavior especially with reference to mass transport limitations in liquid electrolytes.[111-117] It is tempting to aim at a simulation tool that will provide a "total" description of the DSC, but one should evaluate very carefully if this goal is feasible, recognizing the complexity of the system. Many aspects of the DSC need to be separately studied on their own, and simulation by a number of phenomenological equations cannot be a substitute for detailed physical understanding. For example the structure of the three- phase contact at the base of the substrate, mentioned above, or the detailed rates of charge transfer dependence on energy and density, as well as the interactions at semiconductor/dye/hole conductor interface, are issues that have to be properly controlled when describing the system. New solar cell configurations and absorbers are bound to pose their own subtleties.

There has nevertheless been important progress in the formulation of simulation tools that can bring useful results. The first important question is that two or three dimensional modeling [118] is able to deal with effects that are certainly beyond reach of the simple one dimensional modeling, such as the properties of exotic configurations of the solar cell[119] or important practical features such as the distribution of the measured quantities in the solar cell plane due to edge effects.[120,121] The second relevant line of progress is that the main defect of old approaches, which was to compare a model with dozens of parameters, with a measured jV curve that may be described with just two or three, has been corrected. More sophisticated approaches incorporate the physics that has been learned about DSC, such as nonlinear recombination model.[14,116,122,123] An example of realistic modeling including all carriers present in the DSC, as well as free and trapped electrons, is shown in Fig. 10.[123] In addition

researchers have recognized that different experimental techniques have to be combined in order to provide a meaningful and reliable characterization for the solar cell performance.[124-127] In particular the coupling of multidimensional modeling with impedance spectroscopy analysis has become a powerful method in order to establish sound results and interpretation of DSC devices.[121,124]

5. Energy disorder in the semiconductor: combined description of free and trapped electrons

In previous sections we have commented the good success of the fundamental diode model, based on electron density in the conduction band, n_c, and phenomenological β-recombination model in Eq. (13), for a first understanding of current voltage curves of high quality DSC. However, it has been well established that electron density restricted to a single level poses important limitations for the description of measurements of DSC, such as recombination resistance, diffusion coefficient, electron lifetime, diffusion length, etc., due to the fact that the localized states in the bandgap produce strong dynamic effects.[17,128-133] A model that is successful to account for most observed properties, is indicated in Fig. 11(a). It is composed of the transport level that was already discussed above, at energy E_c, and a density of states (DOS) in the bandgap, $g(E)$. A key feature is that an electron in the transport level can be trapped in a localized state in the bandgap and later be thermally ejected to the conduction band. By thermalization the carrier density in the localized states is found as

$$n_L = \int_{-\infty}^{+\infty} g(E) f(E - E_{Fn}) dE \tag{25}$$

where $f(E - E_F)$ is the Fermi-Dirac function. The total carrier density is

$$n = n_c + n_L \tag{26}$$

In the DSC as well as in similar devices, the carrier density is measured in steps at different voltages, or by small perturbation methods. It is important to characterize the differential of the carrier density, which is known as the chemical capacitance.[134]

In general the differential capacitance, that is measured by small perturbation, has the expression

$$C = \frac{dQ}{dV} \tag{27}$$

The textbook example is a *dielectric capacitor*, in which the charge separation creates an

electrical field between the plates. The capacitance, per unit area, is given by

$$C = \frac{\varepsilon_0}{d} \tag{28}$$

We obtain a chemical capacitance when the Fermi level in a semiconductor is displaced with respect to the conduction band edge, because in this case we only change the *chemical potential* of the electrons, and not their electrostatic potential. A structure of selective contacts is also necessary so that the Fermi level variation translates into a voltage as follows

$$dV = dE_{Fn} / q \tag{29}$$

This structure is presented in Figs. 2 and 11, in which the change of voltage implies that the Fermi level of electrons moves toward the conduction band, as stated before in Eq. (6). If L is the thickness of the layer, and A is the area, the charge accumulated in the semiconductor, is $Q = -LAnq$. Hence we obtain the *chemical capacitance*[134,135] per unit area, that is defined as follows

$$C_\mu = LAq^2 \frac{dn}{dE_{Fn}} \tag{30}$$

A specific chemical capacitance per unit volume is defined as

$$c_\mu = q^2 \frac{dn}{dE_{Fn}} \tag{31}$$

For conduction band carriers the chemical capacitance is

$$c_\mu^{cb} = \frac{q^2 n_c}{k_B T} \tag{32}$$

It was first calculated by Shockley for crystalline semiconductors.[136] The concept is very useful in the characterization of disordered materials.[12,137] In the DSC the contribution of trapped electrons is dominant. The calculation of the chemical capacitance for a broad DOS is

$$c_\mu = q^2 \int_{-\infty}^{+\infty} g(E) \frac{df}{dE_{Fn}} (E - E_{Fn}) dE \tag{33}$$

Using the approximation of the zero-temperature limit of the Fermi function, i.e. a step function at $E = E_{Fn}$ separating occupied from unoccupied states, as suggested in Fig. 11(a), it can be shown that Eq. (33) reduces to[12]

$$c_\mu^L = q^2 g(E_{Fn}) \tag{34}$$

In this approximation, the Fermi-Dirac function is a unity step function at the Fermi level.

Therefore, displacing the Fermi level by dE_F simply fills with carriers a slice of the DOS: $dn = g(E_F)dE_F$. c_μ is also denoted a *thermodynamic density of states*.[138]

Measurements of chemical capacitance of nanostructured TiO_2 have shown that the localized states are distributed as an exponential distribution that enters the gap of the semiconductor from the conduction band, as suggested in Fig. 11 and indicated by the expression

$$g(E) = \frac{N_L}{k_B T_0} \exp\left[(E - E_C)/k_B T_0\right] \tag{35}$$

Here N_L is the total density of localized states and T_0 is a parameter with temperature units that determines the depth of the distribution, which can be alternatively expressed as a coefficient $\alpha = T/T_0$. The DOS of nanostructured TiO_2 has been well characterized experimentally.[139] The exponential distribution is observed in measurements of chemical capacitance shown in Fig. 4(d) and 5(c). The DOS resulting from such measurements is indicated in Fig. 7.

An important feature of the DOS of the nanostructured metal oxide is that E_c can be displaced with respect to the redox level, and this method is frequently used to improve the photovoltage, as mentioned before.[93] The change of position of the conduction band is obvious in Fig. 4(d), where a shift ΔE_c is marked, with respect to a reference sample. Note that the shift changes the equilibrium density, n_{c0}, by Eq. (2), and this affects the dark reverse current, j_0. These variations are more generally discussed in the next section. Therefore a control of the DOS of electrons in titania is essential for the meaningful discussion of recombination and any other electronic parameter of the DSC.

In most conditions of measurement we can assume that $n \approx n_L$. The equilibrium value of the carrier density is given by

$$n_{L0} = N_L e^{(E_{F0} - E_c)/k_B T_0} \tag{36}$$

Again using zero-temperature approximation the total electron carrier density is given by the integration of DOS up to the Fermi level, Eq. (25)

$$\begin{aligned} n &= \int_0^{E_{Fn}} g(E)\, dE \\ &= N_L e^{(E_{Fn} - E_c)/k_B T_0} \\ &= n_{L0} e^{qV_F/k_B T_0} \end{aligned} \tag{37}$$

Therefore the chemical capacitance of the localized carriers in the exponential distribution

can be written

$$c_{\mu}^{L} = \frac{q^2 n}{k_B T_0} \tag{38}$$

It should be remarked that now we have two density parameters n and n_c to describe equations modeling the DSC. We have assumed so far that both densities relate to a single Fermi level. Eq. (1) and (37) provide the following condition:

$$\frac{n}{n_{L0}} = \left(\frac{n_c}{n_{c0}} \right)^{\alpha} \tag{39}$$

In fact in steady state conditions, such as in the calculation of current voltage curves, one could formulate equations in terms of either three parameters: n, n_c, or V (or more appropriately, V_F, to discount any series and shunt resistance).[122] Which is the best choice? There is not a single answer, but as shown in Fig. 4, modeling work in DSC often refers to explaining the components of current-density voltage curves, therefore the voltage is a very good choice for the x axis representation of different parameters. If different samples have a similar DOS it is also useful to compare quantities plotted vs. n. But if the DOS is variable then V_F should be preferred, since a value of the Fermi level is stipulated at each voltage. The special feature of the carriers at the transport level, or free electrons, n_c, is that carrier density relates simply to the voltage V_F as (see Eq. (8))

$$n_c = n_{c0} e^{qV_F / k_B T} \tag{40}$$

Therefore actual measurements of carrier density via chemical capacitance or any related stepped technique, will provide the total carrier density n, but since actual measurements are often performed as function of voltage, the *free carrier density* (and not total carrier density) is a useful index of the voltage V_F. This is the advantage of expressing β-recombination model in terms of free carriers as Eq. (15),[14] as then the exponent β immediately translates into the diode quality factor of Eq. (19). Since one can convert from free to total carrier density by the expression (39), recombination of excess carriers can be phenomenologically modeled as a power-law dependence of the total carrier density

$$j_{\text{rec}} = qLB\left[n^{\gamma} - {n_0}^{\gamma} \right] \tag{41}$$

Comparing Eq. (15) we obviously have the relationship $\gamma = \beta / \alpha$. Using (15) or (41) are equivalent expressions that do not speak about the origin of the recombination mechanism, which will be discussed later on.

In summary for the modeling of steady state quantities, one can switch between n and n_c by using Eq. (39). When plotting different measured quantities, one has de choice to use or V or n. The carrier density n is convenient to remove the shift of the conduction band, but in general it is important to present the voltage as the main parameter that changes in the solar cell. For the description of time depending measurements the effects of traps is significant, it is then important to maintain the distinction between n and n_c. Dynamic effects of traps will be discussed below.

6. Shift of conduction band and change of redox level

We have already mentioned that modification of electrolytes and other factors produce a shift of the position of the TiO_2 conduction band, which is an important property of the DSC. E_c affects charge injection from the dye. In addition, the change of the position of the conduction band, produces a strong variation of the recombination resistance, because the parameter j_0 is modified. Indeed note that by Eqs. (2) and (14)

$$j_0 = qLk_{rec}N_c{}^{\beta}e^{\beta(E_{F0}-E_c)/k_BT} \tag{42}$$

In consequence the change of E_c produces a change of R_0, according to Eq. (22). It is important to introduce additional kinetic parameters that specify the properties of j_0. The following expression generalize the suggestions in [28,30] in order to include also the change of redox level.[32] Let us define a kinetic constant j_{0k} that determines the recombination rate, independently of the conduction band position

$$j_{0k} = qLk_{rec}N_c^{\beta} \tag{43}$$

Therefore

$$j_0 = j_{0k}e^{\beta(E_{F0}-E_c)/k_BT} \tag{44}$$

so that Eq. (19) becomes

$$j = j_{sc} - j_{0k}e^{\beta(E_{F0}-E_c)/k_BT}\left(e^{q\beta V_F/k_BT} - 1\right) \tag{45}$$

Equation (44) simplifies the treatment of empirical data by separation in the conventional "dark current" parameter (j_0), of two effects that frequently have an important influence on the behaviour of DSC: E_c, that tracks possible changes of the position of the conduction band of the n-semiconductor, and j_{0k} (or equivalently U_{0k} [32]) that represents changes in the charge transfer rate, e.g. by blocking of the TiO_2 surface. The photovoltage writes:

$$V_{oc} = \frac{E_c - E_{F0}}{q} - \frac{k_B T}{q\beta} \ln \frac{j_{ph}}{j_{0k}} \tag{46}$$

These variations are well illustrated in Fig. 4(c), in which a part of the shift of the recombination resistance is due to the change of the conduction band position that is visible in the chemical capacitance of Fig. 4(d). An important tool to correctly evaluate the recombination rate is therefore to plot the recombination resistances of different devices at the same equivalent value of the position of the conduction band. Therefore we define a suitable potential,

$$V_{ecb} = V_F - \Delta E_c / q + \Delta E_{F0} / q \tag{47}$$

Here "ecb" stands for "common equivalent conduction band", ΔE_c is the shift of the conduction band, and ΔE_{F0} is the change of the redox potential of the hole conductor (for example when comparing different electrolytes), both with respect to a reference sample

$$\Delta E_c = E_c - E_{c,ref} \tag{48}$$

$$\Delta E_{F0} = E_{F0} - E_{F0,ref} \tag{49}$$

We obtain the following expression for the recombination resistance:

$$r_{rec} = \frac{k_B T}{q\beta j_{0k}} e^{-\beta\left(qV_{ecb} - E_{c,ref} + E_{F0,ref}\right)/k_B T} \tag{50}$$

Therefore, when plotted with respect to V_{ecb}, as shown in Fig. 4(e), differences in the recombination resistance correspond exactly to the variation of the reciprocal of the kinetic parameter j_{0k}, removing the influence of change conduction band position. The analysis is more complicated if the samples present different values of the DOS parameter α or recombination exponent β.

7. Electron lifetime

In general the quantities characterizing the recombination flux cannot be obtained from analysis of steady state measurement, which supplies very limited information. Experimentally one uses a method that applies a small perturbation to obtain the recombination kinetics at each value of stationary voltage. Here we discuss the electron lifetime, τ_n, that is a quantity often used to characterize recombination dynamics in DSCs.[50,52,140] We review the definition of the lifetime as a first illustration of small perturbation quantity.[52,140-144]

We take first the simplest recombination model which is that of linear recombination

$$U_n = k_{rec}(n_c - n_0) \tag{51}$$

The decay of a population of electrons is governed by the equation

$$\frac{dn_c}{dt} = -U_n(n_c) \tag{52}$$

Excess electrons injected can be written $\Delta n = n - n_0$, and their decay is controlled by the equation

$$\frac{d(\Delta n_c)}{dt} = -k_{rec}\Delta n_c \tag{53}$$

Therefore the decay with time takes the form

$$\Delta n_c(t) = \Delta n_c(0)e^{-t/\tau_n} \tag{54}$$

In general we define the lifetime as the constant in the denominator of the exponential decay law. In Eq. (54) the lifetime, τ_n, is given by the prefactor of Δn in Eq. (53), that is,

$$\tau_n = k_{rec}^{-1} \tag{55}$$

However, we observe that such decay law depends critically on the fact that our starting recombination law in Eq. (51) is linear, while we have emphasized before that nonlinear recombination is the general rule in a DSC.

Let us take a system that is determined by any general recombination law $U_n(n_c)$. A stationary density is maintained by a photogeneration G_Φ or similar process, so that the quasiequilibrium, stable carrier density, is $\bar{n}_c$. The conservation Eq. (4) can be written

$$\frac{dn_c}{dt} = G_\Phi - U_n(n_c) \tag{56}$$

which in equilibrium sets the stable carrier density by the equation

$$U_n(\bar{n}_c) = G_\Phi \tag{57}$$

Now the small perturbation $\hat{n}$ that is induced on top of the steady state provides the density dependence on time as

$$n_c(t) = \bar{n}_c + \hat{n}_c(t) \tag{58}$$

Using an expansion

$$U_n(n_c) = U_n(\bar{n}_c) + \frac{\partial U}{\partial n_c}\hat{n}_c \tag{59}$$

we obtain from Eq. (56)

$$\frac{d\hat{n}_c}{dt} = -\frac{\partial U_n}{\partial n_c}\hat{n}_c \tag{60}$$

The result we obtain in Eq. (60) is that the linearization procedure always takes the evolution equation to a form of the type (53) that will provide an exponential decay of the small perturbation excess density.

Let us introduce the free carrier lifetime,[52]

$$\tau_f = \left(\frac{\partial U_n}{\partial n_c} \right)^{-1}_{\bar{n}_c} \tag{61}$$

Hence Eq. (60) writes as

$$\frac{d\hat{n}_c}{dt} = -\frac{1}{\tau_f} \hat{n}_c \tag{62}$$

As an example of the small perturbation procedure consider the nonlinear recombination law introduced in Eq. (13). Eq. (4) can be written

$$\frac{d\hat{n}_c}{dt} = G_\Phi - k_{rec} \left[(\bar{n}_c + \hat{n}_c)^\beta - {n_{c0}}^\beta \right] \tag{63}$$

Expanding the sum to first order in $\hat{n}$ and removing the steady state terms (that cancel out) we have

$$\frac{d\hat{n}_c}{dt} = -k_{rec} \beta {\bar{n}_c}^{\beta-1} \hat{n}_c \tag{64}$$

Therefore the lifetime is

$$\tau_f(\bar{n}_c) = \left(k_{rec} \beta {\bar{n}_c}^{\beta-1} \right)^{-1} \tag{65}$$

Obviously the result in Eq. (65) can be derived directly by Eq. (61). Note that the lifetime is a function of the steady state; this is a general feature of nonlinear systems.

The decay of a small population that serves as a probe of the kinetics of the system has therefore been characterized for any recombination rate law and steady state condition. More generally, the decay may require a number of sequential processes coupled to recombination, for example when prior detrapping of localized carriers is required, as we discuss later on. The free carrier lifetime τ_f in Eq. (61) does not yet consider the trapping-detrapping dynamics, but just the charge transfer kinetics. More generally the electron lifetime is defined in terms of the recombination rate $U_n(n)$ and total carrier density as[52]

$$\tau_n = \left(\frac{\partial U_n}{\partial n} \right)^{-1}_{\bar{n}} \tag{66}$$

The relationship with τ_f is provided below.

8. Trapping factors in the kinetic constants

The main effects of traps in the dynamics of electrons in a DSC are indicated in Fig. 11(b). For the long range transport of electrons in the nanostructure, also outlined in Fig. 1(c), we distinguish two classes of electronic states: the transport states above the mobility edge (that may be associated with extended states in the conduction band), and localized states in the bandgap. These assumptions are common in the classical multiple trapping transport,[145-147] which describes the effect of trap levels over the rate of displacement through transport states. Another important effect of traps, and more specifically surfaces states is to provide a variety of pathways in the energy axis for interfacial charge transfer, as indicated in Fig. 12(b).

Let us consider the retarding effect of traps, and how this effect changes the measured kinetic constants.[51] In the presence of traps, the time-dependent conservation equation for free carriers, n_c, contains an additional term, due to the net capture and release by traps, which results in a modified concentration of localized electrons n_L:

$$\frac{\partial n_c}{\partial t} = G(x) - \frac{\partial J}{\partial x} - U_n(n_c) - \frac{\partial n_L}{\partial t} \tag{67}$$

If we use again the small perturbation approach of Eq. (54), Eq. (67) is split in two parts. The first is the steady state equation of Eq. (24). Note that the localized states do not introduce any new effect in the *steady state* conservation equation. Therefore quantities such as the electron conductivity are independent of the number and occupation of traps, as further given below.

The second equation is for the small perturbed density

$$\frac{\partial \hat{n}_c}{\partial t} = -\frac{\partial \hat{J}}{\partial x} - \frac{1}{\tau_f}\hat{n}_c - \frac{\partial \hat{n}_L}{\partial t} \tag{68}$$

where we have included the free carrier lifetime as defined by Eq. (61). Eq (68) may be completed by a kinetic equation for the traps that defines the variation $\partial n_L / \partial t$. However, if the trapping kinetics is fast (with respect to time scale of the transient measurement) we may assume that the traps follow the equilibrium relation with the free carriers

$$\frac{\partial n_L}{\partial t} = \frac{\partial n_L}{\partial n_c}\frac{\partial n_c}{\partial t} \tag{69}$$

We have developed before in Eq. (39) the relationship between free and trapped carrier density when the system rests at equilibrium. Eq. (69) has a different meaning in that it states that equilibrium will be maintained for any time variation during kinetic measurements. Eq.

(69) is termed *the quasistatic approximation* and it was introduced to account for the properties of measured time constants in DSC.[51]

Applying the quasistatic approximation, Eq. (68) becomes

$$\left(1+\frac{\partial n_L}{\partial n_c}\right)\frac{\partial \hat{n}_c}{\partial t} = -\frac{\partial \hat{J}}{\partial x} - \frac{1}{\tau_f}\hat{n}_c \tag{70}$$

We introduce the trapping factor

$$\Theta_L = \left(1+\frac{\partial n_L}{\partial n_c}\right) \tag{71}$$

From the previous definition of lifetimes, Eqs. (61) and (66), we note that

$$\tau_n = \Theta_L \tau_f \tag{72}$$

Eq. (72) now gives the measured lifetime τ_n as a combination of two effects: trapping and detrapping effects in the bulk, and subsequent charge transfer, by a nonlinear dependence on the free carrier density. More complex theories of the electron lifetime extend this model by a combination of mechanisms and will be described later.[50,148,149]

Furthermore we show later that the measured (chemical) diffusion coefficient is given by

$$D_n = \frac{1}{\Theta_L} D_0 \tag{73}$$

The trapping factor can also be expressed in terms of the chemical capacitances of the separate electronic states

$$\Theta_L = \frac{c_\mu}{c_\mu^{cb}} = \frac{c_\mu^{cb} + c_\mu^{L}}{c_\mu^{cb}} \tag{74}$$

We note that, if the trapped electron density dominates, then

$$\Theta_L \approx \frac{\partial n_L}{\partial n_c} = \frac{c_\mu^{L}}{c_\mu^{cb}} \tag{75}$$

For an exponential distribution,

$$\Theta_L = \frac{T}{T_0}\frac{n_L}{n_c} \tag{76}$$

and we obtain the voltage dependence of the trapping factor as follows

$$\Theta_L = \frac{T}{T_0}\frac{n_{L0}}{n_{c0}} \exp\left[qV\left(\frac{1}{k_B T_0} - \frac{1}{k_B T}\right)\right] \tag{77}$$

Using Fick's law, Eq. (5), we convert Eq. (70) to

$$\frac{\partial \hat{n}_c}{\partial t} = \frac{D_0}{\Theta_L}\frac{\partial^2 \hat{n}_c}{\partial x^2} - \frac{1}{\Theta_L \tau_f}\hat{n}_c \tag{78}$$

and therefore

$$\frac{\partial \hat{n}_c}{\partial t} = D_n \frac{\partial^2 \hat{n}_c}{\partial x^2} - \frac{1}{\tau_n}\hat{n}_c \tag{79}$$

Eq. (79) implies that the system of Fig. 11 can be treated with the dynamic equations of a single level, but with kinetic coefficients (lifetime, diffusion coefficient) that depend on the steady state. The essence of the quasistatic approximation is to describe the kinetic factors associated to trapping and detrapping in terms of occupation of free and localized states. The quasistatic approximation is explained in more detail in Refs. [51,52,150,151]. It has been widely used to describe experimental results of DSCs.

Fig. 13 shows electron densities and time constants dependence on voltage according to the model developed above, for an exponential distribution of traps. These features are often observed in experiments.[16,33,43,152,153] One exception is the free carrier density, that will be commented separately later on. It is assumed that D_0, the free electron diffusion coefficient, is a constant. The calculation of the chemical diffusion coefficient in Eq. (73) for an exponential distribution gives an exponential dependence on the Fermi-level position as follows[154]

$$D_n = \frac{T_0}{T}\frac{N_c}{N_L}\exp\left[(E_{Fn} - E_c)\left(\frac{1}{k_B T} - \frac{1}{k_B T_0}\right)\right] D_0 \tag{80}$$

Therefore the electron diffusion coefficient increases when the Fermi level rises. This is because the retarding effect of traps is suppressed when traps become increasingly occupied.

On the other hand, the free carrier lifetime, given in Eq. (61), depends on the voltage as follows

$$\tau_f = \frac{{n_{c0}}^{1-\beta}}{\beta k_{rec}}\exp\left[(1-\beta)\frac{qV}{k_B T}\right] \tag{81}$$

and the lifetime has the expression[52]

$$\tau_n = \frac{T}{T_0}\frac{n_{L0}}{{n_{c0}}^{\beta}\beta k_{rec}}\exp\left[(\alpha-\beta)\frac{qV}{k_B T}\right] \tag{82}$$

We observe in Fig. 13 that the lifetime, τ_n, that is measured by the decay of the Fermi

level, decreases with increasing potential, but this can be attributed mostly to the trapping factor. The change of position of the Fermi level changes the detrapping time in an exponential fashion. Characteristic experimental results are shown in Fig. 14.[155] It should be pointed out that the relevant lifetime *for steady state conditions* is the free carrier lifetime, τ_f, which increases with the bias voltage as indicated in Eq. (81).

Another important quantity is the diffusion length, as mentioned before and indicated in Fig. 1.

$$L_n = \sqrt{D_n \tau_n} \tag{83}$$

By Eq. (72) and (73) it is observed that the trapping factors Θ_L compensate in the diffusion length.[51] However if the free carrier lifetime shows some dependence with the potential, as implied by Eq. (81), then the diffusion length varies with voltage, and it should increase according to[14]

$$L_n = \sqrt{D_0 \tau_f} \tag{84}$$

This feature, indicated in Fig. 13(c), is often observed in experimental results, see Fig. 5(d).[152,156] The connection of the diffusion length with the trap dynamics has been also investigated by Monte Carlo simulation.[13,157,158]

9. Chemical diffusion coefficient and electron conductivity

The results for the Fermi level dependence of the diffusion coefficient, summarized in Eq. (77), can be obtained in the framework of a more general kinetic-thermodynamic formalism.[13,49,154,159]

First the jump diffusion coefficient D_J is introduced, which is proportional to the tracer diffusion coefficient, D^*, that reflects random walks of a particle

$$D^* = \lim_{t \to \infty} \frac{1}{6Nt} \left\langle \sum_{i=1}^{N} (\Delta r_i)^2 \right\rangle \tag{85}$$

Consequently D_J can be calculated by Monte Carlo simulation.[13,160,161] In the multiple trapping framework the jump diffusion coefficient is given by[49]

$$D_J = \frac{n_c}{n} D_0 \tag{86}$$

where $n \approx n_L$ is the total carrier density that coincides with trapped carriers in most conditions ($n_c << n_L$). The diffusion coefficient measured by small perturbation methods D_n is the *chemical diffusion coefficient* and differs of D_J by the quantity χ_n,

$$D_n = \chi_n D_J \tag{87}$$

that is called the *thermodynamic factor*, and is defined as follows

$$\chi_n = \frac{n}{k_B T}\frac{\partial E_{Fn}}{\partial n} \tag{88}$$

Combining the general form of the chemical and jump diffusion coefficient, Eqs. (86) and (87), we have, for the exponential distribution

$$D_n = \frac{T_0}{T}\frac{n_{c0}}{n_{L0}^{1/\alpha}} n_L^{(1-\alpha)/\alpha} D_0 \tag{89}$$

This is exactly the same result as given above in Eq. (80). Another way to arrive at the same conclusion starts from the equation

$$D_n = \frac{k_B T}{q}\chi_n u_n \tag{90}$$

that is an statement of the generalized Einstein relation.[49] In Eq. (90) u_n is the mobility. By Eq. (87) we obtain

$$u_n = \frac{qD_J}{k_B T} \tag{91}$$

u_n is related to the displacement of carriers in the total DOS, and is therefore proportional to the jump diffusion coefficient. Considering both free and trapped carriers, the thermodynamic factor can be written as

$$\chi_n = \frac{n}{n_c}\frac{1}{1+\dfrac{\partial n_L}{\partial n_c}} \approx \frac{n}{n_c}\frac{\partial n_c}{\partial n_L} \tag{92}$$

By combining (90), (91) and (92), one gets

$$D_n = \left(1+\frac{\partial n_L}{\partial n_c}\right)^{-1} D_0 \tag{93}$$

that coincides with Eq. (73).

In summary there is a difference between the jump diffusion coefficient, which reflects the random walk of a particle in the available DOS and geometry, and the chemical diffusion coefficient measured by inducing a gradient by a small step method. The difference is expressed in Eq. (87) and consists on the thermodynamic factor that accounts for the difference between a gradient in concentration, and a gradient in electrochemical potential, thus generalizing Fick's law.[12]

This connection is a fundamental one and it can be expected to operate more generally for other types of quantities. Indeed the same type of relationship can be postulated for the electron lifetime, as shown recently by Ansari-Rad et al.[13,56] On the one hand, the small perturbation lifetime τ_n is related to the decay of the Fermi level after injection of excess carriers. On the other hand a "jump lifetime" τ_J can be calculated by Monte Carlo simulation by following the survival time of a specific carrier that undergoes the sequence of events indicated in Fig. 11(b), i.e., random walk in the total DOS and charge transfer to acceptor species in the electrolyte. τ_J is different from the free carrier lifetime, τ_f, introduced above, in that the latter takes into account the survival time of a free carrier, just by the charge transfer mechanism, without counting the prior random walk. In fact τ_f corresponds to the free electrons diffusion coefficient in the diffusion formalism, D_0. The relationship between these two lifetime quantities is given by[13]

$$\tau_n = \frac{\chi_r}{\chi_n}\tau_J \tag{94}$$

where χ_r is a recombination factor that plays a role similar to thermodynamic factor χ_n.

It can be concluded that a general distinction exists between single particle quantities that can be monitored by random walk simulation methods, and collective quantities that are measured by small perturbation, involving a modification of the chemical potential of the species. Both quantities are related by the classical thermodynamic factor[162] and its generalizations.[13]

While the measurement of diffusion coefficient requires some type of small perturbation methods, the electron conductivity drives dc transport and can be measured in steady state conditions, for example by electrochemical gating.[163,164] The electron conductivity can be given in terms of the total number of carriers and the mobility as[49]

$$\sigma_n = nqu_n \tag{95}$$

Using Eq. (91) we can write

$$\sigma_n = \frac{q^2}{k_B T} nD_J \tag{96}$$

We can also express the conductivity in terms of the free carrier density as follows

$$\sigma_n = \frac{q^2 D_0}{k_B T} n_c \tag{97}$$

Additionally we may provide a formulation of the generalized Einstein relation (90) that

links the conductivity, the chemical diffusion coefficient and the chemical capacitance [49,165]

$$\sigma_n = D_n c_\mu \tag{98}$$

It is important to remark that Eq. (97) indicates that the conductivity is determined exclusively by the transport level and is *completely independent* of the presence and distribution of traps, in the context of the multiple trapping model that we have used herein. The steady-state conduction is not affected by the trapping process, because the traps remain in equilibrium. Alternatively, one can view conduction as the result of the displacement of the whole electron density, n, with a smaller jump diffusion coefficient, Eq. (96).

10.Delocalized electrons in the conduction band

We have already commented that measurement of electron density by the chemical capacitance invariably reveals the exponential distribution associated to the trap states, or in general the shape of the dominant DOS at the Fermi level in the given material. The question arises, if the free carrier density, n_c, is really accessible or is just a theoretical feature that conveniently describes the voltage V_F. We have seen that even if the free electron density is relatively low, the role of the free carrier density is crucial to provide long range transport. This feature is emphasized in Fig. 1(c) and in Fig. 11(b). Even though the general picture of Fig. 13, is very well supported by measurements of the time constants τ_n and D_n, it should be noticed that these parameters depend strongly on the traps in the system. It should be interesting to detect kinetic phenomena that depend exclusively on conduction band carriers.

Experimentally, such observation is, however, far from straightforward. In principle, the method to access the free electrons density seems obvious. One has to apply the potential V_F large enough for rising E_{Fn} close to E_c, see Fig. 11, in which case the large DOS at E_c will make the n_c population larger than n_L. However, this method encounters practical problems of large charging and band unpinning,[166] so that increasing V_{app} does not really change V_F, as a result of which the conduction band capacitance of Eq. (32) has never been detected, as far as we know. (It can be observed, however, in defect-free silicon solar cells[79].) Connected with this question there is also a difficult problem, which is to determine the *exact position* of the conduction band, E_c, which has many implications for electron injection from the absorber and recombination models.

A direct method of detection of free electrons is provided by techniques such as spectroelectrochemistry and microwave conductivity. The first one is based on the detection of the delocalized carrier by the specific absorption features, such as the Burstein shift, which

is caused by intraband absorption in the infrared region of the spectrum.[129,151,167,168] Recently Hamann et al. developed a detailed method based on temperature dependence of the free carrier density to locate the position of the conduction band. [166] The time-resolved microwave conductivity allows for a detection of electron carriers[169,170] although the distinction between free and trapped electrons requires a detailed analysis.[151] A similar concern arises often in the interpretation of absorption data, since there are a number of possible absorption effects and these cannot be simply linked to the concentration.[168]

A very important piece of evidence about the free carrier transport arises from the voltage dependence of the electron conductivity in Eq. (97). According to Eq. (1) the conductivity dependence on Fermi level voltage must satisfy the Boltzmann exponent q/k_BT ,

$$\sigma_n = \frac{q^2 D_0 n_{c0}}{k_B T} e^{qV_F/k_BT} \tag{99}$$

This relationship is often observed to hold almost exactly.[16,34,151,171] An example of the fit is shown in Fig. 5(a),[45] that displays the transport resistance, r_{tr}, that is the reciprocal to the electronic conductivity σ_n

$$r_{tr} = \sigma_n^{-1} \tag{100}$$

as further discussed below. Some authors have introduced additional exponents in the carrier density related to dc conductivity,[116] but the accurate measurement of the transport resistance by IS[34,151] shows that Eq. (99) based on the Boltzmann statistics of the free electrons is well satisfied in good quality cells. Indeed for obtaining meaningful voltage dependence of transport and recombination resistances a number of aspects of the experiment have to be carefully balanced, such as the possible bandshifts, or temperature changes of the redox potential.[39]

The good behavior of electron conductivity according to the multiple transport model is, however, not conclusive about the dynamic effects of the carriers in extended states. One important consequence of the dominance of n_c is that the effect of traps on D_n should be removed, since $\Theta_L \to 1$. As a consequence, at high V_F, D_n must saturate to D_0 and exhibit a constant value.[154] Only a few results have been reported about these effects. Archana et al.[172] suggest that a band-edge type electron diffusion mechanism is observed in doped anatase mesoporous electrodes. Wang and Jennings reported recombination via the conduction band,[173] which follows Eq. (49) by a recombination exponent $\beta = 1$, as further commented below in the sections on recombination. This type of recombination mechanism has also been

observed by Hamann et al. for the redox couple $[Co(Me_2bpy)_3]^{3+/2+}$.[148]

12. Diffusion-recombination in small signal methods

We have discussed above how carrier density transport-kinetic equation is reduced to a linear form, with density dependent parameters, by the small perturbation method. Such approach can be applied also for the measurement of ac current with respect to ac voltage analysis at variable frequency ω. The resulting impedance spectroscopy models for DSC have been presented in several works.[29,44,150,174,175] In brief, the conservation equation (79) for the small perturbation of the carrier density, can be translated to the general expression of the diffusion impedance in a film of thickness L

$$Z(\omega) = [\zeta(\omega) r_{tr}]^{1/2} \coth\left\{L[\zeta(\omega) r_{tr}]^{1/2}\right\} \tag{101}$$

In Eq. (101) r_{tr} is the resistivity of the material (or *distributed* transport impedance, per unit length per area)

$$r_{tr} = A(1-p)R_{tr}/L \tag{102}$$

where R_{tr} is the macroscopic transport resistance of the film of geometric area A and p is porosity. r_{tr} is related to electron conductivity as indicated in Eq. (99). The diffusion impedance of Eq. (101) can be represented as a distributed equivalent circuit, the transmission line of Fig. 15(a), that is closely connected to a class of transmission lines for porous electrodes as shown in Fig. 15(b).

The case of interest for DSC and solar cells in general is the diffusion-recombination impedance with a reflecting boundary condition at the end of the electron transport channel. The model is shown in Fig. 15(c). Recombination process introduces a recombination resistance in parallel with the chemical capacitance in the transmission line.[44] The transverse ζ-impedance in Eq. (101) in this case is

$$\zeta = \frac{r_{rec}}{1 + i\omega/\omega_{rec}} \tag{103}$$

The characteristic frequency of recombination is related to electron lifetime τ_n as

$$\omega_{rec} = \tau_n^{-1} \tag{104}$$

The distributed recombination resistance is given by

$$r_{rec} = LA(1-p)R_{rec} = LA(1-p)\frac{\tau_n}{C_\mu} \tag{105}$$

Here C_μ is the chemical capacitance. R_{rec} is the macroscopic recombination resistance of the layer, that was introduced in Eq. (20) and will be the object of detailed analysis in the remaining sections of this article. The impedance model for diffusion-recombination adopts the form[44]

$$Z(\omega)=\left(\frac{R_{tr}R_{rec}}{1+\mathrm{i}\omega/\omega_{rec}}\right)^{1/2}\coth\left[\left(R_{tr}/R_{rec}\right)^{1/2}\left(1+\mathrm{i}\omega/\omega_{rec}\right)^{1/2}\right] \tag{106}$$

The transmission line circuit and impedance spectra of the model of Eq. (106) are shown in Fig. 16. By fitting the spectra to this model we can obtain:

(a) the electron conductivity, Eq. (99)

(b) the chemical diffusion coefficient, D_n,

$$D_n=\frac{1}{R_{tr}C_\mu}=\frac{\omega_d}{L^2} \tag{107}$$

This last equation corresponds to the generalized Einstein relation given in Eq. (90).

(c) the electron lifetime, that is obtained as follows

$$\tau_n=\omega_{rec}^{-1}=R_{rec}C_\mu \tag{108}$$

The impedance model of Eq. (106) produces different types of spectra, as shown in Fig. 16. The shape of the impedance spectra is determined by the factor relating the characteristic frequencies, which can be expressed in several alternative ways[44]

$$\frac{\omega_d}{\omega_{rec}}=\frac{R_{rec}}{R_{tr}}=\left(\frac{L_n}{L}\right)^2 \tag{109}$$

Note that the diffusion length can be obtained from the measured resistances by the expression

$$L_n=\left(\frac{R_{rec}}{R_{tr}}\right)^{1/2}L \tag{110}$$

The spectrum for $R_{tr}<R_{rec}$, is shown in Fig. 16(b)-(c). It corresponds to a long diffusion length $L_n>L$ and indicates efficient charge collection in a DSC at moderate forward bias.[16] The opposite case, for strong recombination, requires $R_{tr}>R_{rec}$, and it is shown in Fig. 16(e). The intermediate spectrum for $R_{tr}\approx R_{rec}$ is shown in Fig. 16(d). These impedance spectra have been widely described and utilized in experiments.[16,34,37,39,43,45,151,156]

13. General picture of recombination in a DSC

In the discussion of the fundamental diode model, we have already emphasized the outstanding importance of recombination of photogenerated electrons for the energy conversion properties of the DSC device. In practice, the DSC progress has been very much based on the development of better dyes and coadsorbants. Indeed current collection, as generated by dye injection, is not generally a major limitation, and charge collection efficiencies close to unity are routinely obtained in good quality devices. A major problem of the DSC is the loss of voltage, from the dye bandgap about 2 eV to the actual V_{oc} of less than 1 V.[92] Fig. 7 shows the dramatic loss of voltage that occurs due to the deep position of the dye ground state with respect to the redox level of the electrolyte. Optimization of DSC requires to govern the position of the TiO_2 conduction band, as high as possible, while not hindering injection from the dye, and most of all, controlling the recombination rate.[11]

These features occurring at the semiconductor/dye/hole conductor system can be analyzed using a variety of methods.[60,176] We have already commented on how to measure recombination properties, via electrons lifetimes and recombination resistance, among a variety of available methods.[126,127,155,177-179] In the final sections of this chapter we aim to provide deeper insight into the fundamental mechanisms of recombination in a DSC.

Starting from our general knowledge of electronic states, and fundamental properties of charge transfer at semiconductor-electrolyte interface, reviewed in the next section, a general model of recombination by electron transfer from TiO_2 to a redox electrolyte has been developed,[16,50,180,181] based on the scheme of Fig. 12; this model has been well validated by experimental results, as commented later on. We will focus here in the recombination towards a well defined redox species in a redox electrolyte, while other situations, such as the organic hole conductor or the solid absorbers, will not be specifically discussed and we refer the reader to the literature.[40,102,176]

14. Fundamental factors determining rates of electron transfer

When an electron is transferred from one reactant in a solution to another, for example, from a Ru $(NH_3)_6^{2+}$ ion in water to a Fe $(H_2O)_6^{3+}$ ion in the same solvent, the electron cannot simply jump from one ion to the other, because the solvent environment, namely, the ensemble of orientations of the surrounding solvent molecules after the jump, would not be appropriate to the new ionic charges, and so just after the electron transfer, the system would have a much higher total energy than before the jump. The atomic nuclei move so slowly that

they do not have time to adapt their positions or velocities to the new charges during the electron jump (Franck-Condon principle), and so the transfer would violate the law of conversation of energy.

Instead, as discussed in a 1956 article on the theory of electron transfer reactions,[182] before an electron can jump from one reactant to the other, there first has to be a "reorganization" of the solvent molecules around the ions. Similarly, there also has to be a "reorganization" of relevant vibrational bond lengths in each reactant, and sometimes in the bond angles.[183,184] After a suitable configurational reorganization of the relevant coordinates has been achieved such that the total energy of the entire system before and after the electron jump is unchanged, energy is conserved in the jump. This energy is the sum of all contributions to the potential energy and kinetic energy of the molecules and ions present. The reorganization involves suitable changes in the relevant orientations and in the bond lengths and often in the bond angles of the species present prior to the electron transfer. There are, thus, fluctuations in all coordinates of the reactants and their surroundings, ~10^{24} coordinates for a mole of solvent.

If the system has N position and momentum coordinates, where $N \sim 10^{24}$, the transition state for an electron transfer reaction occupies an N-1 dimensional "hypersurface" in this N-dimensional space. Accordingly, in the reacting system when the reacting pair and its surroundings cross that N-1 dimensional hypersurface, they form the reaction products, according to transition state theory. We treated this reorganization for electron transfer between a pair of reactants in a solvent, [182] and subsequently for an electron transfer at metal electrodes,[184-188] electron transfer at semiconductor electrodes,[187,189,190] and electron transfer across liquid-liquid interfaces.[191] In each case, there is a reorganization of the orientations of the solvent molecules, of reactant bond lengths, and sometimes of their bond angles.[183-188,192-194]

The theoretical expressions for these different experimentally studied systems are given in the following, where k_{rate} denotes the reaction rate constant[185]

$$k_{rate} = Ae^{-\Delta G^*/k_B T} \tag{111}$$

where

$$\Delta G^* = w^r + m^2\lambda \tag{112}$$

$$-(2m+1)\lambda = -\Delta G_R^0 \tag{113}$$

$$\Delta G_R^0 = \Delta G^0 + w^p - w^r \tag{114}$$

and

$$\lambda = \lambda_0 + \lambda_i \tag{115}$$

In the case where the electron transfer is to or from an electrode, Eq. (114) is replaced by [184,185,193]

$$\Delta G_R^0 = -z_q q\eta + w^p - w^r \tag{116}$$

In Eq. (114) w^r is the "work" (free energy change) required to bring the reactants from a large distance (sufficiently large that they do not interact at that distance), to a separation distance *R*, or in the case of an electron transfer with an electrode (Eq. 115), to a distance *R* from its electrostatic image in the electrode (twice the distance between the center of charge of the reactant and the electrode surface) and w^p is the corresponding quantity for the products. The ΔG^0 in Eq. (114) is the "standard" free energy of reaction in the existing solvent medium. The *m* in Eq. (112) can actually serve as a reaction coordinate, being 0 for the reactants and -1 for the products and given by Eq. (113) for the transition state.

In Eq. (116) z_q is $-|z|$ $(+|z|)$ for the transfer of $|z|$ electrons (holes), q is positive elementary charge, and η is the overpotential of the electrode, that is defined as $\eta = U - U^{0'}$. Here U is the electrode potential in the electrochemical convention (note that with respect to the voltage V defined in previous sections, $U = -V$) and $U^{0'}$ is the "standard" reduction potential of the electrode for the transfer of electron from the electrode to the reactant in the prevailing solvent. For example if the metal electrode is biased negatively to promote a one electron transfer electrochemical reduction reaction, then $\eta < 0$, $z = -1$. The "work" separating products from reactants is $-q\eta$, so that $\Delta G_R^0 < 0$.

The units of *A* in Eq. (111) depend on the geometry, for example in an electron transfer in solution, the units depend on whether or not the reactants are bound together and in the electrode case, on whether the reactant is or is not bound to the electrode. In the unbound case, *A* could be written as a relevant "collision frequency" *Z* multiplied by κ, an electronic transition probability of electron transfer in the transition state, being about or near unity for an "adiabatic" or a "nearly adiabatic" electron transfer, and substantially less than unity for a highly "nonadiabatic" electron transfer. In a nonadiabatic electron transfer the electronic coupling of the reactant wave functions is small and so the probability of electron transfer when the system reaches the intersection of the reactant and the product potential energy surfaces is also small. In contrast, in an adiabatic electron transfer the electronic coupling element coupling the reactant and the product wave functions near or at the intersection is

substantial and essentially every system reaching that intersection region undergoes an electron transfer. An approximate expression for the transition probability is given by the famous 1932 Landau-Zener expression.[195,196] A recent survey and analysis of these adiabatic-nonadiabatic effects is given in ref. [197]. An example of a nonadiabatic electron transfer to or from an electrode is an electron transfer across a layer of parallel long chain of CH_2's bridging groups in thioalkanes, each bound via its sulfide atom to a gold electrode and at the other end of the chain bound, in a classic experiment, to a ferrocene.[198] We return to the nonadiabatic case later.

The reorganization effects relate the thermodynamic free energy difference ΔG^0 between reactants and products, to the transition state activation free energy ΔG^* that actually determines the rate constant in Eq. (111). Combining Eqs. (112)-(114) we obtain the form of the rate constant for electron transfer

$$k_{rate} = A\exp\left[-\frac{w^r}{k_B T} - \frac{1}{4\lambda k_B T}\left(\lambda + \Delta G_R^0\right)^2\right] \tag{117}$$

The rate constant for both the nonadiabatic and adiabatic electron transfers critically depends on the reorganization energy λ and on a prefactor A whose value depends on the "nonadiabaticity" of the electron transfer. We describe the properties of both parameters in turn.

The λ_0 in Eq. (115) describes the reorganization energy of the dielectric medium (the solvent and, in the semiconductor electrode case, also the solid). The λ_i in Eq. (115) arises from the change in equilibrium values of vibrational coordinates of the reactants, including, in the semiconductor case, any of its relevant vibrational coordinates. For example, if the reactant(s) undergoes a change Δq_i in the equilibrium value of some collective coordinate, a "normal coordinate" of a reactant, and if k_j^r and k_j^p are the "force constants" of that normal mode for the reactant and for the product, respectively, then classically[184]

$$\lambda_i = \sum_j \left[k_j^r k_j^p / \left(k_j^r + k_j^p\right)\right]\left(\Delta q_j\right)^2 \tag{118}$$

where Δq_j is the change in the *j*th normal mode coordinate, normal mode because there are no cross-terms between the different *j*s in Eq. (118). Some ions, such as $Ru(NH_3)_6^{2+}$ + $Ru(NH_3)_6^{3+}$ undergoing electron transfer have a small Δq_j while some others, such as the $Fe(H_2O)_6^{2+}$ + $Fe(H_2O)_6^{3+}$ have a larger Δq_j and hence a larger λ_i. The magnitude of these quantities is understood by electronic structure arguments. In the ions cited above the largest contributor to Δq_j comes from the symmetric stretching ("breathing") coordinate of the

coordination shell of a reactant.

For an electron transfer reaction between two reactants in solution a dielectric continuum treatment for the reorganization energy λ_0 gave [182]

$$\lambda_0 = (\Delta e)^2 \left(\frac{1}{2a_1} + \frac{1}{2a_2} - \frac{1}{R} \right) \left(\frac{1}{\varepsilon_{op}} - \frac{1}{\varepsilon_s} \right) \tag{119}$$

where Δe is the charged transferred, the two a_i's are the radii of the two reactants, ε_{op} is the optical dielectric constant (square of the refractive index) of the solvent, and ε_s is the static dielectric constant.

For electron transfer at a metal electrode, λ_0 is given, instead, by[184,185]

$$\lambda_0 = (\Delta e)^2 \left(\frac{1}{2a} - \frac{1}{R} \right) \left(\frac{1}{\varepsilon_{op}} - \frac{1}{\varepsilon_s} \right) \tag{120}$$

where *R* is the distance between the center of charge of the ion and its electrostatic image in the electrode.

For a semiconductor electrode, the expression for λ_0 is a little more complex, since now there is also a reorganization in the semiconductor electrode itself. The λ_0 is given by[189,190,199]

$$\lambda_0 = \frac{(\Delta e)^2}{2a} \left(\frac{1}{\varepsilon_1^{op}} - \frac{1}{\varepsilon_1^{s}} \right) - \frac{(\Delta e)^2}{2R} \left(\frac{\varepsilon_2^{op} - \varepsilon_1^{op}}{\varepsilon_2^{op} + \varepsilon_1^{op}} \frac{1}{\varepsilon_1^{op}} - \frac{\varepsilon_2^{s} - \varepsilon_1^{s}}{\varepsilon_2^{s} + \varepsilon_1^{s}} \frac{1}{\varepsilon_1^{s}} \right) \tag{121}$$

The λ_0 for electron transfer across the interface of two liquids is more complex, since there are now two media and two reactants. The λ_0 for this case is given in Ref. [191], omitted here since the present main focus is not on electron transfer across a liquid-liquid interface.

The simplest type of electron transfer reaction is the self-exchange reaction, for example, the transfer of an electron from an $Fe(H_2O)_6^{2+}$ to an $Fe(H_2O)_6^{3+}$. The ΔG^0 in Eq. (114) is now zero, w^r and w^p are equal, and $a_1 = a_2$. This class of reactions (known in the literature as "self exchange" or "isotopic exchange" reactions) is the simplest class of reactions in all of chemistry. In a simple electron transfer, no chemical bonds are broken or are formed. The *m* in Eqs. (112) and (113) is now -1/2. Apart from w^r and w^p in Eqs. (114) and (116), the free energy barrier to reaction ΔG^* is $\lambda/4$.

One sees from Eq. (119) that the smaller the radii a_i of the reactants the larger is λ_0. Small ions like Fe^2 have a larger λ_0 than large ions such as $Ru(bpy)_3^{2+}$. A physical interpretation is clear: the smaller the radii a_i the larger the orientating force of the ionic charges on the nearby solvent molecules, and so the greater the difference of the ion-polar

solvent interaction before and after electron transfer, and so the larger is the reorganization energy λ_0. The role of the separation distance *R* that appears in Eqs. (119) - (121) is also clear. When the two ions in solution are close to each other [Eq. (119)], or when an ion approaches a metal electrode [Eq. (120)], or a semiconductor electrode [Eq. (121)], that is, when *R* in each case is smaller, the reorganization energy λ_0 is smaller. This effect is readily understood in physical terms: When *R* is smaller, solvent molecules at every point in the system see less of a change in the electric field acting on them, comparing before and after the electron transfer. These two different fields are the field created by the reactant charges and the field created by product charges. Indeed, when the separation distance *R* of the reactants is small, distant solvent molecules hardly see a change of electric field accompanying the electron transfer. In the case of a charge near an electrode, there is only one ion experiencing that change of electric field, and in that case the image charge tends to nullify the field of the ionic charge, and the nullifying effect is larger the smaller the *R*.

One also sees that when the solvent is nonpolar, that is when $\varepsilon_s = \varepsilon_{op}$, the solvent contribution to λ_0 arising from the orientational and vibrational part of its dielectric polarization disappears. So λ_0 is the smaller the less polar the medium. There may also be specific solvent effects, absent in a dielectric continuum treatment but present in a molecular treatment of the solvent.

There are various estimates one can make for *A* in Eq. (111). For example, if the reaction is between two reactants in solution, and if they are linked together or in a precursor complex, then *A* has units of a first-order rate constant sec^{-1}. For a nonadiabatic reaction (weak electronic coupling element) it can be written as, e.g., [194] and references cited therein,

$$A = \frac{2\pi}{\hbar}\frac{|H|^2}{(4\pi\lambda k_B T)^{1/2}} \tag{122}$$

where H is the electronic matrix element coupling the two reactants. One approximation for the latter for a coupling bridge of length *R* is, see e.g., [194] and references cited therein,

$$|H|^2 \approx 10^{13} e^{-\alpha_b R} / \text{sec} \tag{123}$$

where α_b depends on the nature of the bridge between the reactants. It is about 0.1 nm^{-1} for a chain of CH_2 groups and much smaller for a link of conjugated units. Estimates have been made for various systems and are available from interpretations of experimental data.

For a nonadiabatic electron transfer to or from an electrode, denoting by ε an energy state of the electrode, the first-order rate constant k_{rate} is given by [186,187]

$$k_{rate} = \frac{2\pi \int d\varepsilon\, e^{-\Delta G^*(\varepsilon)/k_B T} \left|H(\varepsilon)\right|^2 f(\varepsilon) d\varepsilon}{\hbar (4\pi\lambda k_B T)^{1/2}} \tag{124}$$

where $\Delta G^*(\varepsilon)$ is, apart from the work terms (if the reactant is brought from infinity), given by [184] for the case of transfer from the metal electrode,

$$\Delta G^*(\varepsilon) = \frac{\left[\lambda - z_q q \eta - \varepsilon\right]^2}{4\lambda} \tag{125}$$

$f(\varepsilon)$ is the Fermi-Dirac distribution function for the probability that a state **k** in the electrode with an energy $\varepsilon(\mathbf{k})$ is occupied, and $\left|H(\varepsilon)\right|^2$ is an electron wave number **k**-weighted interaction coupling element,[186,187]

$$\left|H(\varepsilon)\right|^2 \equiv \int d^3k \left|H_{kA}\right|^2 \delta\left[\varepsilon(\mathbf{k}) - \varepsilon\right] \tag{126}$$

where H_{kA} is the electronic matrix element coupling the reactant A and a state **k** of the electrode, and δ is the Dirac delta function.

Often for depicting the energetics of chemical reactions one plots some quantity such as the potential energy or free energy along a reaction coordinate. When a reaction involves a breaking of one bond and forming another a commonly used reaction coordinate is some linear combination of the two bond lengths. In the present case we have an overwhelmingly large number of relevant coordinates and even, in a dielectric continuum model, an infinite number of relevant coordinates. So in this case a quite different type of reaction coordinate is needed. One possibility is to introduce a linear combination of the equilibrium values for the reactants and for the products and to plot various quantities as a function of that coordinate. For example, for a vibrational coordinate q_j one could introduce a reaction coordinate x, via $q_j(x) = q_j^r + x(q^p - q_j^r)$ and for a vectorial quantity $\mathbf{P}_u(\mathbf{r})$ related to the orientation-vibrational dielectric polarization of the solvent at each point **r** of the system and introduced in the 1956 article,[182] one would write $\mathbf{P}_u(\mathbf{r},\mathbf{n}) = \mathbf{P}_u^r(\mathbf{r}) + x[\mathbf{P}_u^p(\mathbf{r}) - \mathbf{P}_u^r(\mathbf{r})]$, where the $\mathbf{P}_u(\mathbf{r})$'s denote the equilibrium value of that quantity when the charges are those of the reactants (superscript r) and when they are those of the products (superscript p).

In terms of this reaction coordinate x the free energy of the reactants and surroundings, relative to their initial value, $\Delta G^*(x)$ is a function of a reaction coordinate x, given by

$$\Delta G^{*r}(x) = w^r + x^2\lambda \tag{127}$$

Along this curve for the reactant free energy versus x, x =0 corresponds to the reactants but

in surroundings appropriate to the reactant charges, x = 1 correspond to the products but in surroundings appropriate to the product charges, and x = -m where m is given by Eq. (113) corresponds to the transition state. The free energy for the products relative to their initial configuration is given by

$$\Delta G^{*p}(x) = w^p + (1-x)^2 \lambda \tag{128}$$

A plot of the free energy changes is given in Figure 17. *R* denotes the free energy curve given by Eq. (127) and *P* denotes the curve given by Eq. (128). The difference in vertical heights of the bottoms of the two wells is $\Delta G_R^{0'}$, the "standard" free energy of reaction in the prevailing medium at the separation distance *R* and contains all three terms in Eq. (114). Reaction proceeds via fluctuations of all the coordinates, starting from $x = 0$ on the *R* curve, transitioning to the *P* curve at the intersection, and proceeding on the *P* curve to the region at x = 1.

When instead one uses a purely statistical mechanical approach, and perhaps with a view to also do computer simulations of the free energy curves, a reaction coordinate grounded in statistical mechanics is needed. One introduced in [183], and later elaborated in [184] is an energy difference coordinate. The potential energy of all particles in the reacting system U^r is a function of all the coordinates, whose totality is denoted by $\mathbf{Q}$ and written as $\mathrm{U^r}(\mathbf{Q})$. Similarly, the reaction products and their environment have a potential energy function $\mathrm{U^p}(\mathbf{Q})$. The potential energy difference $U^r(\mathbf{Q}) - U^r(\mathbf{Q})$, a function of the *N* coordinates, has a fixed value on an N=1 dimensional surface in the N-dimensional space and so can be used as a reaction coordinate in a statistical mechanical treatment of the electron transfer, as in [183,184]. One can calculate a free energy of the system with the reactant charges and a free energy of a system with the product charges, as a function of that coordinate. The free energy plots for the reactant and for the products would look the same as in Fig. 17.

Some of the factors discussed earlier in this section can be seen in Fig. 17. When the bond length change from reactants to products is less, it corresponds to shifting the two parabolas in Fig. 17 closer horizontally, so reducing the height of the intersection. Similarly when the radii of the reactants are larger the difference in ion-solvent interaction before and after the electron transfer is less and again corresponds to shifting the curves horizontally closer together and so reduces the height of the intersection. When because of a more favorable standard free energy of reaction, *i.e.*, more negative or more favorable standard potential the *P* curve in the Figure is shifted vertically downward relative to the *R* curve, the free energy barrier is smaller for the

system depicted by the Figure.

15. Carrier transfer at semiconductor/electrolyte interface

The mechanism of charge transfer that constitutes recombination in a DSC can be formulated as a product of three quantities: the electron density, the concentration of the acceptor (the oxidized half of the redox electrolyte), c_{ox}, and the probability of single transfer event ν_{el}, that is described by the electron transfer model of the previous section, as shown in Fig. 12(a). Due to the disorder in the energy axis of the metal oxide, we have a variety of possible electronic channels that constitute parallel recombination mechanisms, as indicated in Fig. 12(b).

For the direct charge transfer of conduction band electrons, we have the recombination rate given by

$$U_{cb} = \nu_{el}^{cb}(E_c) c_{ox} [n_c - n_{c0}] \tag{129}$$

This formula is also expressed as

$$U_{cb} = [n_c - n_{c0}] e_{ox}^{cb} \tag{130}$$

where

$$e_{ox}^{cb} = c_{ox} \nu_{el}^{cb}(E_c) \tag{131}$$

The model of Eq. (129) leads to a linear recombination rate, as stated in Eq. (51). In addition, the charge transfer from the metal oxide may occur via a distribution of surface states, as shown in Fig. 12(b), and the recombination rate has the form

$$dU_{ss}(E) = g_{ss}(E) f_{ss}(E) e_{ox}^{ss}(E) dE \tag{132}$$

where $g_{ss}(E)$ is the density of surface states, $f_{ss}(E)$ is the fractional occupancy, and

$$e_{ox}^{ss}(E) = c_{ox} \nu_{el}^{ss}(E) \tag{133}$$

The total rate of recombination via surface states is

$$U_{ss} = c_{ox} \int_{E_{redox}}^{E_c} g_{ss}(E) f_{ss}(E) \nu_{el}^{ss}(E) dE \tag{134}$$

In the situation of Fig. 12(a), the starting state of the electron in the semiconductor surface has energy E, while the free energy of electrons in the electrolyte is E_{redox}. The probability for an elementary electron transfer event is given in Ref. [186]. For a planar interface

$$\nu_{el}(E) = \frac{2\pi}{\hbar}|H|^2 \frac{l_{sc}}{\alpha_{sc}\,\delta_{np}\,d_{sc}{}^{2/3}(6/\pi)^{1/3}} FC \tag{135}$$

$$FC = \frac{1}{\sqrt{4\pi k_B T\lambda}} \exp\left[-\frac{(\lambda+\Delta G)^2}{4\lambda k_B T}\right] \tag{136}$$

$$\Delta G = E_{redox} - E \tag{137}$$

In Eq. (135) l_{sc}(cm^{-1}) is the effective coupling length between the oxidized redox ion and the electrode, α_{sc}(cm^{-1}) is the coupling attenuation factor as in Eq. (123), and d_{sc} (cm^{-3}) is the density of the atoms that contribute to the density of states of either the surface states or the band of concern.[200,201] δ_{np}(cm) is a volume to area ratio in the nanoparticulate semiconductor electrode.

The electron transfer rate is therefore given by the following formula

$$\nu_{el}(E) = k_0 \exp\left[-\frac{(E_{redox}-E+\lambda)^2}{4\lambda k_B T}\right] \tag{138}$$

where $k_0 = Al_{sc}/\left[\alpha_{sc}\,\delta_{np}\,d_{sc}{}^{2/3}(6/\pi)^{1/3}\right]$ being A that in Eq. (122), so that k_0 is measured in units cm^3 s^{-1}. $E_{redox}-E$ is negative in the situation of Fig. 12(a). Eq. (138) applies to each of the recombination channels indicated in Fig. 12(b), according to the actual distribution of surface states that allow the electron transfer to the oxidized ion at the semiconductor surface.

It should be remarked that when the energy difference $E - E_{redox}$ becomes larger than the reorganization energy λ, as for example for the transference from the conduction band states in Fig. 12(b), the rate of charge transfer decreases (the "Marcus inverted region"). This reduction of the rate at high energy difference has an outstanding importance in biological systems for sunlight energy conversion in order to avoid recombination of spatially separated charges.

We have discussed in section 7 that differences in the parameter j_{0k} could be attributed to changes of surface blocking, catalysis of charge transfer, etc. It should be desirable to pinpoint specific causes for the changes of recombination rates. As mentioned before, the usual shape of the recombination resistance dependence on voltage V_F is an exponential shape, Eq. (21), that relates to the phenomenological nonlinear recombination model of Eq. (13). Usually it is observed that $\beta = 0.6 - 0.75$, as mentioned before, but one report[173] has obtained the value $\beta = 1$, from the diode quality factor. This result corresponds to cells in which the conduction band edge was extremely low, so that conduction band transfer of Eq. (129), becomes the

dominant mechanism. This is an exception, however, and one important task of the model is to explain the normal values $\beta = 0.6 - 0.75$, by a combination of charge transfer pathways, as indicated in Eq. (134). This result will be demonstrated in section 16. The combined measurement of capacitance, recombination resistance, etc., and application of the recombination model, has allowed researchers to provide a very detailed picture of energetics and kinetics of recombination.

A number of studies have discussed the Marcus model in DSC.[39,179,201-206] In general, however, detailed insight to the basic charge transfer mechanisms has been prevented by the exceedingly complex reaction rate steps of the iodide/triodide redox couple, that shows very special characteristics, in which even the nature of the predominant electron acceptor is not clear yet, since it could be either via reduction of I_3^- or free iodine I_2.[207-211] An example of the study of recombination is shown in Fig. 14, in which the electron lifetime is measured for a series of DSCs with triphenylamine (TPA) dyes in which the conjugation length is varied.[155] Larger dyes showed enhanced electron recombination while reducing the dye size increases surface blocking of the dye layer and hence the electron lifetime. It was suggested an interaction between the dye molecular structure and I_3^- and/or I_2, that may be correlated to the increased polarizability of the larger TPA dyes. It is likely that dye-shuttle interaction[212] and a variety of reaction pathways associated to I_3^-/I^- prevents the successful application of outer sphere electron transfer in the Marcus model to this specific redox couple. Nonetheless it is also important to explain why this couple works so well in kinetic terms, i.e., why the injected electrons do not reduce I_3^- efficiently. Meyer et al.[213] have applied the Marcus model to one electron reduction of I_3^- and conclude that electrons trapped in TiO_2 react slowly with I_3^-. A different and very promising approach, which provides access to specific fundamental quantities governing charge transfer rates in a DSC, is the utilization of outer sphere redox couples, since these allow the observation of the lifetime features associated to the Marcus model.[148,179] These last results are reviewed in the next section.

16. Recombination resistance and lifetime models

In this section we aim to obtain the model calculation of the recombination flux, recombination resistance, and the electron lifetime, in a DSC, associated to the electron transfer by a combination of surface states that form an exponential distribution, with a DOS $g_{ss}(E)$, as shown in Fig. 12(b), and considering also the direct transfer from the conduction band.[16,50,52,180,181,206,214]

The current per unit macroscopic area of an electrode of thickness L is

$$\begin{aligned} j_{rec} &= qLU_{ss} \\ &= qLc_{ox}\int_{E_{redox}}^{E_c} g_{ss}(E)\, f_{ss}(E)\nu_{el}^{ss}(E)dE \end{aligned} \tag{139}$$

The calculation of j_{rec} requires a stipulation of the surface states that are occupied. Since surface states exchange electrons both with the conduction band and the electrolyte, the statistics is more complex than in a bulk trap. The occupation of the surface states is determined by a demarcation level and in general it is not possible to define a Fermi level.[180,215] For simplicity we assume here that the trapping-release rate is sufficiently fast, so that the surface state is in equilibrium with the transport states, and the occupancy of both is described by Fermi-Dirac distribution, with a single Fermi level.

The recombination resistance is

$$R_{rec}^{ss}(E_{Fn})^{-1} = A\frac{dj_{rec}(E_{Fn})}{dV} \tag{140}$$

Thus

$$R_{rec}^{ss}(E_{Fn})^{-1} = q^2 LAc_{ox}\int g_{ss}(E)\nu_{el}^{ss}(E)\frac{df_{ss}(E-E_{Fn})}{dE_{Fn}}dE \tag{141}$$

Applying the zero temperature limit of the Fermi-Dirac distribution, the following result is obtained[16]

$$R_{rec}^{ss}(E_{Fn})^{-1} = q^2 LAg_{ss}(E_{Fn})e_{ox}^{ss}(E_{Fn}) \tag{142}$$

Eq. (142) states that the reciprocal charge-transfer resistance is proportional to the product of the density of surface states at the Fermi level, and the probability of electron transfer from such states. The calculation of the recombination resistance involves a small displacement of the Fermi level that fills the surface states precisely at the Fermi level, hence the resistance detects only those states. In summary we have

$$R_{rec}^{ss}(E_{Fn})^{-1} = C_{\mu}^{ss}(E_{Fn})e_{ox}^{ss}(E_{Fn}) \tag{143}$$

The free carrier lifetime can now be calculated from Eq. (108), by selecting the capacitance just of those electron states that participate in charge transfer.[50,52] Therefore

$$\tau_f = R_{rec}C_{\mu}^{ss} \tag{144}$$

where

$$C_{\mu}^{ss} = LAq^2 g_{ss}(E_{Fn}) \tag{145}$$

is the chemical capacitance of the surface states. Using Eq. (143) we get

$$\tau_f(E_{Fn}) = \frac{1}{e_{ox}^{ss}(E_{Fn})} = \frac{1}{c_{ox}\nu_{el}^{ss}(E_{Fn})} \tag{146}$$

The free carrier lifetime is inversely proportional to the fundamental charge transfer rate at the Fermi level. If we consider also bulk traps, described by the DOS $g_b(E)$, and a chemical capacitance

$$C_\mu^b = LAq^2 g_b(E_{Fn}) \tag{147}$$

then the measured lifetime contains a trapping factor as shown in Eq. (71), and we obtain the expression

$$\tau_n(E_{Fn}) = \frac{C_\mu^b + C_\mu^{ss}}{C_\mu^{ss} e_{ox}^{ss}(E_{Fn})} \tag{148}$$

If both bulk traps and surface states consist on an exponential distribution with a similar T_0, and number density N_s for surface states and N_L for total number of traps, the trapping factor is just a numerical constant that does not influence the voltage dependence of the lifetime. Eq. (148) can therefore be stated as function of voltage as follows

$$\tau_n(V) = \tau_{n0} \exp\left[\frac{(qV-\lambda)^2}{4\lambda k_B T}\right] \tag{149}$$

where

$$\tau_{n0} = \frac{N_L}{N_s}\sqrt{\frac{\pi\lambda}{k_B T}}\frac{1}{c_{ox}k_0^{ss}} \tag{150}$$

There is no functional difference between τ_n and τ_f. The significance of this result must be emphasized. In a DSC we measure recombination resistance, chemical capacitance, electron lifetime. But when we wish to study fundamental charge transfer questions we really want to determine ν_{el}. Eq. (145) states that we have access to the electron transfer probability.

The model of Eq. (149) is illustrated in Fig. 18.[50] First Fig. 18(a) shows the electron transfer probability according to Marcus model as stated in Eq. (138). Here $V = \lambda/q$ is the point of maximum charge transfer rate, where activationless charge transfer occurs, and the Marcus inverted region occurs when $V > \lambda/q$. In the Fig. 18(b) we observe the reciprocal product of chemical capacitance and transfer rate, which is the recombination resistance of Eq. (142) that is further discussed below. The lifetime is plotted in Fig. 18(c). Note that the carrier transference at the interface through the exponential distribution of surface states corresponds

to the curved region at low voltage. The lifetime has a parabolic shape (semilogarithmic), as it follows exactly the Marcus rate ν_{el} dependence on the Fermi level.[50]

The expression (148) can be generalized very easily to include additional parallel recombination pathways. For example we can incorporate the direct transference from the conduction band, that has a recombination resistance

$$R_{rec}^{cb}(E_{Fn})^{-1} = C_{\mu}^{cb}(E_{Fn})e_{ox}^{cb} \tag{151}$$

We observe that the denominator of Eq. (148) is the reciprocal of the total recombination resistance, Eq. (151), and the numerator is the total chemical capacitance. Since the reciprocal parallel resistances are added to obtain a total resistance, we have more generally[50]

$$\tau_n(E_{Fn}) = \frac{C_{\mu}^{b} + C_{\mu}^{ss} + C_{\mu}^{cb}}{C_{\mu}^{ss}e_{ox}^{ss}(E_{Fn}) + C_{\mu}^{cb}e_{ox}^{cb}(E_{Fn})} \tag{152}$$

Now according to Eq. (152) there are three regions in the lifetime plot of Fig. 18(c). The curved region at low voltage corresponds to the combination of the exponential surface state distribution, and the curvature of the Marcus transfer model indicated in Fig. 18(a). It should be remarked that the minimum of the lifetime occurs at the same point of the maximum charge transference. A second region is due to charge transfer via the conduction band, in which τ_f is independent of voltage, and the lifetime decreases at increasing voltage due to the trapping factors indicated in Eq. (71). Finally conduction band electrons become dominant when the Fermi level approaches the conduction band, and here $\Theta_L \to 1$ in Eq. (71) so that $\tau_n \approx \tau_f$ is a constant.

Alternatively we may analyze the recombination resistance dependence on voltage. The resistance in Eq. (142) takes the form[16]

$$R_{rec}(E_{Fn}) = R_{0\lambda}\exp\left[\frac{(E_{Fn} - E_{redox} - \lambda)^2}{4\lambda k_B T} - \frac{E_{Fn} - E_c}{k_B T_0}\right] \tag{153}$$

where

$$R_{0\lambda} = \frac{\sqrt{\pi\lambda k_B T}}{q^2 L A k_0^{ss} c_{ox} N_s \alpha} \tag{154}$$

Eq. (153) can also be expressed as

$$R_{rec}(E_{Fn}) = R_{0\lambda}\exp\left[\frac{q^2(V - V_{\mu})^2}{4\lambda k_B T} + \frac{E_c - E_{redox} - \lambda(1+\alpha)}{k_B T_0}\right] \tag{155}$$

where the following constant has been introduced:

$$V_\mu = \left(1 + 2\frac{T}{T_0}\right)\frac{\lambda}{q} \tag{156}$$

Fig. 21(a) shows the characteristic probability of electron transfer according to Marcus model, for different values of the reorganization energy. According to Eq. (155) the resistance dependence on voltage, shown in Fig. 21(b), consists in a Gaussian function, an inverted parabola (semilogarithmic), centered at the energy V_μ indicated in Eq. (156). The minimum of the parabola of R_{rec}, is shifted positive in the scale of the Fermi level, with respect to the point of maximum charge transfer, at the voltage λ / q, by an amount $2\lambda\alpha = 2\lambda T / T_0$, as it is illustrated in Fig. 21(b). The displacement of the minimum of the resistance with respect to that of ν_{el} is due to the product of the chemical capacitance of the exponential distribution.

In previous sections we have remarked that R_{rec} usually shows in DSC an exponential dependence on voltage, as stated in Eq. (21). While the result in Eq. (155) produces a parabolic shape, we can observe in Fig. 19(b) that for a large λ, the shape observed at $V << \lambda$ is a straight line. Thus the model of Eq. (21) can be obtained as a limit case of Eq. (155). Let us write the recombination resistance in the form

$$R_{rec}(V) = R_0 \exp\left[-\frac{q\beta V}{k_B T} + \frac{q^2 V^2}{4\lambda k_B T}\right] \tag{157}$$

where

$$R_0 = R_{0\lambda} \exp\left[\frac{E_c - E_{redox}}{k_B T_0} + \frac{\lambda}{4k_B T}\right] \tag{158}$$

$$\beta = \frac{1}{2} + \frac{T}{T_0} \tag{159}$$

When $V << \lambda$, Eq. (155) reduces to the exponential dependence that was suggested above as a phenomenological approach. Furthermore, based on the microscopic model, the parameter β accepts the form (159).[16]

Summarizing the model results, we obtain that despite many simplifications the model of Fig. 12(b) provides a detailed description of the lifetime and recombination resistance, quantities that can be measured as a function of the voltage in a DSC. The main feature is that the parabola in the exponential of the Marcus model electron transfer rate between the semiconductor surface and redox acceptor in the electrolyte, translates in curvatures of τ_n and R_{rec}. These quantities have been reported in hundreds of publications, but usually a linear

behavior in semilogarithmic plot is observed, as reported in representative measurements of Figs. 4, 5 and 14. The absence of curvature could be evidence for a large reorganization energy in the DSC with I_3^-/I^- redox couples, and the value $\lambda = 1\,\mathrm{eV}$ is often used.[213] Simpler explanation is that the outer sphere transfer model is not satisfied because this couple causes a complex reaction scheme.[207-209] It is nonetheless deceptive that all the microscopic complexity of charge transference between TiO_2 and the redox couple, as described in Fig. 12(b), ends up in just two parameters for recombination, j_{0k} and β. It is really highly desirable to obtain and explain with theory more structured data sets. Some early results[50] showed a curvature for the lifetime in I_3^-/I^- redox, however it was suggested that the recombination from the substrate would produce such results.[216] This problem has been, however, controlled by employing suitable TiO_2 blocking layers on top of the conducting substrate. Recently, very promising results have been obtained for the understanding of recombination in a DSC by Hamann et al.[148] They used outer-sphere redox shuttles $[Co(Me_2bpy)_3]^{3+/2+}$ and $[Ru(bpy)_2(MeIm)_2]^{3+/2+}$ that should follow well Marcus model and they obtain the results in Fig. 20. These results can be explained by a combination of charge transfer mechanisms. The remarkable point is that the curved lifetime, devoid of any substrate effects, is well observed in the case of $[Ru(bpy)_2(MeIm)_2]^{3+/2+}$, while $[Co(Me_2bpy)_3]^{3+/2+}$ has a much more negative redox potential and provides the usual exponential dependence. This observation allows to obtain detailed information about the physical characteristics of charge transfer,[179] such as the reorganization energy that has been indicated in Fig. 20(b).

Further investigation of this type is required, to confirm the validity of the model of Eq. (155), getting closer to a microscopic picture of the events occurring at the semiconductor/electrolyte interface in a DSC, which may finally serve also for the characterization of more complex mechanisms such as the redox couple I_3^-/I^- or the recombination in solid absorbers and organic hole conductors.[40,41,102]

17. Conclusion

Modelling of the dye solar cell has been very much developed in the last decade, until establishing very detailed models that allow to extract significant information about the device and materials properties and on the operation mechanisms. Modelling the device is quite challenging because of the necessity to deal with a large number of features: a combination of phases, energy disorder in low temperature processed semiconductor networks, and a multiplicity of interfaces. A variety of experimental techniques have been developed that are

up to this task, and the convergence of independent techniques speaks about the reality of the concepts that have been proposed. Especially important are those techniques that employ small perturbation methods, since they allow linearization to quantities that depend on local Fermi level, and therefore that are well defined in the framework of a highly nonlinear system. This is why we have emphasized quantities such as electron lifetime in their different meanings. Any quantity that is well defined physically can be checked by different experimental and computational methods and it can also be related to other quantities, if necessary. In contrast, a quantity that is linked to one particular measurement may be practical in some respects but cannot enter the larger conceptual pool that broadens the knowledge about these systems.

The confirmation that jump and chemical diffusion coefficient concepts can be also realized for the lifetimes has closed a general interpretation of transport that implements the basic multiple trapping model to a broad set of measurements and stochastic simulation. This theory can be considered very advanced now. The main challenge is to obtain a more detailed theoretical and experimental understanding of the details of interfacial carrier transfer. So far most of the works prefer to study a comparison of several samples that usually show too similar behavior. The use of model systems that allow to isolate specific experimental behavior concerning charge transfer, should be highly recommended, and can bring new light to the implementation of charge transfer in nanostructured systems, and a better control of recombination in these solar cells.

18. Acknowledgments

We thank the following agencies for support of this research. JB’s research is supported by Ministerio de Educacion y Ciencia under project HOPE CSD2007-00007, Generalitat Valenciana (ISIC/2012/008). RAM's research is supported by ARO, ONR and NSF agencies. RAM contributed in sections 14 and 15 of this article.

References

(1) O' Regan, B.; Grätzel, M. A low-cost high-efficiency solar cell based on dye-sensitized colloidal TiO2 films, *Nature* **1991**, *353*, 737-740.

(2) Yella, A.; Lee, H.-W.; Tsao, H. N.; Yi, C.; Chandiran, A. K.; Nazeeruddin, M. K.; Diau, E. W.-G.; Yeh, C.-Y.; Zakeeruddin, S. M.; Grätzel, M. Porphyrin-Sensitized Solar Cells with Cobalt (II/III)Based Redox Electrolyte Exceed 12 Percent Efficiency, *Science* **2011**, *334*, 629-634.

(3) Chang, J. A.; Rhee, J. H.; Im, S. H.; Lee, Y. H.; Kim, H.-J.; Seok, S. I.; Nazeeruddin, M. K.; Grätzel, M. High-Performance Nanostructured Inorganic−Organic Heterojunction Solar Cells, *Nano Letters* **2010**, *10*, 2609–

2612.

(4) Kim, H.-S.; Lee, C.-R.; Im, J.-H.; Lee, K.-B.; Moehl, T.; Marchioro, A.; Moon, S.-J.; Humphry-Baker, R.; Yum, J.-H.; Moser, J. E.; Grätzel, M.; Park, N.-G. Lead Iodide Perovskite Sensitized All-Solid-State Submicron Thin Film Mesoscopic Solar Cell with Efficiency Exceeding 9%, *Scientific Reports* **2012**, *2*, 591.

(5) Lee, M. M.; Teuscher, J.; Miyasaka, T.; Murakami, T. N.; Snaith, H. J. Efficient Hybrid Solar Cells Based on Meso-Superstructured Organometal Halide Perovskites, *Science* **2012**, *338*, 643-647.

(6) Bignozzi, C. A.; Argazzi, R.; Boaretto, R.; Busatto, E.; Carli, S.; Ronconi, F.; Caramori, S. The role of transition metal complexes in dye sensitized solar devices, *Coordination Chemistry Reviews* **2012**.

(7) Mora-Seró, I.; Bisquert , J. Breakthroughs in the Development of Semiconductor-Sensitized Solar Cells, *Journal of Physical Chemistry Letters* **2010**, *1*, 3046–3052.

(8) Hodes, G. Comparison of Dye- and Semiconductor-Sensitized Porous Nanocrystalline Liquid Junction Solar Cells, *The Journal of Physical Chemistry C* **2008**, *112*, 17778–17787.

(9) Dittrich, T.; Belaidi, A.; Ennaoui, A. Concepts of inorganic solid-state nanostructured solar cells, *Solar Energy Materials and Solar Cells* **2011**, 10.1016/j.solmat.2010.1012.1034.

(10) Fabregat-Santiago, F.; Bisquert, J.; Palomares, E.; Otero, L.; Kuang, D.; Zakeeruddin, S. M.; Grätzel, M. Correlation between Photovoltaic Performance and Impedance Spectroscopy of Dye-Sensitized Solar Cells Based on Ionic Liquids, *The Journal of Physical Chemistry C* **2007**, *111*, 6550-6560.

(11) Barea, E. M.; Ortiz, J.; Payá, F. J.; Fernández-Lázaro, F.; Fabregat-Santiago, F.; Sastre-Santos, A.; Bisquert, J. Energetic factors governing injection, regeneration and recombination in dye solar cells with phthalocyanine sensitizers, *Energy and Environmental Science* **2010**, *3*, 1985–1994.

(12) Bisquert, J. Physical electrochemistry of nanostructured devices, *Physical Chemistry Chemical Physics* **2008**, *10*, 49-72.

(13) Ansari-Rad, M.; Anta, J. A.; Bisquert, J. Interpretation of Diffusion and Recombination in Nanostructured and Energy Disordered Materials by Stochastic Quasiequilibrium Simulation, *The Journal of Physical Chemistry C* **2013**, 10.1021/jp403232b.

(14) Bisquert, J.; Mora-Seró, I. Simulation of Steady-State Characteristics of Dye-Sensitized Solar Cells and the Interpretation of the Diffusion Length, *Journal of Physical Chemistry Letters* **2010**, *1*, 450–456.

(15) Södergren, S.; Hagfeldt, A.; Olsson, J.; Lindquist, S. E. Theoretical Models for the Action Spectrum and the Current-Voltage Characteristics of Microporous Semiconductor Films in Photoelectrochemical Cells, *The Journal of Physical Chemistry* **1994**, *98*, 5552-5556.

(16) Wang, Q.; Ito, S.; Grätzel, M.; Fabregat-Santiago, F.; Mora-Seró, I.; Bisquert, J.; Bessho, T.; Imai, H. Characteristics of High Efficiency Dye-sensitized Solar Cells, *The Journal of Physical Chemistry B* **2006**, *110*, 19406-19411.

(17) Nayak, P. K.; Garcia-Belmonte, G.; Kahn, A.; Bisquert, J.; Cahen, D. Photovoltaic efficiency limits and material disorder, *Energy & Environmental Science* **2012**, *5*, 6022-6039.

(18) Halme, J.; Boschloo, G.; Hagfeldt, A.; Lund, P. Spectral Characteristics of Light Harvesting, Electron Injection, and Steady-State Charge Collection in Pressed TiO2 Dye Solar Cells, *The Journal of Physical Chemistry C* **2008**, *112*, 5623-5637.

(19) Li, L.-L.; Diau, E. W.-G. Porphyrin-sensitized solar cells, *Chemical Society Reviews* **2012**, *42*, 291-304.

(20) Bertoluzzi, L.; Ma, S. On the methods of calculation of the charge collection efficiency of dye sensitized solar cells, *Physical Chemistry Chemical Physics* **2013**, *15*, 4283-4285.

(21) Usami, A. Rigorous solutions of light scattering of neighboring TiO2 particles in nanocrystalline films, *Solar Energy Materials and Solar Cells* **1999**, *59*, 163-166.

(22) Usami, A. A theoretical simulation of light scattering of nanocrystalline films in photoelectrochemical solar cells, *Solar Energy Materials and Solar Cells* **2000**, *62*, 239-246.

(23) Usami, A. Theoretical simulations of optical confinement in dye-sensitized nanocrystalline solar cells, *Solar Energy Materials and Solar Cells* **2000**, *64*, 73-83.

(24) Tachibana, Y.; Hara, K.; Sayama, K.; Arakawa, H. Quantitative Analysis of Light-Harvesting Efficiency and Electron-Transfer Yield in Ruthenium-Dye-Sensitized Nanocrystalline TiO2 Solar Cells, *Chemistry of Materials* **2002**, *14*, 2527–2535.

(25) Galvez, F. E.; Kemppainen, E.; Miguez, H.; Halme, J. Effect of Diffuse Light Scattering Designs on the Efficiency of Dye Solar Cells: An Integral Optical and Electrical Description, *The Journal of Physical Chemistry C* **2012**, *116*, 11426-11433.

(26) Lin, Y.; Ma, Y. T.; Yang, L.; Xiao, X. R.; Zhou, X. W.; Li, X. P. Computer simulations of light scattering and mass transport of dye-sensitized nanocrystalline solar cells, *Journal of Electroanalytical*

Chemistry **2006**, *588*, 51-58.

(27) Raga, S. R.; Barea, E. M.; Fabregat-Santiago, F. Analysis of the Origin of Open Circuit Voltage in Dye Solar Cells, *The Journal of Physical Chemistry Letters* **2012**, *3*, 1629-1634.

(28) Fabregat-Santiago, F.; Garcia-Belmonte, G.; Mora-Seró, I.; Bisquert, J. Characterization of Nanostructured Hybrid and Organic Solar Cells by Impedance Spectroscopy, *Physical Chemistry Chemical Physics* **2011**, *13*, 9083–9118.

(29) Bisquert, J.; Fabregat-Santiago, F. Impedance Spectroscopy: A general Introduction and Application to Dye-Sensitized Solar Cells. In *Dye-sensitized solar cells.*; Kalyanasundaram, K., Ed.; CRC Press: Boca Raton, 2010.

(30) Barea, E. M.; Zafer, C.; Gultein, B.; Aydin, B.; Koyuncu, S.; Icli, S.; Fabregat-Santiago, F.; Bisquert, J. Quantification of the effects of recombination and injection in the performance of dye-sensitized solar cells based on N-substituted Carbazole dyes *The Journal of Physical Chemistry C* **2010**, *114*, 19840–19848.

(31) Barea, E. M.; Gonzalez-Pedro, V.; Ripolles-Sanchis, T.; Wu, H.-P.; Li, L.-L.; Yeh, C.-Y.; Diau, E. W.-G.; Bisquert, J. Porphyrin Dyes with High Injection and Low Recombination for Highly Efficient Mesoscopic Dye-Sensitized Solar Cells, *The Journal of Physical Chemistry C* **2011**, *115*, 10898-10902.

(32) Zhou, D.; Bai, Y.; Zhang, J.; Cai, N.; Su, M.; Wang, Y.; Zhang, M.; Wang, P. Anion Effects in Organic Dye-Sensitized Mesoscopic Solar Cells with Ionic Liquid Electrolytes: Tetracyanoborate vs Dicyanamide, *The Journal of Physical Chemistry C* **2010**, *115*, 816–822.

(33) Xu, X.; Cao, K.; Huang, D.; Shen, Y.; Wang, M. Disulfide/Thiolate Based Redox Shuttle for Dye-Sensitized Solar Cells: An Impedance Spectroscopy Study, *The Journal of Physical Chemistry C* **2012**, *116*, 25233-25241.

(34) Yu, Q.; Zhou, D.; Shi, Y.; Si, X.; Wang, Y.; Wang, P. Stable and efficient dye-sensitized solar cells: photophysical and electrical characterizations, *Energy & Environmental Science* **2010**, *3*, 1722-1725.

(35) Bai, Y.; Yu, Q.; Cai, N.; Wang, Y.; Zhang, M.; Wang, P. High-efficiency organic dye-sensitized mesoscopic solar cells with a copper redox shuttle, *Chemical Communications* **2011**, *47*, 4376-4378.

(36) Zhang, M.; Liu, J.; Wang, Y.; Zhou, D.; Wang, P. Redox couple related influences of pi-conjugation extension in organic dye-sensitized mesoscopic solar cells, *Chemical Science* **2011**, *2*, 1401-1406.

(37) Zhou, D.; Yu, Q.; Cai, N.; Bai, Y.; Wang, Y.; Wang, P. Efficient organic dye-sensitized thin-film solar cells based on the tris(1,10-phenanthroline)cobalt(II/III) redox shuttle, *Energy & Environmental Science* **2011**, *4*, 2030-2034.

(38) Bai, Y.; Zhang, J.; Zhou, D.; Wang, Y.; Zhang, M.; Wang, P. Engineering Organic Sensitizers for Iodine-Free Dye-Sensitized Solar Cells: Red-Shifted Current Response Concomitant with Attenuated Charge Recombination, *Journal of the American Chemical Society* **2011**, *133*, 11442-11445.

(39) Liu, Y.; Jennings, J. R.; Zakeeruddin, S. M.; Grätzel, M.; Wang, Q. Heterogeneous Electron Transfer from Dye-Sensitized Nanocrystalline TiO2 to [Co(bpy)3]3+: Insights Gained from Impedance Spectroscopy, *Journal of the American Chemical Society* **2013**, *135*, 3939-3952.

(40) Mora-Seró, I.; Giménez, S.; Fabregat-Santiago, F.; Gomez, R.; Shen, Q.; Toyoda, T.; Bisquert, J. Recombination in quantum dot sensitized solar cells *Accounts in Chemical Research* **2009**, *42*, 1848–1857.

(41) Gónzalez-Pedro, V.; Xu, X.; Mora-Seró, I.; Bisquert , J. Modeling High-Efficiency Quantum Dot Sensitized Solar Cells, *ACS Nano* **2010**, *4*, 5783–5790.

(42) Boix, P. P.; Guerrero, A.; Marchesi, L. F.; Garcia-Belmonte, G.; Bisquert, J. Current-Voltage Characteristics of Bulk Heterojunction Organic Solar Cells: Connection Between Light and Dark Curves, *Advanced Energy Materials* **2011**, *1*, 1073–1078.

(43) Wang, H.; Peter, L. M. A Comparison of Different Methods To Determine the Electron Diffusion Length in Dye-Sensitized Solar Cells, *The Journal of Physical Chemistry C* **2009**, *113*, 18125–18133.

(44) Bisquert, J. Theory of the Impedance of Electron Diffusion and Recombination in a Thin Layer, *The Journal of Physical Chemistry B* **2002**, *106*, 325-333.

(45) Jennings, J. R.; Liu, Y.; Safari-Alamuti, F.; Wang, Q. Dependence of Dye-Sensitized Solar Cell Impedance on Photoelectrode Thickness, *The Journal of Physical Chemistry C* **2012**, *116*, 1556-1562.

(46) Jaegermann, W. The semiconductor/electrolyte interface: a surface science approach, *Modern Aspects of Electrochemistry, Number 30* **1996**.

(47) Bisquert, J.; Cahen, D.; Rühle, S.; Hodes, G.; Zaban, A. Physical chemical principles of photovoltaic conversion with nanoparticulate, mesoporous dye-sensitized solar cells., *The Journal of Physical Chemistry B* **2004**, *108*, 8106-8118.

(48) Bisquert, J. Hopping transport of electrons in dye-sensitized solar cells, *The Journal of Physical*

Chemistry C **2007**, *111*, 17163-17168.

(49) Bisquert, J. Interpretation of electron diffusion coefficient in organic and inorganic semiconductors with broad distributions of states, *Physical Chemistry Chemical Physics* **2008**, *10*, 3175-3194.

(50) Bisquert, J. ; Zaban, A.; Greenshtein, M.; Mora-Seró, I. Determination of rate constants for charge transfer and the distribution of semiconductor and electrolyte electronic energy levels in dye-sensitized solar cells by open-circuit photovoltage decay method., *Journal of the American Chemical Society* **2004**, *126*, 13550.

(51) Bisquert, J.; Vikhrenko, V. S. Interpretation of the time constants measured by kinetic techniques in nanostructured semiconductor electrodes and dye-sensitized solar cells., *The Journal of Physical Chemistry B* **2004**, *108*, 2313-2322.

(52) Bisquert, J.; Fabregat-Santiago, F.; Mora-Seró, I.; Garcia-Belmonte, G.; Giménez, S. Electron Lifetime in Dye-Sensitized Solar Cells: Theory and Interpretation of Measurements, *The Journal of Physical Chemistry C* **2009**, *113*, 17278–17290.

(53) van de Lagemaat, J.; Frank, A. J. Nonthermalized Electron Transport in Dye-Sensitized Nanocrystalline TiO2 Films: Transient Photocurrent and Random-Walk Modeling Studies, *The Journal of Physical Chemistry B* **2001**, *105*, 11194-11205.

(54) Benkstein, K. D.; Kopidakis, N.; Van de Lagemaat, J.; Frank, A. J. Influence of the percolation network geometry on the electron transport in dye-sensitized titanium dioxide solar cells., *The Journal of Physical Chemistry B* **2003**, *107*, 7759 -7767.

(55) Anta, J. A. Random walk numerical simulation for solar cell applications, *Energy and Environmental Science* **2009**, *2*, 387-392.

(56) Ansari-Rad, M.; Abdi, Y.; Arzi, E. Simulation of non-linear recombination of charge carriers in sensitized nanocrystalline solar cells, *Journal of Applied Physics* **2012**, *112*, 074319-074317.

(57) Mendels, D.; Tessler, N. Drift and Diffusion in Disordered Organic Semiconductors: The Role of Charge Density and Charge Energy Transport, *The Journal of Physical Chemistry C* **2013**, *117*, 3287-3293.

(58) Amat, A.; Angelis, F. D. Challenges in the simulation of dye-sensitized ZnO solar cells: quantum confinement, alignment of energy levels and excited state nature at the dye/semiconductor interface, *Physical Chemistry Chemical Physics* **2012**, *14*, 10662-10668.

(59) Ronca, E.; Pastore, M.; Belpassi, L.; Tarantelli, F.; De Angelis, F. Influence of the dye molecular structure on the TiO2 conduction band in dye-sensitized solar cells: disentangling charge transfer and electrostatic effects, *Energy & Environmental Science* **2012**, *6*, 183-193.

(60) Pastore, M.; de Angelis, F. Intermolecular Interactions in Dye-Sensitized Solar Cells: A Computational Modeling Perspective, *Journal of Physical Chemistry Letters* **2013**, *4*, 956-974.

(61) Baumeier, B.; May, F.; Lennartz, C.; Andrienko, D. Challenges for in silico design of organic semiconductors, *Journal of Materials Chemistry* **2012**, *22*, 10971-10976.

(62) Ruhle, V.; Lukyanov, A.; May, F.; Schrader, M.; Vehoff, T.; Kirkpatrick, J.; Baumeier, B.; Andrienko, D. Microscopic Simulations of Charge Transport in Disordered Organic Semiconductors, *Journal of Chemical Theory and Computation* **2011**, *7*, 3335-3345.

(63) Coehoorn, R.; Bobbert, P. A. Effects of Gaussian disorder on charge carrier transport and recombination in organic semiconductors, *physica status solidi (a)* **2012**, *209*, 2354-2377.

(64) Cao, F.; Oskam, G.; Meyer, G. J.; Searson , P. C. Electron transport in porous nanocrystalline TiO_2 photoelectrochemical cells, *The Journal of Physical Chemistry* **1996**, *100*, 17021-17027.

(65) Villanueva, J.; Anta, J. A.; Guillen, E.; Oskam, G. Numerical Simulation of the Current-Voltage Curve in Dye-Sensitized Solar Cells, *J. Phys. Chem. C* **2009**, *113*, 19722-19731.

(66) Cai, J. H.; Chen, H.; Han, L. Y. MODELS OF ELECTRON INJECTION, DIFFUSION AND RECOMBINATION IN DYE-SENSITIZED SOLAR CELLS, *Int. J. Mod. Phys. B* **2012**, *26*, 19.

(67) Cass, M. J.; Qiu, F. L.; Walker, A. B.; Fisher, A. C.; Peter, L. M. Influence of Grain Morphology on Electron Transport in Dye Sensitized Nanocrystalline Solar Cells, *The Journal of Physical Chemistry B* **2003**, *107*, 113-119.

(68) Kambili, A.; Walker, A. B.; Qiu, F. L.; Fisher, A. C.; Savin, A. D.; Peter, L. M. Electron transport in the dye sensitized nanocrystalline cell, *Physica E* **2002**, *14*, 203-209.

(69) Duffy, N. W.; Peter, L. M.; Rajapakse, R. M. G.; Wijayantha, K. G. U. Investigation of the kinetics of the back reaction of electrons with tri-Iodide in dye-sansitized nanocrystalline photovoltaic cells, *The Journal of Physical Chemistry B* **2000**, *104*, 8916-8919.

(70) Duffy, N. W.; Peter, L. M.; Rajapakse, R. M. G.; Wijayantha, K. G. U. A novel charge extraction method for the study of electron transport and interfacial transfer in dye sensitized nanocrystalline solar cells,

Electrochemistry Communications **2000**, *2*, 658-662.

(71) Jennings, J. R.; Peter, L. M. A Reappraisal of the Electron Diffusion Length in Solid-State Dye-Sensitized Solar Cells, *The Journal of Physical Chemistry C* **2007**, *111*, 16100-16104.

(72) Lobato, K.; Peter, L. M.; Wurfel, U. Direct Measurement of the Internal Electron Quasi-Fermi Level in Dye Sensitized Solar Cells Using a Titanium Secondary Electrode, *The Journal of Physical Chemistry B* **2006**, *110*, 16201-16204.

(73) Paasch, G.; Micka, K.; Gersdorf, P. Theory of the electrochemical impedance of macrohomogeneous porous electrodes, *Electrochimica Acta* **1993**, *38*, 2653-2662.

(74) Stangl, R.; Ferber, J.; Luther, J. On the modeling of the dye-sensitized solar cell, *Solar Energy Materials and Solar Cells* **1998**, *54*, 255-264.

(75) Ferber, J.; Stangl, R.; Luther, J. An electrical model of the dye-sensitized solar cell, *Solar Energy Materials and Solar Cells* **1998**, *53*, 29-54.

(76) Burgelman, M.; Grasso, C. Network of flatband solar cells as a model for solid-state nanostructured solar cells, *Journal of Applied Physics* **2004**, *95*, 2020-2024.

(77) Newman, J. S. *Electrochemical Systems*; Prentice-Hall: Englewoods Cliffs, 1973.

(78) Sze, S. M. *Physics of Semiconductor Devizes*, 2nd ed.; John Wiley and Sons: New York, 1981.

(79) Mora-Seró, I.; Garcia-Belmonte, G.; Boix, P. P.; Vázquez, M. A.; Bisquert, J. Impedance characterisation of highly efficient silicon solar cell under different light illumination intensities *Energy and Environmental Science* **2009**, *2*, 678–686.

(80) Rickert, H. *Electrochemistry of Solids*; Springer Verlag: Berlin, 1982.

(81) Riess, I. What does a voltmeter measure?, *Solid State Ionics* **1997**, *95*, 327-328.

(82) Schwarzburg, K.; Willig, F. Origin of photovoltage and photocurrent in the nanoporous dye-sensitized electrochemical solar cell, *The Journal of Physical Chemistry B* **1999**, *28*, 5743-5746.

(83) Pichot, F.; Gregg, B. A. The photovoltage-determining mechanism in dye-sensitized solar cells, *The Journal of Physical Chemistry B* **2000**, *104*, 6-10.

(84) Cahen, D.; Hodes, G.; Grätzel, M.; Guillemoles, J. F.; Riess, I. Nature of Photovoltaic Action in Dye-Sensitized Solar Cells, *The Journal of Physical Chemistry B* **2000**, *104*, 2053-2059.

(85) Levy, B.; Liu, W.; Gilbert, S. E. Directed photocurrents in nanostructured TiO_2 /SnO_2 heterojunction diodes, *The Journal of Physical Chemistry B* **1997**, *101*, 1810-1816.

(86) Turrión, M.; Bisquert, J.; Salvador, P. Flatband potential of F:SnO2 in a TiO2 dye-sensitized solar cell: An interference reflection study., *The Journal of Physical Chemistry B* **2003**, *107*, 9397-9403.

(87) Fabregat-Santiago, F.; Garcia-Belmonte, G.; Bisquert, J.; Bogdanoff, P.; Zaban, A. Mott-Schottky analysis of nanoporous semiconductor electrodes in the dielectric state deposited on SnO2(F) conducting substrates., *Journal of the Electrochemical Society* **2003**, *150*, E293-E298.

(88) Rühle, S.; Dittrich, T. Investigation of the Electric Field in TiO2/FTO Junctions Used in Dye-Sensitized Solar Cells by Photocurrent Transients, *The Journal of Physical Chemistry B* **2005**, *109*, 9522-9526.

(89) Ruhle, S.; Cahen, D. Electron Tunneling at the TiO2/Substrate Interface Can Determine Dye-Sensitized Solar Cell Performance, *The Journal of Physical Chemistry B* **2004**, *108*, 17946-17951.

(90) Liu, W. Q.; Kou, D. X.; Hu, L. H.; Dai, S. Y. The kinetics of electron transfer across the multi-point contact interface through simplifying the complex structure in dye-sensitized solar cell, *Chemical Physics Letters* **2011**, *513*, 145-148.

(91) van de Lagemaat, J.; Park, N.-G.; Frank, A. J. Influence of Electrical Potential Distribution, Charge Transport, and Recombination on the Photopotential and Photocurrent Conversion Efficiency of Dye-Sensitized Nanocrystalline TiO2 Solar Cells: A Study by Electrical Impedance and Optical Modulation Techniques, *The Journal of Physical Chemistry B* **2000**, *104*, 2044-2052.

(92) Bisquert, J. Dilemmas of Dye-Sensitized Solar Cells, *ChemPhysChem* **2011**, *12*, 1633-1636.

(93) Zhang, Z.; Zakeeruddin, S. M.; O'Regan, B. C.; Humphry-Baker, R.; Grätzel, M. Influence of 4-Guanidinobutyric Acid as Coadsorbent in Reducing Recombination in Dye-Sensitized Solar Cells, *The Journal of Physical Chemistry B* **2005**, *109*, 21818-21824.

(94) Guerrero, A.; Marchesi, L. F.; Boix, P. P.; Ruiz-Raga, S.; Ripolles-Sanchis, T.; Garcia-Belmonte, G.; Bisquert, J. How the Charge-Neutrality Level of Interface States Controls Energy Level Alignment in Cathode Contacts of Organic Bulk-Heterojunction Solar Cells, *ACS Nano* **2012**, *6*, 3453-3460.

(95) Mora-Seró, I.; Fabregat-Santiago, F.; Denier, B.; Bisquert, J.; Tena-Zaera, R.; Elias, J.; Lévy-Clement, C. Determination of carrier density of ZnO nanowires by electrochemical techniques, *Applied Physics Letters* **2006**, *89*, 203117.

(96) Tena-Zaera, R.; Elias, J.; Lévy-Clément, C.; Bekeny, C.; Voss, T.; Mora-Seró, I.; Bisquert, J. Influence of the Potassium Chloride Concentration on the Physical Properties of Electrodeposited ZnO Nanowire Arrays, *The Journal of Physical Chemistry C* **2008**, *112*, 16318–16323.

(97) Foley, J. M.; Price, M. J.; Feldblyum, J. I.; Maldonado, S. Analysis of the operation of thin nanowire photoelectrodes for solar energy conversion, *Energy & Environmental Science* **2012**, *5*, 5203-5220.

(98) Kambe, S.; Nakade, S.; Kitamura, T.; Wada, Y.; Yanagida, S. Influence of the electrolytes on electron transport in mesoporous TiO2-electrolyte systems, *The Journal of Physical Chemistry B* **2002**, *106*, 2967-2972.

(99) Feldt, S. M.; Gibson, E. A.; Gabrielsson, E.; Sun, L.; Boschloo, G.; Hagfeldt, A. Design of Organic Dyes and Cobalt Polypyridine Redox Mediators for High-Efficiency Dye-Sensitized Solar Cells, *Journal of the American Chemical Society* **2010**, *132*, 16714–16724.

(100) Bignozzi, C. A.; Argazzi, R.; Boaretto, R.; Busatto, E.; Carli, S.; Ronconi, F.; Caramori, S. The role of transition metal complexes in dye sensitized solar devices, *Coordination Chemistry Reviews* **2013**, doi:10.1016/j.ccr.2012.1009.1008.

(101) Snaith, H. J.; Grätzel, M. Light-enhanced charge mobility in a molecular hole transporter, *Physical Review Letters* **2007**, *98*, 177402.

(102) Fabregat-Santiago, F.; Bisquert, J.; Cevey, L.; Chen, P.; Wang, M.; Zakeeruddin, S. M.; Grätzel, M. Electron transport and recombination in solid state Dye solar cell with spiro-OMeTAD as hole conductor, *Journal of the American Chemical Society* **2009**, *131*, 558–562.

(103) Wang, M.; Chen, P.; Humphry-Baker, R.; Zakeeruddin, S. M.; Grätzel, M. The Influence of Charge Transport and Recombination on the Performance of Dye-Sensitized Solar Cells, *ChemPhysChem* **2009**, *10*, 290-299.

(104) Boix, P. P.; Larramona, G.; Jacob, A.; Delatouche, B.; Mora-Sero, I.; Bisquert, J. Hole Transport and Recombination in All-Solid Sb2S3-Sensitized TiO2 Solar Cells Using CuSCN As Hole Transporter, *The Journal of Physical Chemistry C* **2011**, *116*, 1579-1587.

(105) Boix, P. P.; Lee, Y. H.; Fabregat-Santiago, F.; Im, S. H.; Mora-Sero, I.; Bisquert, J.; Seok, S. I. From Flat to Nanostructured Photovoltaics: Balance between Thickness of the Absorber and Charge Screening in Sensitized Solar Cells, *ACS Nano* **2012**, *6*, 873-880.

(106) Dualeh, A.; Moehl, T.; Nazeeruddin, M. K.; Grätzel, M. Temperature Dependence of Transport Properties of Spiro-MeOTAD as a Hole Transport Material in Solid-State Dye-Sensitized Solar Cells, *ACS Nano* **2013**, *7*, 2292-2301.

(107) Noh, J. H.; Im, S. H.; Heo, J. H.; Mandal, T. N.; Seok, S. I. Chemical Management for Colorful, Efficient, and Stable Inorganic-Organic Hybrid Nanostructured Solar Cells, *Nano Letters* **2013**, 10.1021/nl400349b.

(108) Kopidakis, N.; Schiff, E. A.; Park, N. G.; van de Lagemaat, J.; Frank, A. J. Ambipolar Diffusion of Photocarriers in Electrolyte-Filled, Nanoporous TiO2â€ *The Journal of Physical Chemistry B* **2000**, *104*, 3930-3936.

(109) Champlain, J. G. On the use of the term ``ambipolar'', *Applied Physics Letters* **2011**, *99*, 123502.

(110) Ritter, D.; Zeldov, E.; Weiser, K. Ambipolar transport in amorphous semiconductors in the lifetime and relaxation-time regimes investigated by the steady-state photocarrier grating technique, *Physical Review B* **1988**, *38*, 8296.

(111) Papageorgiou, N.; Grätzel, M.; Infelta, P. P. On the relevance of mass transport in thin layer nanocrystalline photoelectrochemical solar cells, *Solar Energy Materials and Solar Cells* **1996**, *44*, 405-438.

(112) Kalaignan, G. P.; Kang, Y. S. A review on mass transport in dye-sensitized nanocrystalline solar cells, *J. Photochem. Photobiol. C-Photochem. Rev.* **2006**, *7*, 17-22.

(113) Usami, A.; Ozaki, H. Computer Simulations of Charge Transport in Dye-Sensitized Nanocrystalline Photovoltaic Cells, *The Journal of Physical Chemistry B* **2001**.

(114) Usami, A. Theoretical study of charge trasportation in dye-sensitized nanocristalline TiO2 electrodes, *Chemical Physics Letters* **1998**, *292*, 223-228.

(115) Hyk, W.; Augustynski, J. Steady-State Operation of Porous Photoelectrochemical Cells Under the Conditions of Mixed Diffusional and Migrational Mass Transport *Journal of the Electrochemical Society* **2006**, *153*, A2326.

(116) Barnes, P. R. F.; Anderson, A. Y.; Durrant, J. R.; O'Regan, B. C. Simulation and measurement of complete dye sensitised solar cells: Including the influence of trapping, electrolyte, oxidised dyes and light intensity on steady state and transient device behaviour, *Physical Chemistry Chemical Physics* **2011**, *13*, 5798-5816.

(117) Andrade, L.; Sousa, J.; Aguilar Ribeiro, H.; Mendes, A. Phenomenological modeling of dye-sensitized solar cells under transient conditions, *Solar Energy* **2012**, *85*, 781-793.

(118) Gagliardi, A.; der Maur, M. A.; Gentilini, D.; Di Carlo, A. Simulation of dye solar cells: through and beyond one dimension, *J. Comput. Electron.* **2011**, *10*, 424-436.

(119) Chua, J.; Mathews, N.; Jennings, J. R.; Yang, G.; Wang, Q.; Mhaisalkar, S. G. Patterned 3-dimensional metal grid electrodes as alternative electron collectors in dye-sensitized solar cells, *Physical Chemistry Chemical Physics* **2011**, *13*, 19314-19317.

(120) Miettunen, K.; Halme, J.; Visuri, A.-M.; Lund, P. Two-Dimensional Time-Dependent Numerical Modeling of Edge Effects in Dye Solar Cells, *The Journal of Physical Chemistry C* **2011**, *115*, 7019-7031.

(121) Mastroianni, S.; Lanuti, A.; Penna, S.; Reale, A.; Brown, T. M.; Di Carlo, A.; Decker, F. Physical and Electrochemical Analysis of an Indoor–Outdoor Ageing Test of Large-Area Dye Solar Cell Devices, *ChemPhysChem* **2012**, *13*, 2925-2936.

(122) Anta, J. A.; Idigoras, J.; Guillen, E.; Villanueva-Cab, J.; Mandujano-Ramirez, H. J.; Oskam, G.; Pelleja, L.; Palomares, E. A continuity equation for the simulation of the current-voltage curve and the time-dependent properties of dye-sensitized solar cells, *Physical Chemistry Chemical Physics* **2012**, *14*, 10285-10299.

(123) Gagliardi, A.; Mastroianni, S.; Gentilini, D.; Giordano, F.; Reale, A.; Brown, T. M.; Di Carlo, A. Multiscale Modeling of Dye Solar Cells and Comparison With Experimental Data, *IEEE Journal of Selected Topics in Quantum Electronics* **2010**, *16*, 1611-1618.

(124) Halme, J.; Vahermaa, P.; Miettunen, K.; Lund, P. Device Physics of Dye Solar Cells, *Advanced Materials* **2010**, *22*, E210–E234.

(125) Peter, L. M. Characterization and Modeling of Dye-Sensitized Solar Cells, *The Journal of Physical Chemistry C* **2007**, *111*, 6601-6612.

(126) Barnes, P. R. F.; Miettunen, K.; Li, X.; Anderson, A. Y.; Bessho, T.; Gratzel, M.; O'Regan, B. C. Interpretation of Optoelectronic Transient and Charge Extraction Measurements in Dye-Sensitized Solar Cells, *Advanced Materials* **2013**, *25*, 1881-1922.

(127) Li, L.-L.; Chang, Y.-C.; Wu, H.-P.; Diau, E. W.-G. Characterisation of electron transport and charge recombination using temporally resolved and frequency-domain techniques for dye-sensitised solar cells, *International Reviews in Physical Chemistry* **2012**, *31*, 420-467.

(128) Schwarzburg, K.; Willig, F. Influence of trap filling on photocurrent transients in polycrystalline TiO2, *Applied Physics Letters* **1991**, *58*, 2520-2522.

(129) Franco, G.; Gehring, J.; Peter, L. M.; Ponomarev, E. A.; Uhlendorf, I. Frequency-Resolved Optical Detection of Photoinjected Electrons in Dye-Sensitized Nanocrystalline Photovoltaic Cells, *The Journal of Physical Chemistry B* **1999**, *103*, 692-698.

(130) van de Lagemaat, J.; Frank, A. J. Effect of the surface state distribution on electron transport in dye sensitized TiO2 solar cells: nonlinear electron-transport kinetics, *The Journal of Physical Chemistry B* **2000**, *104*, 4292-4294.

(131) Vanmaekelbergh, D.; de Jongh, P. E. Driving force for electron transport in porous nanostructured photoelectrodes, *The Journal of Physical Chemistry B* **1999**, *103*, 747-750.

(132) Vanmaekelbergh, D.; de Jongh, P. E. Electron transport in disordered semiconductors studied by a small harmonic modulation of the steady state, *Physical Review B* **2000**, *61*, 4699-4707.

(133) Nelson, J. Continuous-time random-walk model of electron transport in nanocrystalline TiO2 electrodes, *Physical Review B* **1999**, *59*, 15374.

(134) Bisquert, J. Chemical capacitance of nanostructured semiconductors: its origin and significance for heterogeneous solar cells, *Phys. Chem. Chem. Phys.* **2003**, *5*, 5360-5364.

(135) Jamnik, J.; Maier, J. Generalised equivalent circuits for mass and charge transport: chemical capacitance and its implications, *Physical Chemistry Chemical Physics* **2001**, *3*, 1668-1678.

(136) Shockley, W. Electrons, Holes, and Traps, *Proceedings of the IRE* **1958**, *46*, 973-990.

(137) Garcia-Belmonte, G.; Guerrero, A.; Bisquert, J. Elucidating Operating Modes of Bulk-Heterojunction Solar Cells from Impedance Spectroscopy Analysis, *Journal of Physical Chemistry Letters* **2013**.

(138) Lee, P. A. Density of states and screening near the mobility edge, *Physical Review B* **1982**, *26*, 5882-5885.

(139) Berger, T.; Monllor-Satoca, D.; Jankulovska, M.; Lana-Villarreal, T.; Gomez, R. The Electrochemistry of Nanostructured Titanium Dioxide Electrodes, *ChemPhysChem* **2012**.

(140) Zaban, A.; Greenshtein, M.; Bisquert, J. Determination of the electron lifetime in nanocrystalline dye solar cells by open-circuit voltage decay measurements, *ChemPhysChem* **2003**, *4*, 859-864.

(141) van Roosbroeck, W. The transport of added current carriers in a homogeneous semiconductor, *Physical Review* **1953**, *91*, 282-289.

(142) Rose, A. *Concepts in Photoconductivity and Allied Problems*; Interscience: New York, 1963.

(143) van Roosbroeck, W.; Shockley, W. Photon-radiative recombination of electrons and holes in germanium, *Physical Review* **1954**, *94*, 1558-1560.

(144) Schmidt, J. Measurement of differential and actual recombination parameters in crystalline silicon wafers, *IEEE Transactions on Electron Devices* **1999**, *46*, 2018-2025.

(145) Tiedje, T.; Rose, A. A physical interpretation of dispersive transport in disordered semiconductors, *Solid State Communications* **1981**, *37*, 49.

(146) Orenstein, J.; Kastner, M. Photocurrent transient spectroscopy: mesurament of the density of localized states in a -As2Se3, *Physical Review Letters* **1981**, *46*, 1421-1424.

(147) Hoesterey, D. C.; Letson, G. M. The trapping of photocarriers in anthracene, *Journal of Physical Chemistry of Solids* **1963**, *24*, 1609.

(148) Ondersma, J. W.; Hamann, T. W. Measurements and Modeling of Recombination from Nanoparticle TiO2 Electrodes, *Journal of the American Chemical Society* **2011**, *133*, 8264-8271.

(149) Ansari-Rad, M.; Abdi, Y.; Arzi, E. Reaction Order and Ideality Factor in Dye-Sensitized Nanocrystalline Solar Cells: A Theoretical Investigation, *The Journal of Physical Chemistry C* **2012**, *116*, 10867–10872.

(150) Bisquert, J. Beyond the quasi-static approximation: Impedance and capacitance of an exponential distribution of traps, *Physical Review B* **2008**, *77*, 235203.

(151) Dunn, H. K.; Peter, L. M.; Bingham, S. J.; Maluta, E.; Walker, A. B. In Situ Detection of Free and Trapped Electrons in Dye-Sensitized Solar Cells by Photo-Induced Microwave Reflectance Measurements, *The Journal of Physical Chemistry C* **2012**, *116*, 22063-22072.

(152) Chen, J.; Li, B.; Zheng, J.; Jia, S.; Zhao, J.; Jing, H.; Zhu, Z. Role of One-Dimensional Ribbonlike Nanostructures in Dye-Sensitized TiO2-Based Solar Cells, *The Journal of Physical Chemistry C* **2011**, *115*, 7104-7113.

(153) Ondersma, J. W.; Hamann, T. W. Impedance Investigation of Dye-Sensitized Solar Cells Employing Outer-Sphere Redox Shuttles, *The Journal of Physical Chemistry C* **2009**, *114*, 638-645.

(154) Bisquert, J. Chemical diffusion coefficient in nanostructured semiconductor electrodes and dye-sensitized solar cells., *The Journal of Physical Chemistry B* **2004**, *108*, 2323-2332.

(155) Marinado, T.; Nonomura, K.; Nissfolk, J.; Karlsson, M. K.; Hagberg, D. P.; Sun, L.; Mori, S.; Hagfeldt, A. How the Nature of Triphenylamine-Polyene Dyes in Dye-Sensitized Solar Cells Affects the Open-Circuit Voltage and Electron Lifetimes, *Langmuir* **2009**, *26*, 2592–2598.

(156) Jennings, J. R.; Li, F.; Wang, Q. Reliable Determination of Electron Diffusion Length and Charge Separation Efficiency in Dye-Sensitized Solar Cells, *The Journal of Physical Chemistry C* **2010**, *114*, 14665–14674.

(157) González-Vázquez, J. P.; Anta, J. A.; Bisquert, J. Random walk numerical simulation for hopping transport at finite carrier concentrations: diffusion coefficient and transport energy concept, *Physical Chemistry Chemical Physics* **2009**, *11*, 10359-10367.

(158) Gonzalez-Vazquez, J. P.; Oskam, G.; Anta, J. A. Origin of Nonlinear Recombination in Dye-Sensitized Solar Cells: Interplay between Charge Transport and Charge Transfer, *The Journal of Physical Chemistry C* **2012**, *116*, 22687-22697.

(159) van de Lagemaat, J.; Kopidakis, N.; Neale, N. R.; Frank, A. J. Effect of nonideal statistics on electron diffusion in sensitized nanocrystalline TiO2, *Physical Review B* **2005**, *71*, 035304.

(160) Anta, J. A.; Mora-Seró, I.; Dittrich, T.; Bisquert, J. Interpretation of diffusion coefficients in nanostructured materials from random walk numerical simulation, *Physical Chemistry Chemical Physics* **2008**, *10*, 4478-4485.

(161) Gonzalez-Vazquez, J. P.; Anta, J. A.; Bisquert, J. Determination of the Electron Diffusion Length in Dye-Sensitized Solar Cells by Random Walk Simulation: Compensation Effects and Voltage Dependence, *The Journal of Physical Chemistry C* **2010**, *114*, 8552-8558.

(162) Darken, L. S., *Trans. Am. Inst. Min. Eng.* **1948**, *175*, 184.

(163) Paul, E. W.; Ricco, A. J.; Wrighton, M. S. Resistance of polyaniline films as a function of electrochemical potential and the fabrication of polyaniline based microelectronic devices, *The Journal of Physical Chemistry* **1985**, *89*, 1441.

(164) Vanmaekelbergh, D.; Houtepen, A. J.; Kelly, J. J. Electrochemical gating: A method to tune and

monitor the (opto)electronic properties of functional materials, *Electrochimica Acta* **2007**, *53*, 1140-1149.

(165) Pomerantz, Z.; Zaban, A.; Ghosh, S.; Lellouche, J.-P.; Garcia-Belmonte, G.; Bisquert, J. Capacitance, spectroelectrochemistry and conductivity of polarons and bipolarons in a polydicarbazole based conducting polymer, *Journal of Electroanalytical Chemistry* **2008**, doi: 10.1016/j.jelechem.2007.1011.1005.

(166) Ondersma, J. W.; Hamann, T. W. Conduction band energy determination by variable temperature spectroelectrochemistry, *Energy & Environmental Science* **2012**, *5*, 9476-9480.

(167) Boschloo, G.; Fitzmaurice, D. Electron Accumulation in Nanostructured TiO2 (Anatase) Electrodes, *The Journal of Physical Chemistry B* **1999**, *103*, 7860-7868.

(168) Berger, T.; Anta, J. A.; Morales-Florez, V. Electrons in the Band Gap: Spectroscopic Characterization of Anatase TiO2 Nanocrystal Electrodes under Fermi Level Control, *The Journal of Physical Chemistry C* **2012**, *116*, 11444-11455.

(169) Kroeze, J. E.; Savenije, T. J.; Warman, J. M. Electrodeless determination of the trap density, decay kinetics and charge separation efficiency of dye-sensitized nanocrystalline TiO2, *Journal of the American Chemical Society* **2003**, *126*, 7608.

(170) Friedrich, D.; Kunst, M. Analysis of Charge Carrier Kinetics in Nanoporous Systems by Time Resolved Photoconductance Measurements, *The Journal of Physical Chemistry C* **2011**, *115*, 16657-16663.

(171) Fabregat-Santiago, F.; Garcia-Belmonte, G.; Bisquert, J.; Zaban, A.; Salvador, P. Decoupling of transport, charge-storage and interfacial charge-transfer in the nanocrystalline TiO2/electrolyte system by impedance methods, *The Journal of Physical Chemistry B* **2002**, *106*, 334-339.

(172) Archana, P. S.; Jose, R.; Yusoff, M. M.; Ramakrishna, S. Near band-edge electron diffusion in electrospun Nb-doped anatase TiO[sub 2] nanofibers probed by electrochemical impedance spectroscopy, *Applied Physics Letters* **2011**, *98*, 152106.

(173) Jennings, J. R.; Wang, Q. Influence of Lithium Ion Concentration on Electron Injection, Transport, and Recombination in Dye-Sensitized Solar Cells, *The Journal of Physical Chemistry C* **2010**, *114*, 1715–1724.

(174) Bisquert, J.; Grätzel, M.; Wang, Q.; Fabregat-Santiago, F. Three-channel transmission line impedance model for mesoscopic oxide electrodes functionalized with a conductive coating, *The Journal of Physical Chemistry B* **2006**, *110*, 11284-11290.

(175) Bisquert, J. Influence of the boundaries in the impedance of porous film electrodes, *Physical Chemistry Chemical Physics* **2000**, *2*, 4185-4192.

(176) Barea, E. M.; Bisquert, J. Properties of chromophores determining recombination at TiO2-dye-electrolyte interface *Langmuir* **2013**, 10.1021/jp2018378.

(177) Clifford, J. N.; Martinez-Ferrero, E.; Palomares, E. Dye mediated charge recombination dynamics in nanocrystalline TiO2 dye sensitized solar cells, *Journal of Materials Chemistry* **2012**, *22*, 12415-12422.

(178) de Vries, M. J.; Pellin, M. J.; Hupp, J. T. Dye-Sensitized Solar Cells: Driving-Force Effects on Electron Recombination Dynamics with Cobalt-Based Shuttles, *Langmuir* **2010**, 10.1021/la904643t.

(179) Ondersma, J. W.; Hamann, T. W. Recombination and redox couples in dye-sensitized solar cells, *Coordination Chemistry Reviews* **2012**, dx.doi.org/10.1016/j.ccr.2012.1009.1010.

(180) Bisquert, J.; Zaban, A.; Salvador, P. Analysis of the mechanism of electron recombination in nanoporous TiO2 dye-sensitized solar cells. Nonequilibrium steady state statistics and transfer rate of electrons in surface states., *The Journal of Physical Chemistry B* **2002**, *106*, 8774-8782.

(181) Salvador, P.; González-Hidalgo, M.; Zaban, A.; Bisquert, J. Illumination intensity dependence of the photovoltage in nanostructured TiO2 dye-sensitized solar cells., *The Journal of Physical Chemistry B* **2005**, *109*, 15915-15926.

(182) Marcus, R. A. On the theory of oxidation-reduction reactions involving electron transfer. I, *The Journal of Chemical Physics* **1956**, *24*, 966.

(183) Marcus, R. A. Exchange reactions and electron transfer reactions inclunding isotopic exchange. Theory of oxidation-reduction reactions involving electron transfer. Part 4., *Faraday Discussion Chemical Society* **1960**, *29*, 21.

(184) Marcus, R. A. On the theory of electron-transfer reactions. VI. Unified treatment for homogeneous and electrode reactions, *The Journal of Chemical Physics* **1965**, *43*, 679.

(185) Marcus, R. A. On the theory of electrochemical and chemical electron transfer processes, *Canadian Journal of Chemistry* **1959**, *37*, 155-163.

(186) Gosavi, S.; Marcus, R. A. Nonadiabatic Electron Transfer at Metal Surfaces, *The Journal of Physical Chemistry B* **2000**, *104*, 2067-2072.

(187) Gosavi, S.; Qin Gao, Y.; Marcus, R. A. Temperature dependence of the electronic factor in the

nonadiabatic electron transfer at metal and semiconductor electrodes, *Journal of Electroanalytical Chemistry* **2001**, *500*, 71-77.

(188) Marcus, R. A. Electron transfer at electrodes and in solution: Comparison of theory and experiment, *Electrochimica Acta* **1968**, *13*, 995-1004.

(189) Marcus, R. A. Reorganization free energy for electron transfers at liquid-liquid and dielectric semiconductor-liquid interfaces, *The Journal of Physical Chemistry* **1990**, *94*, 1050-1055.

(190) Gao, Y. Q.; Georgievskii, Y.; Marcus, R. A. On the theory of electron transfer reactions at semiconductor electrode/liquid interfaces, *The Journal of Chemical Physics* **2000**, *112*, 3358-3369.

(191) Marcus, R. A. Theory of electron-transfer rates across liquid-liquid interfaces, *The Journal of Physical Chemistry* **1990**, *94*, 4152-4155.

(192) Marcus, R. A. On the theory of oxidation-reduction reactions involving electron transfer. V. Comparison and properties of electrochemical and chemical rate constants, *The Journal of Physical Chemistry* **1963**, *67*, 853.

(193) Marcus, R. A. Chemical and electrochemical electron-transfer theory, *Annual Revue of Physical Chemistry* **1964**, *15*, 155-196.

(194) Marcus, R. A.; Sutin, N. Electron transfers in chemistry and biology, *Biochimica et Biophysica Acta (BBA) - Reviews on Bioenergetics* **1985**, *811*, 265-322.

(195) Landau, L. D. Assotsiatsiya dvukhatomnykh molekul, *Sovetskii Fizicheskii Zhurnal* **1932**, *2*, 46-52.

(196) Zener, C. Dissociation of Excited Diatomic Molecules by External Perturbations, *Proceedings of the Royal Society of London. Series A* **1933**, *140*, 660-668.

(197) Feldberg, S. W.; Sutin, N. Distance dependence of heterogeneous electron transfer through the nonadiabatic and adiabatic regimes, *Chemical Physics* **2006**, *324*, 216-225.

(198) Chidsey, C. E. D. Free energy and temperature dependence of electron transfer at the metal-electrolyte interface, *Science* **1991**, *251*, 918-922.

(199) Hamann, T. W.; Gstrein, F.; Brunschwig, B. S.; Lewis, N. S. Measurement of the Dependence of Interfacial Charge-Transfer Rate Constants on the Reorganization Energy of Redox Species at n-ZnO/H2O Interfaces, *Journal of the American Chemical Society* **2005**, *127*, 13949-13954.

(200) Royea, W. J.; Fajardo, A. M.; Lewis, N. S. Fermi Golden Rule Approach to Evaluating Outer-Sphere Electron-Transfer Rate Constants at Semiconductor/Liquid Interfaces, *The Journal of Physical Chemistry B* **1997**, *101*, 11152-11159.

(201) Kuciauskas, D.; Freund, M. S.; Gray, H. B.; Winkler, J. R.; Lewis, N. Electron transfer dynamics in nanocrystaline titanium dioxide solar cells sensitized with ruthenium or osmium polypyridyl complexes, *The Journal of Physical Chemistry B* **2001**, *105*, 392-403.

(202) Lyon, L. A.; Hupp, J. T. Energetics of the nanocrystalline titanium dioxide/aqueous solution interface: approximate conduction band edge variations, *The Journal of Physical Chemistry B* **1999**, *103*, 4623-4628.

(203) Miyashita, M.; Sunahara, K.; Nishikawa, T.; Uemura, Y.; Koumura, N.; Hara, K.; Mori, A.; Abe, T.; Suzuki, E.; Mori, S. Interfacial Electron-Transfer Kinetics in Metal-Free Organic Dye-Sensitized Solar Cells: Combined Effects of Molecular Structure of Dyes and Electrolytes, *Journal of the American Chemical Society* **2008**, *130*, 17874–17881.

(204) Gaal, D. A.; Hupp, J. T. Thermally Activated, Inverted Interfacial Electron Transfer Kinetics:â€‰ High Driving Force Reactions between Tin Oxide Nanoparticles and Electrostatically-Bound Molecular Reactants, *Journal of the American Chemical Society* **2000**, *122*, 10956-10963.

(205) Maggio, E.; Martsinovich, N.; Troisi, A. Theoretical study of charge recombination at the TiO2-electrolyte interface in dye sensitised solar cells, *The Journal of Chemical Physics* **2012**, *137*, 22A508.

(206) Sun, Z.; Zhang, R.-K.; Xie, H.-H.; Wang, H.; Liang, M.; Xue, S. Non-ideal Charge Recombination and Conduction Band Edge Shifts in Dye-Sensitized Solar Cells Based on Adsorbent Doped Poly(ethylene oxide) Electrolytes, *The Journal of Physical Chemistry C* **2013**, *117*, 4364–4373.

(207) Boschloo, G.; Hagfeldt, A. Characteristics of the Iodide/Triiodide Redox Mediator in Dye-Sensitized Solar Cells, *Accounts of Chemical Research* **2009**, *42*, 1819-1826.

(208) Ardo, S.; Meyer, G. J. Photodriven heterogeneous charge transfer with transition-metal compounds anchored to TiO2 semiconductor surfacesw, *Chemical Society Reviews* **2009**, *38*, 115–164.

(209) Richards, C. E.; Anderson, A. Y.; Martiniani, S.; Law, C.; O'Regan, B. C. The Mechanism of Iodine Reduction by TiO2 Electrons and the Kinetics of Recombination in Dye-Sensitized Solar Cells, *The Journal of Physical Chemistry Letters* **2012**, *3*, 1980-1984.

(210) Rowley, J. G.; Farnum, B. H.; Ardo, S.; Meyer, G. J. Iodide Chemistry in Dye-Sensitized Solar Cells: Making and Breaking Iâˆ’I Bonds for Solar Energy Conversion, *The Journal of Physical Chemistry Letters* **2011**,

1, 3132-3140.

(211) Rowley, J. G.; Ardo, S.; Sun, Y.; Castellano, F. N.; Meyer, G. J. Charge Recombination to Oxidized Iodide in Dye-Sensitized Solar Cells, *The Journal of Physical Chemistry C* **2011**, *115*, 20316-20325.

(212) O'Regan, B. C.; K., W.; Juozapavicius, M.; Anderson, A.; Matar, F.; Ghaddar, T.; Zakeeruddin, S. M.; Klein, C.; Durrant, J. R. Structure/Function Relationships in Dyes for Solar Energy Conversion: A Two-Atom Change in Dye Structure and the Mechanism for Its Effect on Cell Voltage, *Journal of the American Chemical Society* **2009**, *131*, 3541–3548.

(213) Farnum, B. H.; Gardner, J. M.; Meyer, G. J. Flash-Quench Technique Employed To Study the One-Electron Reduction of Triiodide in Acetonitrile: Evidence for a Diiodide Reaction Product, *Inorganic Chemistry* **2010**, *49*, 10223-10225.

(214) Shi, Y.; Dong, X. Coupled analysis of steady-state and dynamic characteristics of dye-sensitized solar cells for determination of conduction band movement and recombination parameters, *Physical Chemistry Chemical Physics* **2013**, *15*, 299-306.

(215) Mora-Seró, I.; Bisquert, J. Fermi level of surface states in TiO2 nanoparticles, *Nano Letters* **2003**, *3*, 945-949.

(216) Cameron, P. J.; Peter, L. M. How Does Back-Reaction at the Conducting Glass Substrate Influence the Dynamic Photovoltage Response of Nanocrystalline Dye-Sensitized Solar Cells?, *The Journal of Physical Chemistry B* **2005**, *109*, 7392.

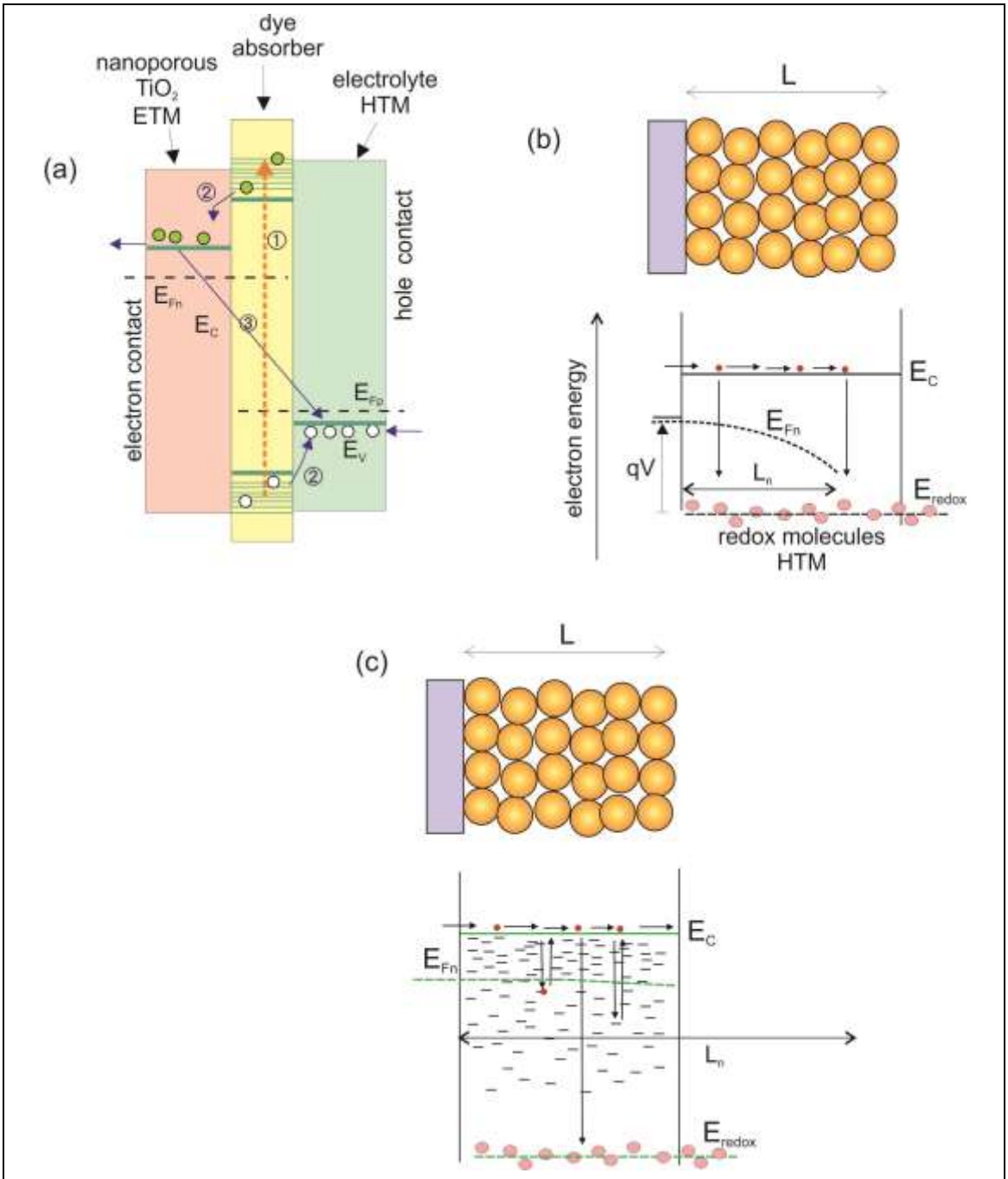

Fig. 1. Energy diagrams of a DSC, formed by several (spatially mixed) materials that function, as the absorber (indicating vibronic levels), the electron (ETM) and hole (HTM) transport materials, or redox electrolyte. Carriers relax to the conduction band of the ETM, E_C, and the valence band (E_V) of the HTM, producing a splitting of the quasi-Fermi levels of electrons (E_{Fn}) in the ETM and holes (E_{Fp}) in the HTM, or redox level in electrolyte E_{redox}. E_{Fn} is the Fermi level in the semiconductor when the TiO_2 photoelectrode is at the potential V. (a) The arrows indicate the following processes: (1) absorption of light, generating electrons and holes in the absorber. (2) Charge separation: Injection from the absorber to the ETM and HTM. (b) Mesoporous structure that forms the ETM in a DSC. It is formed by interconnected particles that

allow the transport of electrons via extended states. The potential V at the substrate fixes the electron density at the edge of the nanostructured semiconductor. Injected electrons at the contact have a probability to diffuse and recombine by charge transfer to the acceptor species in the HTM, so that the effective penetration in the layer is governed by the diffusion length L_n. (c) In this case transport in the extended level is coupled with trapping and release from localized states in the bandgap. The right contact is reflecting to electrons. If the diffusion length is long with respect to film thickness then the concentration is nearly homogeneous.

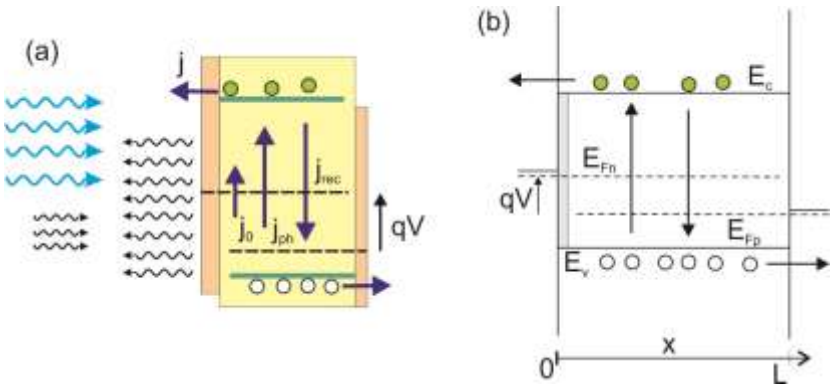

Fig. 2. Energy diagram of semiconductor layer with electron selective contact at the left side and hole selective contact at the right side. Under illumination, absorbed photons promote excitation of the absorber creating an electron-hole pair. Charge separation produces an electron in the ETM conduction band and a hole in the transport level of the HTM. (a) The diagram indicates the balance of radiation in the ideal diode. The diode receives thermal background radiation, and emits photons by radiative recombination. (b) Processes of carrier generation, recombination and extraction that lead to the different fluxes indicated in (a).

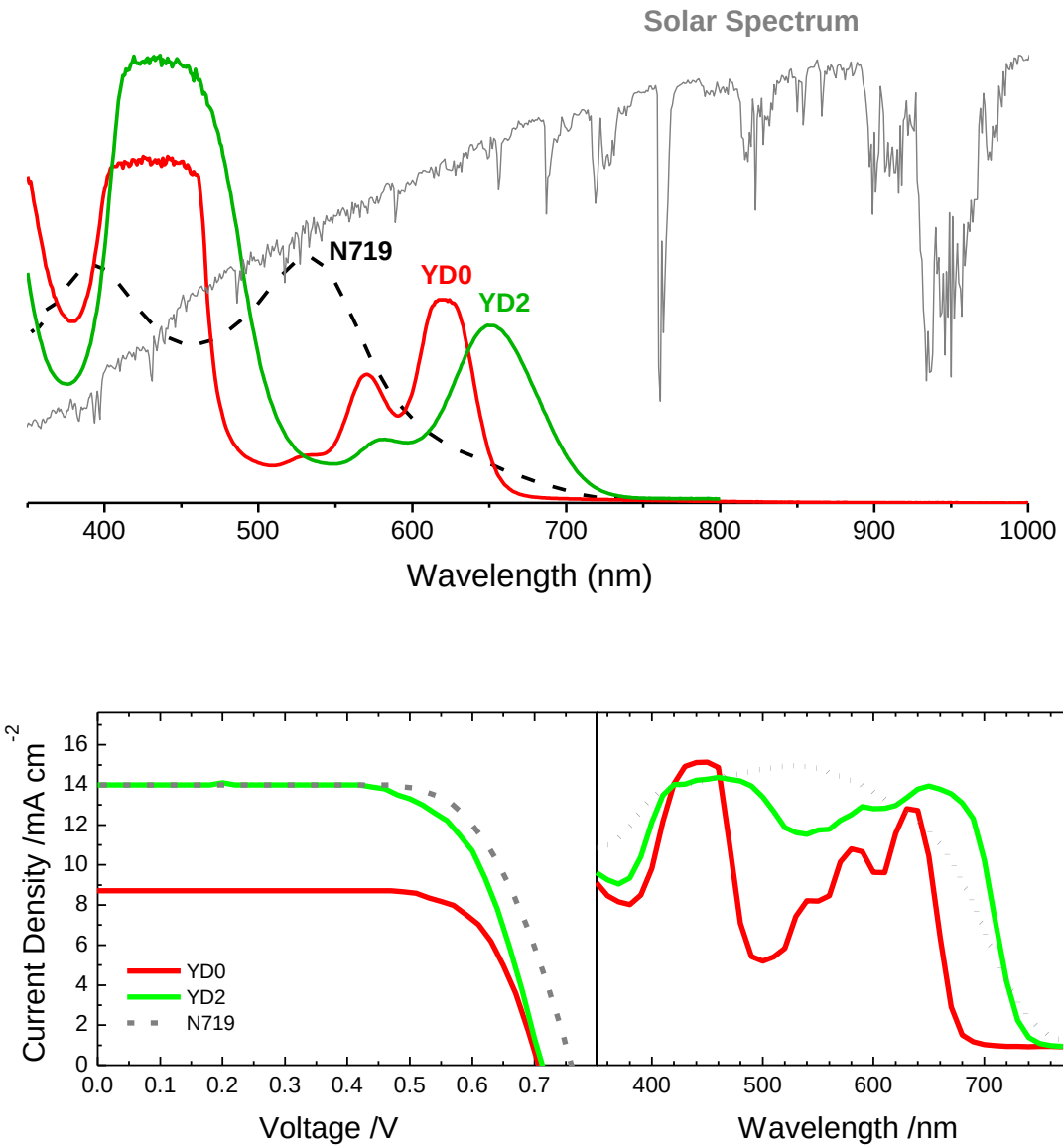

Fig. 3. Absorption coefficient of N719 and two porphyrin dyes, in comparison with the spectral photon flux, and the corresponding photovoltaic performance and IPCE. Adapted from [1] by courtesy of Lu-Lin Li and Eric W. Diau.

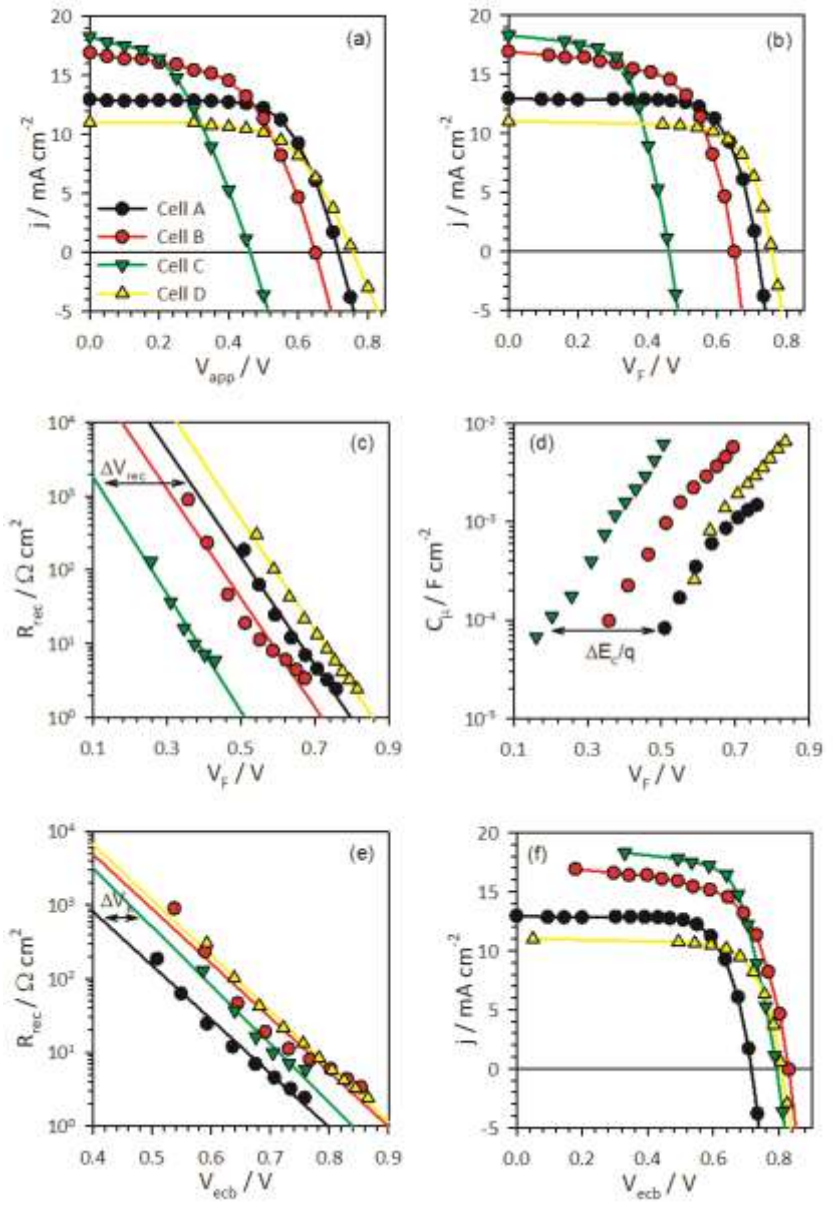

Fig. 4. (a) Current density-voltage curves of a set of DSCs with different electrolytes. Points are obtained from Impedance Spectroscopy measurements and lines by an integration procedure. (b) The current density-voltage curves with respect to Fermi level voltage V_F, in which the voltage drop due to internal series resistance has been corrected. (c) Recombination resistance between the semiconductor and the acceptor species in the electrolyte. (d) Chemical capacitance of the TiO_2. (e) The recombination resistance with respect to equivalent conduction band potential V_{ecb}, in which the voltage V_F is shifted so that all capacitances match to the same line. (f) The current density-voltage curves with respect to voltage V_{ecb}. Adapted from [2] by courtesy of Sonia R. Raga and Fran Fabregat-Santiago.

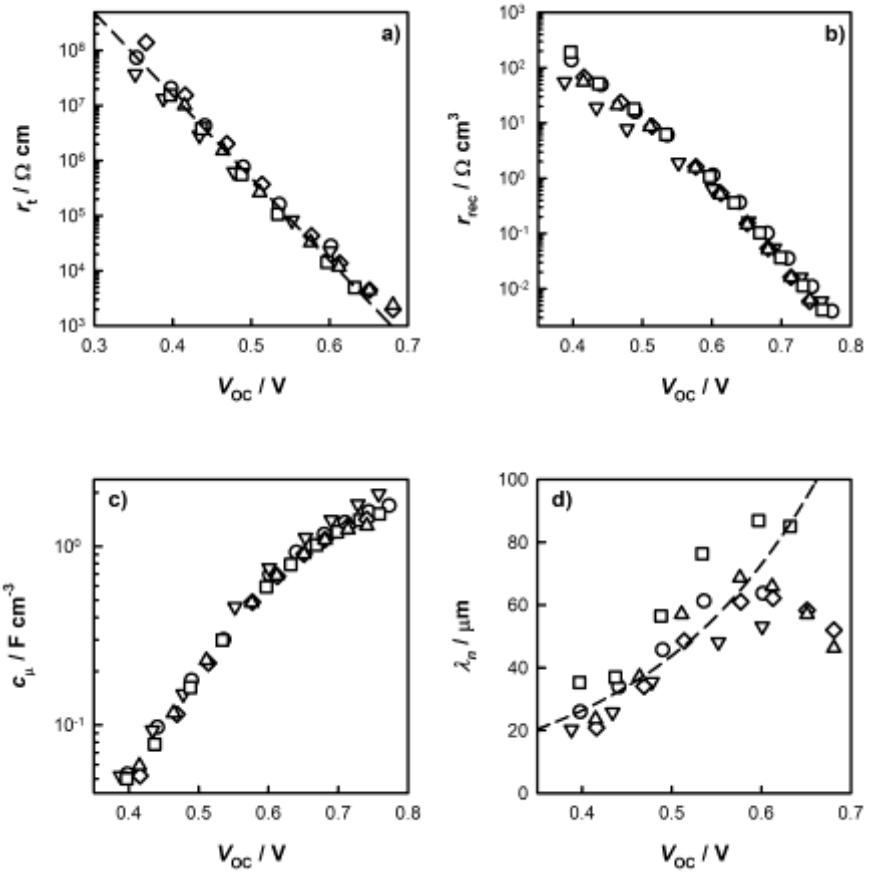

Figure 5. Plots of distributed transport resistance (a), charge transfer resistance (b), electrode capacitance (c), and electron diffusion length (d) versus open-circuit photovoltage for a series of cells with average TiO2 layer thicknesses of 4 (circles), 8 (downward triangles), 14 (squares), 16 (upward triangles), and 18 µm (diamonds). The dashed line in (a) is a fit with a slope of $q/k_BT = 15.2$ V^{-1}, while the dashed line in (d) is just a guide to the eye. Adapted from [3] by courtesy of James Jennings and Qing Wang.

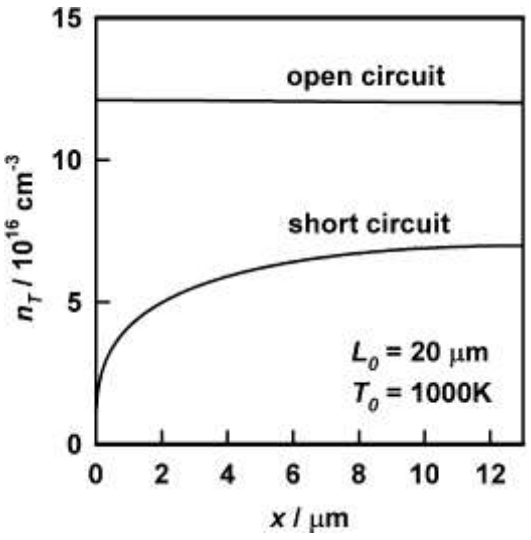

Fig. 6. Trapped carrier density profiles calculated from the steady-state continuity equation for open and short circuit conditions. $N_{L,0}$ = 10^{19} cm^{-3}, T_0 = 1000 K, τ_0 = 10^{-5} s, α = 500 cm−1, L = 13 μm, diffusion length L_0 = 20 μm. Reproduced with permission from [4].

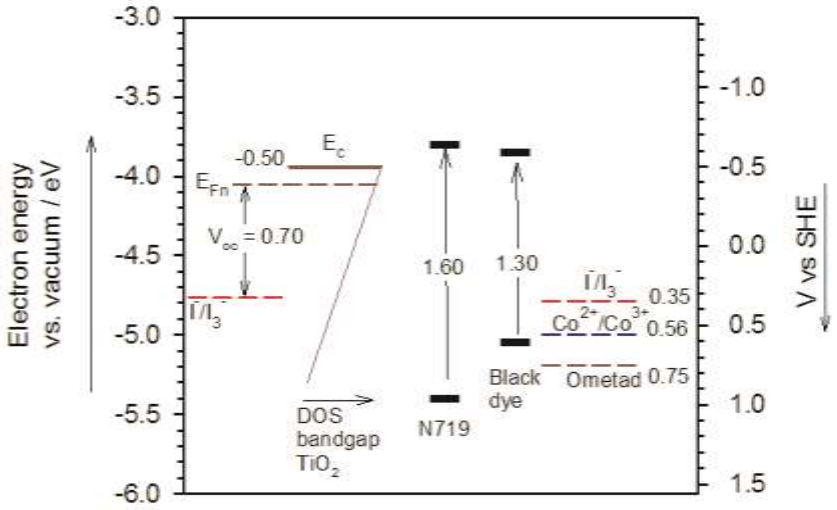

Figure 7. Energetic scheme of the components of a DSC. The position of the conduction band of TiO_2 and the density of states (DOS) in the bandgap is indicated. Also shown is the photovoltage by difference of the Fermi level of electrons and the redox potential in the electrolyte. At the right are shown the redox potential of conventional hole conductors. In the center is shown ground and excited state of standard dyes. More accurately, the excited and ground state are spread over an energy interval. Energy differences are expressed in eV.

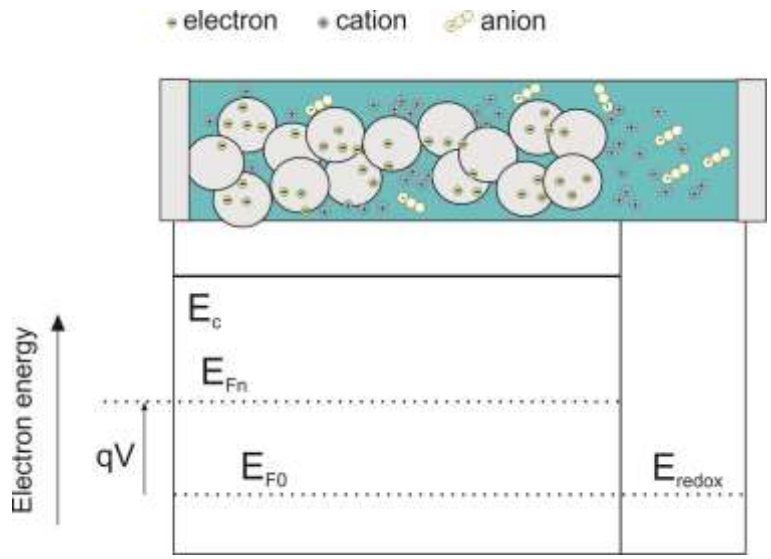

Fig. 8. Scheme showing electron accumulation in a nanocrystalline semiconductor electrode and the compensation by positive charge in the electrolyte to produce local electroneutrallity. The electrolyte may contain several species of anions, cations, redox molecules, as well molecules that have the role of modifying the surface to produce some beneficial effects. The energy diagram shows the change of electrons Fermi level that causes a photovoltage.

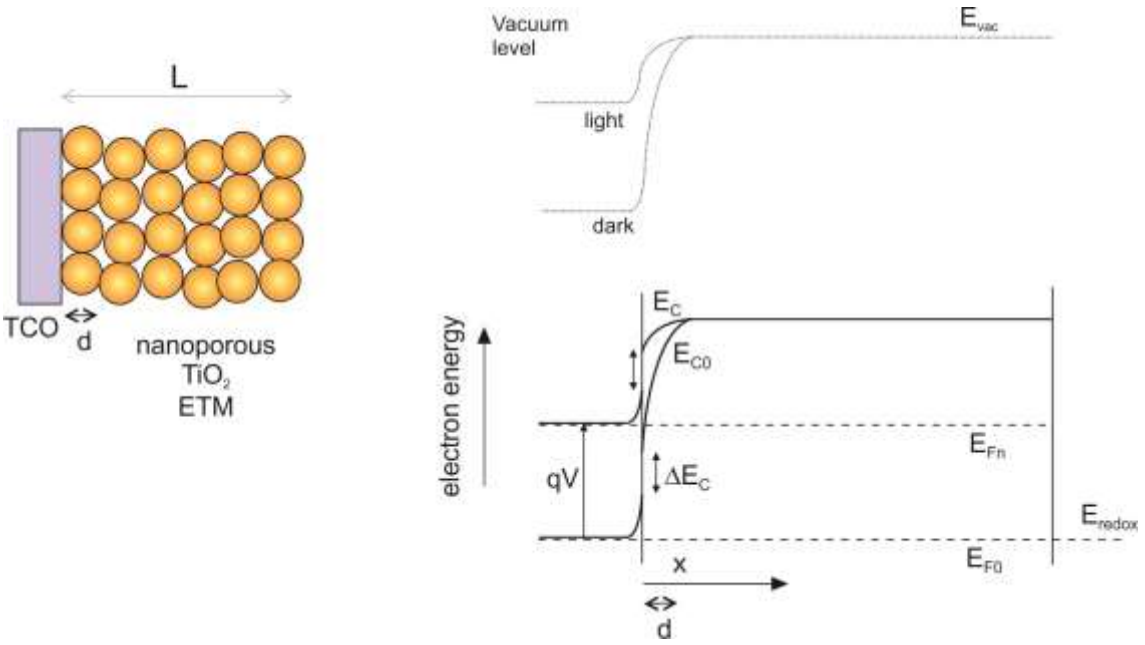

Figure 9. Energy diagram showing the contact of the nanocrystalline semiconductor electrode with the transparent conducting oxide (TCO) substrate, and the change of Fermi levels and the vacuum level under illumination, with respect to the dark equilibrium. ΔE_c is the energy offset between the conduction band of the TiO_2 and the transparent conducting oxide (TCO).

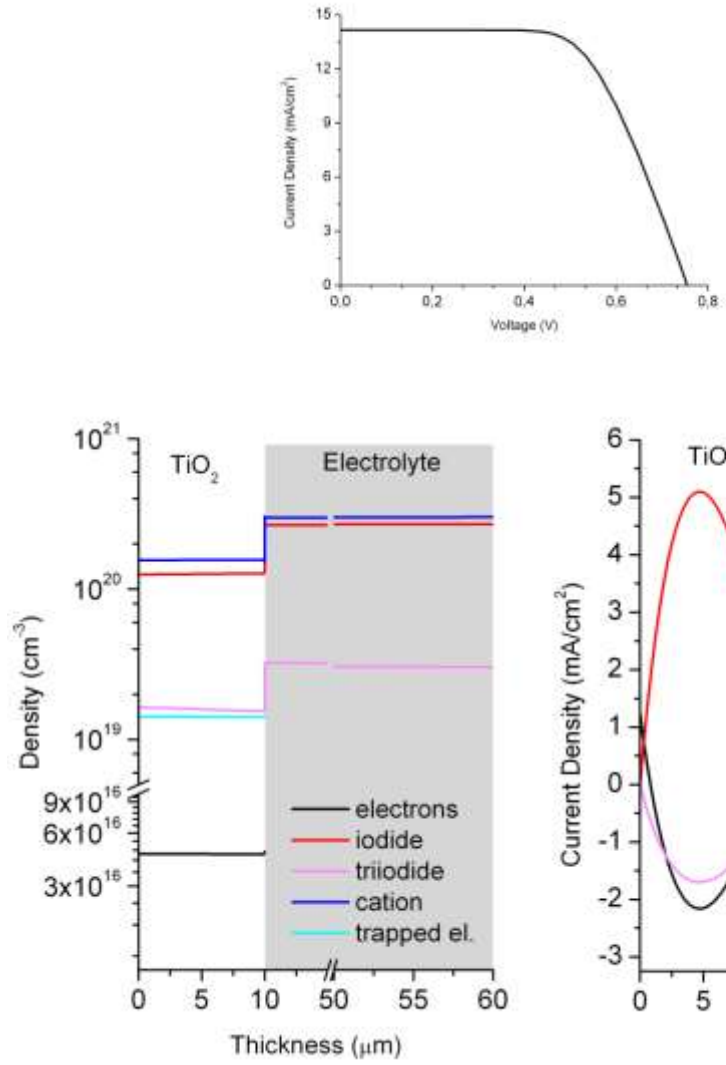

Figure 10. Upper panel: simulation of a current-voltage characteristic for a typical DSC (10 μm of mesoporous TiO_2/electrolyte, 50 μm of pure electrolyte) with N719 dye. Lower panel: the density distribution (left) and current density (right) within the cell at at 737 mV (close to open-circuit condition). The left picture shows all the charged species in the system: electrons (free and trapped), iodide and triiodide, positive counter-ion. For the current density only the charged species which contribute to the total current are shown: free electrons, iodide and triiodide ions. Simulation performed using TiberCAD software, courtesy of Alessio Gagliardi and Aldo di Carlo.

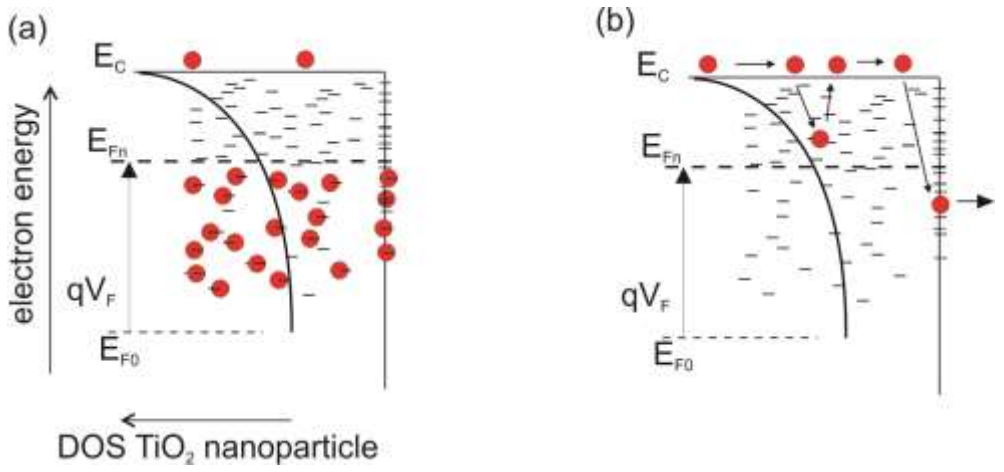

Fig. 11. The schemes shows the characteristic distribution of electronic states in the metal oxide nanoparticulate framework of a DSC, and their role in different electronic processes. (a) The electronic states consist on the transport states in the conduction band level, E_c, the localized states in the bandgap, which form an exponential distribution, and the surface states, whose energy distribution depends drastically on surface treatment. For an exponential distribution it is a good approximation to assume that localized states in the bandgap below the Fermi level are occupied and those above nearly empty. The occupation of the transport level is an important consideration as it gives rise to dc conductivity. The occupation of surface states depends on their charge transfer properties. (b) Electron displacement in transport states is interrupted by trapping and release processes. Trapping occurs mainly to unoccupied states above the Fermi level. Electrons are trapped in surface states from which charge transfer to acceptor species in solution occurs.

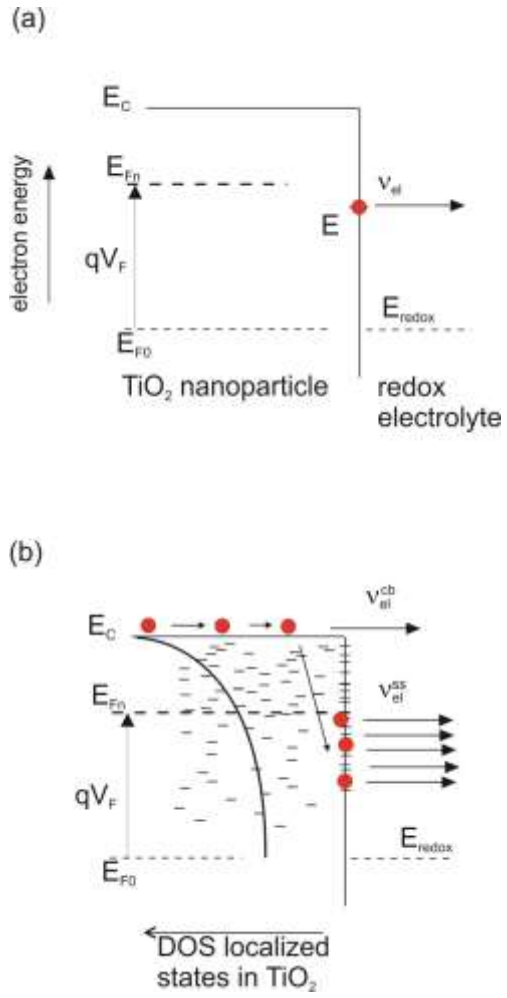

Fig. 12. Energy diagrams indicating recombination event in a DSC of electrons in TiO_2 semiconductor nanoparticle by transfer to the oxidized acceptor species of the redox couple in the electrolyte. On the left we show the bulk and surface of TiO_2. E_c is the energy of the conduction band, E_{F0} is the equilibrium Fermi level in the semiconductor, that initially is in equilibrium with the redox level in the electrolyte, E_{Fn} is the Fermi level in the semiconductor when the TiO_2 photoelectrode is at the potential V_F. (a) Electron transfer from a surface state at the energy E to an oxidized ion in electrolyte with probability ν_{el}. (b) Model including the various channels for electron transfer between the surface of TiO_2 nanoparticles and the oxidized species in the electrolyte (or hole conductor) in a DSC, namely, the transfer from extended states of the semiconductor conduction band with probability ν_{el}^{cb}, and the transfer from a distribution of surface states, each with a probability $\nu_{el}^{ss}(E)$.

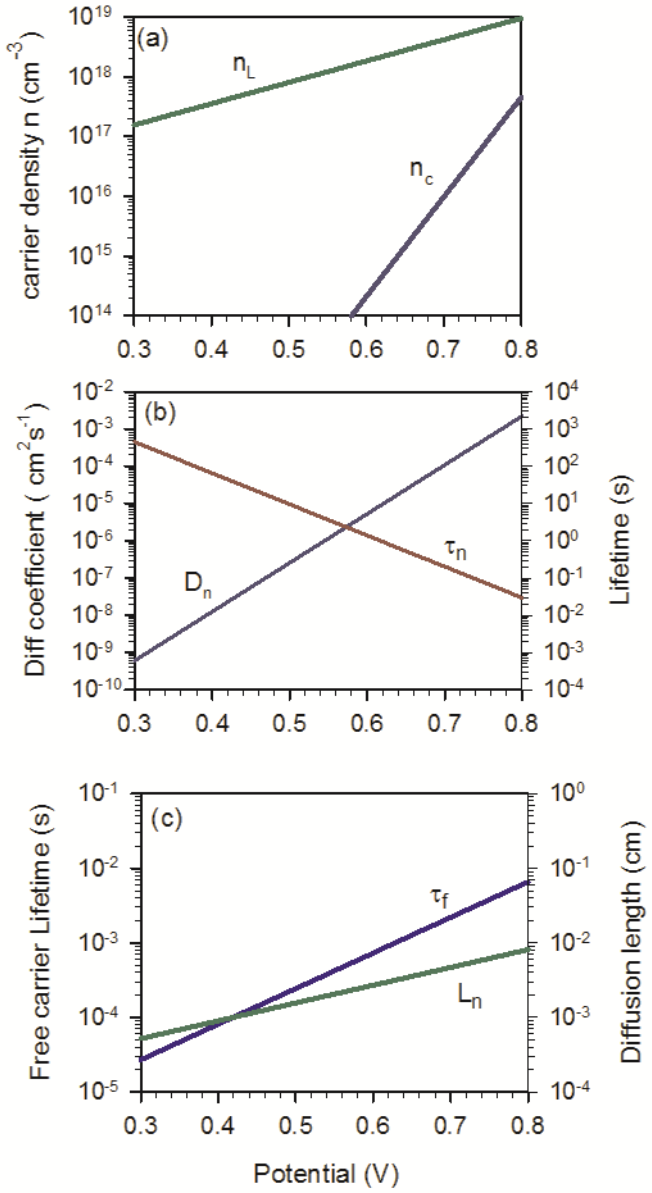

Fig. 13. (a) Representation of the free and localized carrier density, as a function of potential (Fermi level position), for an exponential distribution of localized states ($T = 300\,\mathrm{K}$, $T_0 = 1400\,\mathrm{K}$, $\beta = 0.5 + T/T_0 = 0.71$). (b) Electron lifetime, τ_n, and the diffusion coefficient, D_n, measured by small perturbation. (c) The free carrier lifetime, τ_f, and diffusion length $L_n = \sqrt{D_n \tau_n} = \sqrt{D_0 \tau_f}$.

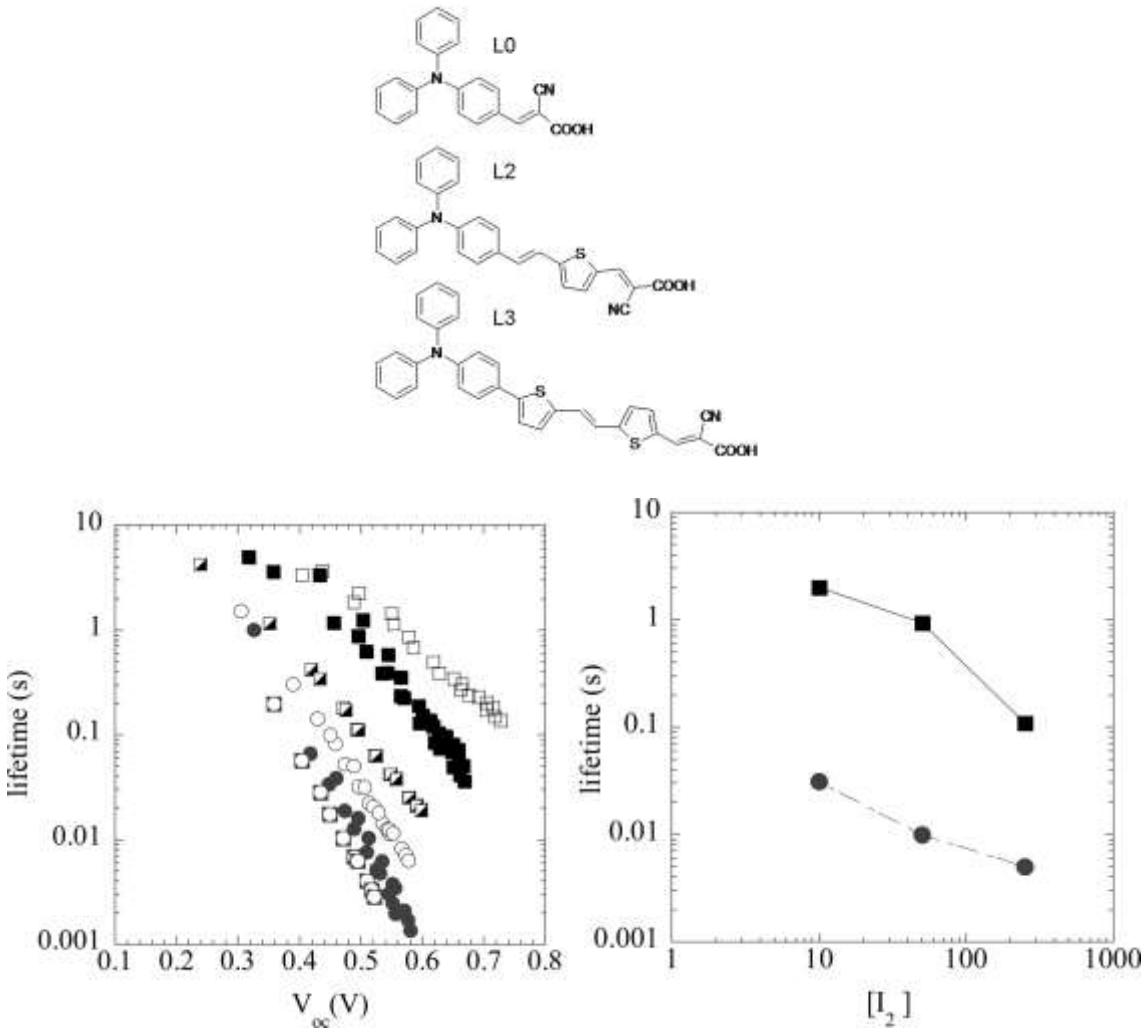

Fig. 14. (Top) a series of triphenylamine (TPA)-based dyes where the linker conjugation is systematically increased with vinylene and thiophene units. (left) Electron lifetime as function of V_{oc} for DSCs based on L0 (squares) and L3 (circles) using three different I_2 concentrations: (open symbols) 10 mM, (solid symbols) 50 mM, and (half-filled squares, gray circles in squares) 250 mM in the redox electrolyte. Electrolyte: 0.6 M TBAI, 0.1 M LiI, and 0.5 M 4-*tert*-butylpyridine with different I_2 concentrations in acetonitrile. (Right) Electron lifetimes for DSCs based on L0 (squares) and L3 (circles) at V_{oc} = 0.5 V as a function of I_2 concentration. Reproduced with permission.[5]

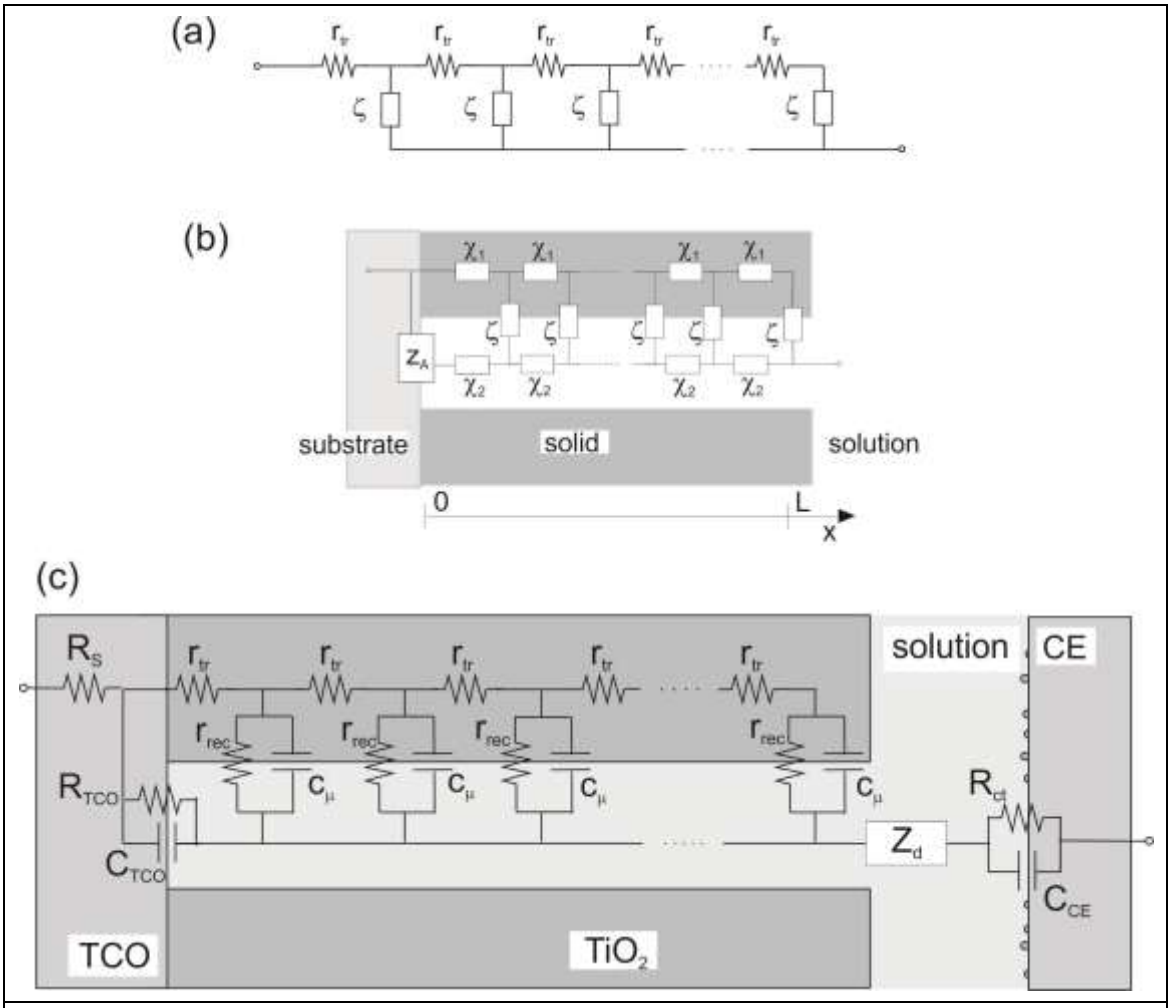

Fig. 15. (a) Transmission line model for the generalized diffusion impedance. (b) Transmission line model for a porous electrode. (c) Transmission line impedance model for diffusion-recombination in a mesoporous TiO_2 electrode, including also interfacial impedances and mass transport impedance in electrolyte.

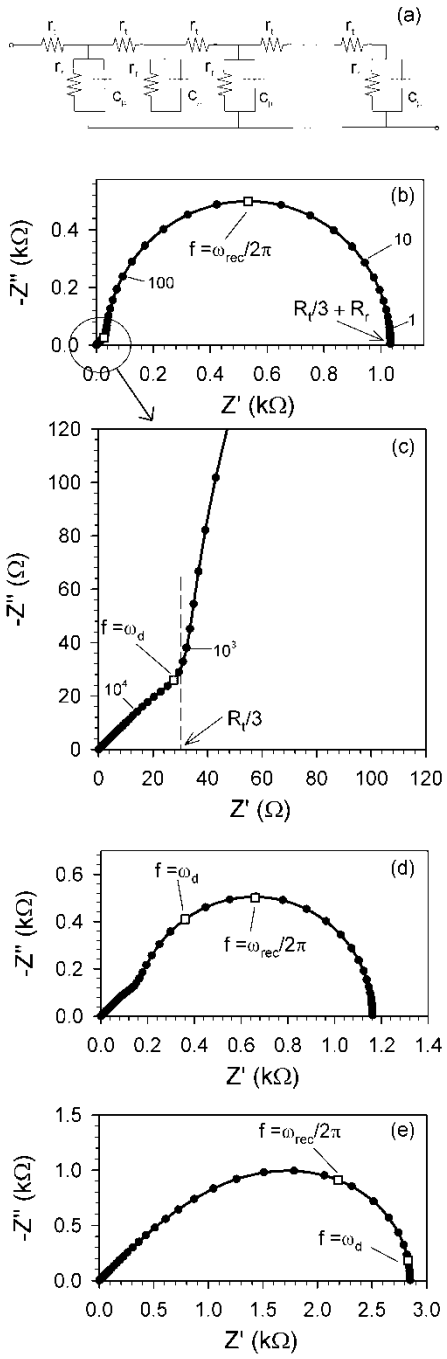

Fig. 16. Diffusion-recombination transmission line with reflecting boundary conditions (a). Simulation of the impedance with parameters $R_{rec} = 10^3\ \Omega$, $C_\mu = 5\times10^{-6}$ F and increasing transport resistance, (b,c) $R_{tr} = 10^2\ \Omega$, (d) $R_{tr} = 10^3\ \Omega$, (e) $R_{tr} = 10^4\ \Omega$. Shown are the frequencies in Hz at selected points, the characteristic frequency of the low frequency arc (square point), related to the angular frequency $\omega_{rec} = \tau_n^{-1} = 1/R_{rec}C_\mu$, and the low frequency resistance. The frequency (Hz) of the turnover from Warburg behaviour to low frequency recombination arc (square point), related to the characteristic frequency $\omega_d = 1/R_{tr}C_\mu$ is also shown.

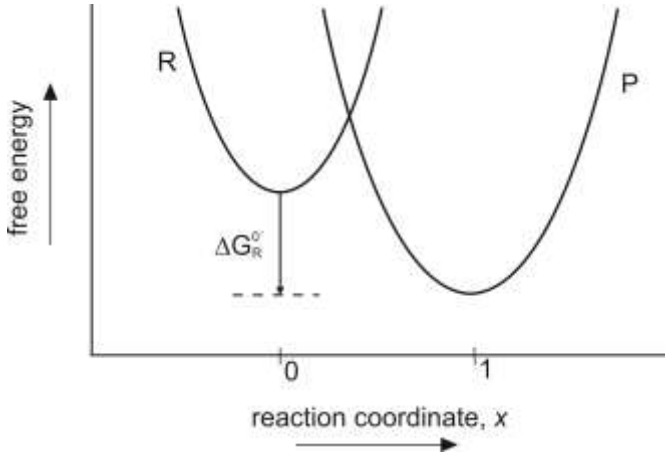

Fig. 17. Free energy curves as a function of the reaction coordinate. ΔG_R^0 indicates the "standard" change of free energy from reactants (R) to products (P) and is negative in the illustrated case in the Figure.

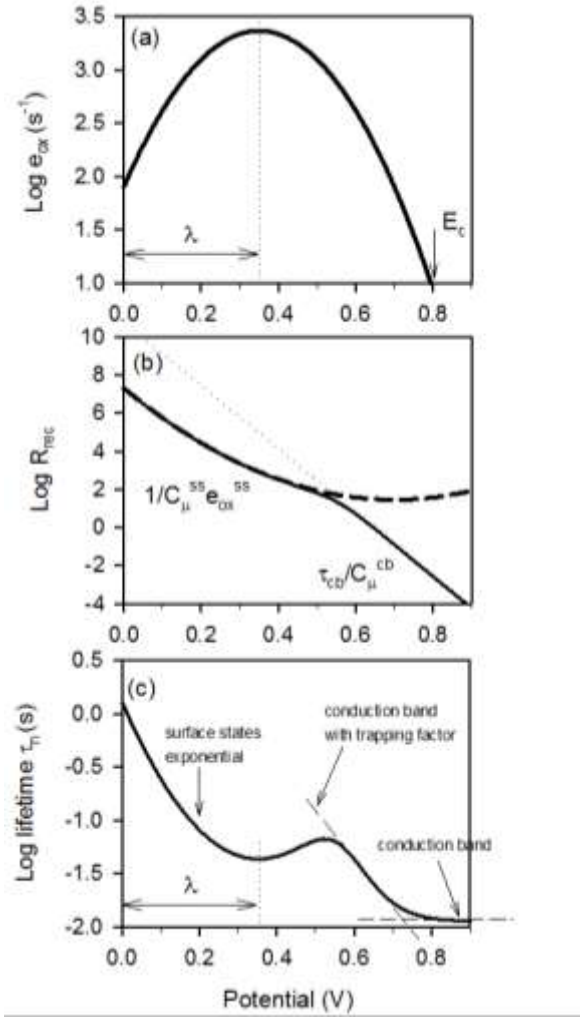

Fig. 18. Recombination in a DSC according to Marcus model of charge transfer in an exponential distribution of surface states. Horizontal axis is the voltage or equivalently the electron Fermi level. (a) Probability of isoenergetic electron transfer to the electronic levels of oxidized species in solution. (b) The inverse of charge transfer rates, both for conduction band and surface trap transfer mechanisms, and total charge transfer resistance in thick line. These quantities correspond to the recombination resistance. (c) The lifetime, indicating the charge transfer mechanism that corresponds to each domain. Simulation parameters are: $\lambda = 0.35\,\mathrm{eV}$, $T = 300\,\mathrm{K}$, $L = 10\,\mu\mathrm{m}$, $E_c = 0.8\,\mathrm{eV}$ vs. E_{redox}, $N_c = 6.8\times10^{20}\,\mathrm{cm}^{-3}$, $N_b = 1\times10^{20}\,\mathrm{cm}^{-3}$, $N_s = 1\times10^{18}\,\mathrm{cm}^{-3}$, $T_{0s} = T_{0b} = 600\,\mathrm{K}$, $c_{ox} = 3\times10^{19}\,\mathrm{cm}^{-3}$, $k_0^{(cb)} = 5\times10^{-15}\,\mathrm{cm}^3\mathrm{s}^{-1}$, $k_0^{(ss)} = 5\times10^{-16}\,\mathrm{cm}^3\mathrm{s}^{-1}$. Reproduced with permission.[6]

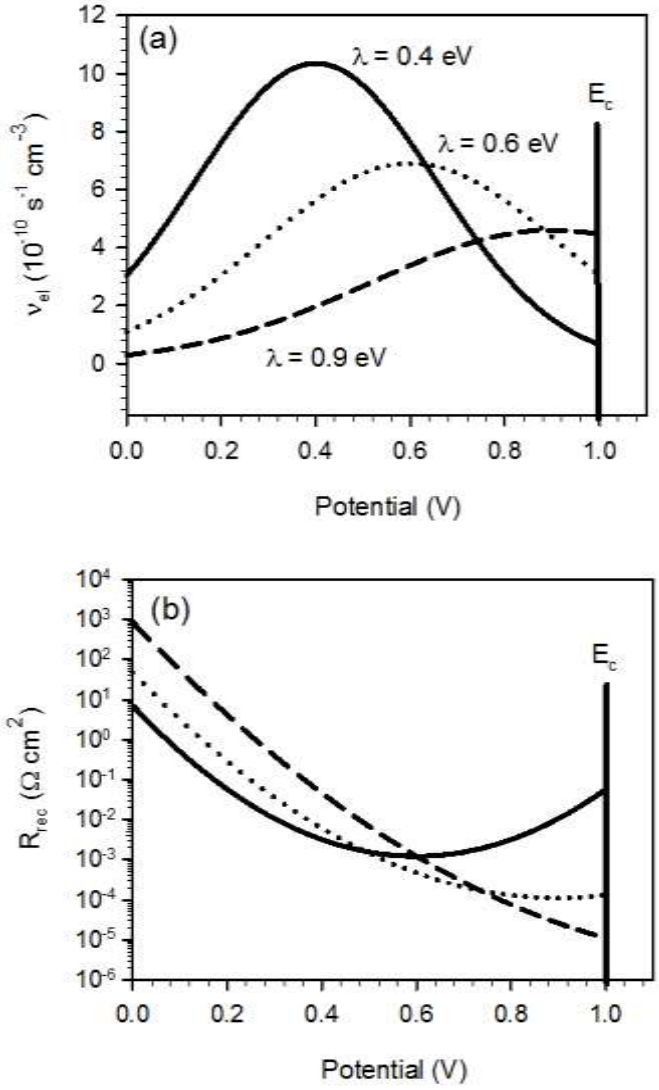

Fig. 19. Recombination in a DSC according to Marcus model of charge transfer in an exponential distribution of surface states. Horizontal axis is the voltage or equivalently the electron Fermi level. The position of the conduction band, E_C, is indicated. Plots at different values of reorganization energy as indicated. (a) Electron transfer probability. (b) Electron recombination resistance. Simulation parameters are:, $T = 300\,\mathrm{K}$, $T_0 = 1200\,\mathrm{K}$, $\alpha = 0.25$, $\beta = 0.75$, $E_c = 1\,\mathrm{eV}$ vs. E_{redox}, $k_0{}^{ss} = 1\times10^{-7}\ \mathrm{cm^{-3}s^{-1}}$, $R_{0\lambda} = 10^{-5}\ \Omega\,\mathrm{cm}^2$.

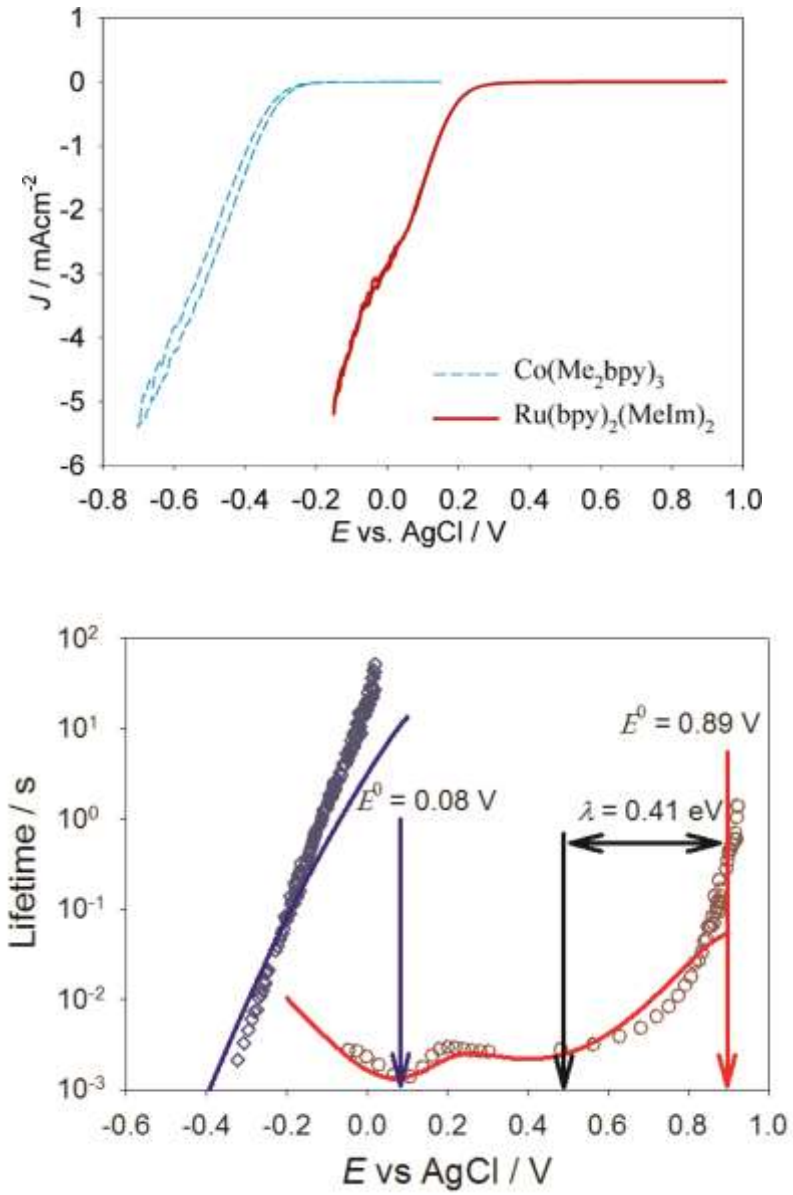

Fig. 20. (a) Current density versus applied potential curves and (b) electron lifetimes in DSCs. The two data sets correspond to different redox carriers $[Co(Me_2bpy)_3]^{3+/2+}$ (◊) and $[Ru(bpy)_2(MeIm)_2]^{3+/2+}$ (O) with redox potential indicated in (b). The reorganization energy λ has been determined for the Co-based redox carrier and it is indicated in (b). Note that the potential V is more negative when the Fermi level of electrons raises (electrochemical convention). Courtesy of Tom Hamann, adapted from [7], reproduced with permission.

(1) Li, L.-L.; Diau, E. W.-G. Porphyrin-sensitized solar cells, *Chemical Society Reviews* **2012**, *42*, 291-304.

(2) Raga, S. R.; Barea, E. M.; Fabregat-Santiago, F. Analysis of the Origin of Open Circuit Voltage in Dye Solar Cells, *The Journal of Physical Chemistry Letters* **2012**, *3*, 1629-1634.

(3) Jennings, J. R.; Liu, Y.; Safari-Alamuti, F.; Wang, Q. Dependence of Dye-Sensitized Solar Cell Impedance on Photoelectrode Thickness, *The Journal of Physical Chemistry C* **2012**, *116*, 1556-1562.

(4) Wang, H.; Peter, L. M. A Comparison of Different Methods To Determine the Electron Diffusion Length in Dye-Sensitized Solar Cells, *The Journal of Physical Chemistry C* **2009**, *113*, 18125–18133.

(5) Marinado, T.; Nonomura, K.; Nissfolk, J.; Karlsson, M. K.; Hagberg, D. P.; Sun, L.; Mori, S.; Hagfeldt, A. How the Nature of Triphenylamine-Polyene Dyes in Dye-Sensitized Solar Cells Affects the Open-Circuit Voltage and Electron Lifetimes, *Langmuir* **2009**, *26*, 2592–2598.

(6) Bisquert, J. ; Zaban, A.; Greenshtein, M.; Mora-Seró, I. Determination of rate constants for charge transfer and the distribution of semiconductor and electrolyte electronic energy levels in dye-sensitized solar cells by open-circuit photovoltage decay method., *Journal of the American Chemical Society* **2004**, *126*, 13550.

(7) Ondersma, J. W.; Hamann, T. W. Measurements and Modeling of Recombination from Nanoparticle TiO2 Electrodes, *Journal of the American Chemical Society* **2011**, *133*, 8264-8271.